CRCLEME

Cooperative Research Centre for
Landscape Evolution & Mineral Exploration

OPEN FILE
REPORT
SERIES

CSIRO
EXPLORATION
AND MINING

AMIRA

Australian Mineral Industries Research Association Limited ACN 004 448 266

BEASLEY CREEK ORIENTATION STUDY GEOCHEMISTRY, PETROGRAPHY AND MINERALOGY OF FERRUGINOUS LAG OVERLYING THE BEASLEY CREEK GOLD MINE - LAVERTON, WESTERN AUSTRALIA

Volume 1

I.D.M. Robertson

CRC LEME OPEN FILE REPORT 10

September 1998

(CSIRO Division of Exploration Geoscience Report 27R, 1989.
Second impression 1998)

CRC LEME is an unincorporated joint venture between The Australian National University, University of Canberra, Australian Geological Survey Organisation and CSIRO Exploration and Mining, established and supported under the Australian Government's Cooperative Research Centres Program.

AMIRA
Australian Mineral Industries Research Association Limited ACN 004 448 266

CRCLEME
Cooperative Research Centre for Landscape Evolution & Mineral Exploration

CSIRO
EXPLORATION AND MINING

BEASLEY CREEK ORIENTATION STUDY GEOCHEMISTRY, PETROGRAPHY AND MINERALOGY OF FERRUGINOUS LAG OVERLYING THE BEASLEY CREEK GOLD MINE -LAVERTON, WESTERN AUSTRALIA

Volume 1

I.D.M. Robertson

CRC LEME OPEN FILE REPORT 10

September 1998

(CSIRO Division of Exploration Geoscience Report 27R, 1989.
Second impression 1998)

CRC LEME is an unincorporated joint venture between The Australian National University, University of Canberra, Australian Geological Survey Organisation and CSIRO Exploration and Mining
Headquarters: CRC LEME c/o CSIRO Exploration and Mining, Private Bag, PO Wembley, Western Australia, 6014

RESEARCH ARISING FROM CSIRO/AMIRA REGOLITH GEOCHEMISTRY PROJECTS 1987-1993

In 1987, CSIRO commenced a series of multi-client research projects in regolith geology and geochemistry which were sponsored by companies in the Australian mining industry, through the Australian Mineral Industries Research Association Limited (AMIRA). The initial research program, "Exploration for concealed gold deposits, Yilgarn Block, Western Australia" (1987-1993) had the aim of developing improved geological, geochemical and geophysical methods for mineral exploration that would facilitate the location of blind, buried or deeply weathered gold deposits. The program included the following projects:

P240: Laterite geochemistry for detecting concealed mineral deposits (1987-1991). Leader: Dr R.E. Smith.
Its scope was development of methods for sampling and interpretation of multi-element laterite geochemistry data and application of multi-element techniques to gold and polymetallic mineral exploration in weathered terrain. The project emphasised viewing laterite geochemical dispersion patterns in their regolith-landform context at local and district scales. It was supported by 30 companies.

P241: Gold and associated elements in the regolith - dispersion processes and implications for exploration (1987-1991). Leader: Dr C.R.M. Butt.
The project investigated the distribution of ore and indicator elements in the regolith. It included studies of the mineralogical and geochemical characteristics of weathered ore deposits and wall rocks, and the chemical controls on element dispersion and concentration during regolith evolution. This was to increase the effectiveness of geochemical exploration in weathered terrain through improved understanding of weathering processes. It was supported by 26 companies.

These projects represented "an opportunity for the mineral industry to participate in a multi-disciplinary program of geoscience research aimed at developing new geological, geochemical and geophysical methods for exploration in deeply weathered Archaean terrains". This initiative recognised the unique opportunities, created by exploration and open-cut mining, to conduct detailed studies of the weathered zone, with particular emphasis on the near-surface expression of gold mineralisation. The skills of existing and specially recruited research staff from the Floreat Park and North Ryde laboratories (of the then Divisions of Minerals and Geochemistry, and Mineral Physics and Mineralogy, subsequently Exploration Geoscience and later Exploration and Mining) were integrated to form a task force with expertise in geology, mineralogy, geochemistry and geophysics. Several staff participated in more than one project. Following completion of the original projects, two continuation projects were developed.

P240A: Geochemical exploration in complex lateritic environments of the Yilgarn Craton, Western Australia (1991-1993). Leaders: Drs R.E. Smith and R.R. Anand.
The approach of viewing geochemical dispersion within a well-controlled and well-understood regolith-landform and bedrock framework at detailed and district scales continued. In this extension, focus was particularly on areas of transported cover and on more complex lateritic environments typified by the Kalgoorlie regional study. This was supported by 17 companies.

P241A: Gold and associated elements in the regolith - dispersion processes and implications for exploration. Leader: Dr. C.R.M. Butt.
The significance of gold mobilisation under present-day conditions, particularly the important relationship with pedogenic carbonate, was investigated further. In addition, attention was focussed on the recognition of primary lithologies from their weathered equivalents. This project was supported by 14 companies.

Although the confidentiality periods of the research reports have expired, the last in December 1994, they have not been made public until now. Publishing the reports through the CRC LEME Report Series is seen as an appropriate means of doing this. By making available the results of the research and the authors' interpretations, it is hoped that the reports will provide source data for future research and be useful for teaching. CRC LEME acknowledges the Australian Mineral Industries Research Association and CSIRO Division of Exploration and Mining for authorisation to publish these reports. It is intended that publication of the reports will be a substantial additional factor in transferring technology to aid the Australian Mineral Industry.

This report (CRC LEME Open File Report 10) is a first revision of CSIRO, Division of Exploration Geoscience Restricted Report 027R, first issued in 1989, which formed part of the CSIRO/AMIRA Project P240 .

Copies of this publication can be obtained from:
The Publication Officer, CRC LEME, CSIRO Exploration and Mining, PMB, Wembley, WA 6014, Australia. Information on other publications in this series may be obtained from the above or from http://leme.anu.edu.au/
Bibliographic reference:
This publication should be referred to as Robertson, I.D.M., 1998. Geochemistry, petrography and mineralogy of ferruginous lag overlying the Beasley Creek Gold Mine - Laverton WA. Open File Report 10, Cooperative Research Centre for Landscape Evolution and Mineral Exploration, Perth, Australia.
Cataloguing-in-Publication:
Robertson, I.D.M.
Geochemistry, petrography and mineralogy of ferruginous lag overlying the Beasley Creek Gold Mine - Laverton WA
ISBN v1: 0 642 28224 2 v2: 0 642 28230 7 set: 0 642 28236 6
1. Geochemistry 2. Laterite 3. Mineralogy 4. Gold - Western Australia.
I. Title
CRC LEME Open File Report 10.
ISSN 1329-4768

FRONTISPIECE

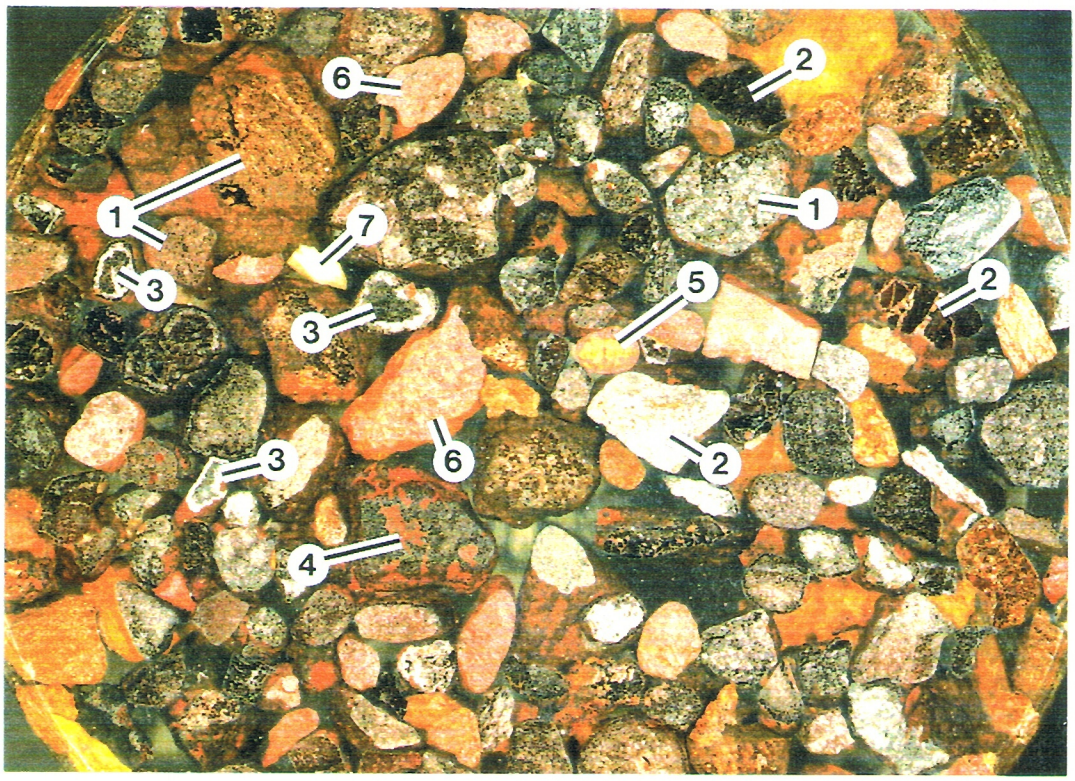

A polished section of fine lag in oblique reflected light. This illustrates the wide variety of granule colours and fabrics and underlines the inhomogeneous nature of this geochemical sampling medium. It consists of numerous brown to grey lithorelics (1), containing remnant micas and pseudomorphs of goethite after probable clay minerals, granules of bright, porous, secondary goethite (2), some with cutans of bright, dense goethite (3) and others with clay-filled solution cavities (4). Also there are yellow clay pisoliths, some with a red rim of goethite and hematite (5), and complex granules of yellowish-brown clay (6), invaded by later goethite, as well as a few shards of quartz (7). Specimen 08-216. Co-ordinates 33975E, 38940N. Photo J. L. Perdrix.

PREFACE

The CSIRO-AMIRA Research Programme, Exploration for Concealed Gold Deposits, Yilgarn Block, Western Australia, has, as its overall aim, the development of improved geological, geochemical and geophysical methods for mineral exploration that will facilitate the location of blind, concealed or deeply weathered gold deposits. This report presents some of the results of an integrated study at the essentially non-outcropping Beasley Creek gold mine, a locality which is being investigated by the Laterite Geochemistry (P240), the Weathering Processes (P241) and WA Remote Sensing (P243) modules of the CSIRO-AMIRA Yilgarn Gold Programme.

At Beasley Creek it was necessary to first thoroughly map the regolith, and associated landforms, and describe them, using standardized terminology. This has been covered in a previous report (26R). The current report concerns the origin, characteristics and use in exploration of ferruginous lag. Coarse lag, fine lag as well as the magnetic and non-magnetic components of the fine lag have been compared and assessed as geochemical sampling media. It is necessary to understand the nature of a geochemical sampling medium in order to focus on the source of a geochemical signature and so to assess the value of the medium and improve its use. The origins of the ferruginous lag have been traced to the underlying saprolite. Saprolite fabrics have been preserved in the lag and it is hoped that, as the Weathering Processes study (P241) progresses, these fabrics will be better understood.

Considerable multi-element geochemical, mineralogical and petrographic detail has been gathered. This information is essential for meaningful multivariate statistical interpretation of geochemical data and this research will form the basis of a later study at Beasley Creek. Ultimately the Beasley Creek orientation study will provide geochemical reference groups for a broader phase of the Laterite Geochemistry Project, that of establishing multivariate data interpretation procedures appropriate to Yilgarn lateritic weathering environments.

Interpretation of the results has made extensive use of petrographic and geochemical information gained during a complementary study of the saprolite for the Weathering Processes P241 Project (Report MG67R) in part by the same author. Report 27R and Report MG67R, have been issed to the sponsors of both P240 and P241 as these investigations are inseparable and synergy has enhanced the interpretation.

R.E. Smith
Project Leader
November, 1989

TABLE OF CONTENTS

LIST OF FIGURES

LIST OF TABLES

GEOCHEMISTRY, PETROGRAPHY AND MINERALOGY OF FERRUGINOUS LAG OVERLYING THE BEASLEY CREEK GOLD MINE - LAVERTON, WA

I.D.M. Robertson

1.0 ABSTRACT

Two fractions (0.2 to 4.0 and 10 to 50 mm) of the black ferruginous lag that used to overlie the Beasley Creek gold mine have been studied physically, petrographically, mineralogically and geochemically. The fine lag was split into magnetic and non-magnetic components.

The coarse lag fraction consists of goethite and hematite with minor quantities of mica, kaolinite and quartz. It contains ferruginised lithorelics with remnant and pseudomorphed minerals and fabrics. These are related to both primary and authigenic features of the underlying saprolite. These relics occur as islands in several cycles of secondary goethite and hematite, which have obliterated much of the original fabric. In many instances hematite can be shown to be a dehydration product of goethite. Later history of the coarse lag is shown by skins and nodules of ferruginous clay, which have undergone several cycles of solution, clay precipitation and permeation by iron-bearing solutions. Careful study of original fabrics could be used to aid the geological mapping of lag-covered areas.

In addition to black ferruginous nodules and red-brown and yellow-brown nodules, analogous to the coarse lag, the fine lag contains minor components of calcrete, quartz and a cellular ironstone, as well as very small quantities of silica-cemented red, aeolian sand and organic debris. The fine lag shows similar fabrics and components to the coarse lag but its finer and more fragmentory nature and wider dispersion make elucidation of the original rock type more difficult.

The orebody and its host, the weathered black phyllite, are depicted by positive anomalies in Au, As, Ba, Co, Cu, Mn, Mo (weak), Pb (possible), Sb, W and Zn in the lag. The cellular ironstone component is strongly anomalous in the target elements As, Au, Co, Cu, Mn, Sb, Se and Zn. Similar anomalies in Mg, Ca and Sr mark the occurrence of calcrete, which occurs near the hill crest and coincides with the orebody. Gold is the best indicator and shows strong anomalies (1000 ppb over a 10 ppb background) which are 600 - 900 m in width. Other elements show narrower dispersions. Superimposed on these broad gold anomalies are narrow, subsidiary peaks (10 000 ppb), specifically in the coarse lag, which accurately locate the ore. The wide dispersion of gold reflects chemical dispersion in the saprolite and lateritic duricrust, prior to mechanical dispersion of the lag on the surface. This is supported by the association of gold grains with vesicles and late goethite and even clay phases in the lag.

The fine lag is the most useful sampling medium and is best suited as a regional tool. The coarse lag, which is more tedious to collect, has use in follow-up work. No advantage is gained in analysis of the magnetic component, as it fails to give anomalies in Co, Cu, Se and Zn and the Au anomaly is not as distinct. This occurs because the important, non-magnetite, cellular ironstone or gossan component is excluded.

2.0 INTRODUCTION

A substantial study of the Beasley Creek Gold Deposit, owned by Western Mining Corporation Ltd., is being carried out within the CSIRO/AMIRA Research Programme "Exploration for Concealed Gold Deposits, Yilgarn Block, Western Australia". This deposit lies about 12 km west north-west of Laverton at 122° 18'E, 28° 34'S. Here, Archaean rocks appear to occupy a small window in the surrounding Permian glacial sediments. The Archaean and Permian rocks have been deeply weathered. Only the saprolite of the Archaean rocks outcrops in a few places.

Proved and probable ore reserves of 2.1 million tonnes at 2 g/t have been outlined by Western Mining Corp. Ltd. The CSIRO research programme commenced prior to disturbances by mining. Open pit mining began at the end of 1987 and the pit was well advanced at the time of writing this report.

2.1 CSIRO Work Programme

Research being carried out by CSIRO at Beasley Creek comprises studies of the surface geology and geomorphology, the geochemistry of surface materials and the geochemistry of and dispersions in the saprolite. A report on the geology, geochemistry and mineralogy of the ore zone and footwall rocks is complete (Robertson and Gall, 1988) and so is a summary of the pre-mining geomorphology and surface geology (Robertson and Churchward, 1989). This report covers the geochemistry, petrography and mineralogy of the ferruginous lag. Further reports on the surface ironstones, lateritic duricrust and ore at shallow depth are in preparation. Geochemical investigations of a profile from surface to about 80-m depth, and of the soils and calcrete are in progress and will be the subject of future reports.

In November 1987, when the mine was at an advanced assessment stage and mining was considered to be imminent, the occurrence of surface materials (soils, lag, vein quartz fragments, calcrete, ironstone and saprolite) were mapped and samples of both surface lag and soil were collected along two lines, 38820 N and 38940 N. Percussion drilling along line 38820 was later sampled to determine the dispersions of key elements in the deep saprolite. Samples of ironstone and calcrete were collected over the southern part of the mine site after mining had commenced on the northern part.

2.2 Geological Summary

The solid geology, as determined by WMC from percussion drilling, is illustrated in Figure 1A. The orebody lies in a black shale zone, some 15 - 40 m thick, which dips at 45° to the east. It strikes generally north but swings to the west at its southern end and flattens. This black shale unit is intensely weathered to considerable depth (>200 m) and gold is associated with ferruginous zones within it. The black shale is enclosed in a narrow, north-striking mafic amphibolite schist, which is less intensely weathered, particularly where distant from the black shale. Small porphyry, granitoid and meta-dolerite lenses intrude the stratigraphy and are associated with north-west striking faults and shears. The amphibolite schist is in turn enclosed in komatiitic lithologies of the Mt. Margaret Anticline.

The regolith at Beasley Creek has been partly stripped. This is indicated by the absence of a lateritic duricrust over all but the eastern flank of the hill. The western edge of the ferruginous lateritic duricrust closely follows the upper surface of the ore-bearing black shale unit and it seems likely that iron in this unit, probably originally as sulphides, formed much of the source of iron for the lateritic duricrust. Ironstones overlie both the ore-bearing black shale unit and meta-dolerites. Extensive calcretes occur near the top of the hill. Saprolitic Permian sediments overlap the mafic and ultramafic saprolites in the eastern margin of the pit (Figure 1A).

FIGURE 1
(Scale 1 : 5000)

A	Solid Geology
B	Physiography
C	Distribution of coarse lag
D	Distribution of very fine lag
E	Distribution of the coarse fraction of the fine lag
F	Distribution of the Khaki lag
G	Location of sampling of surficial materials

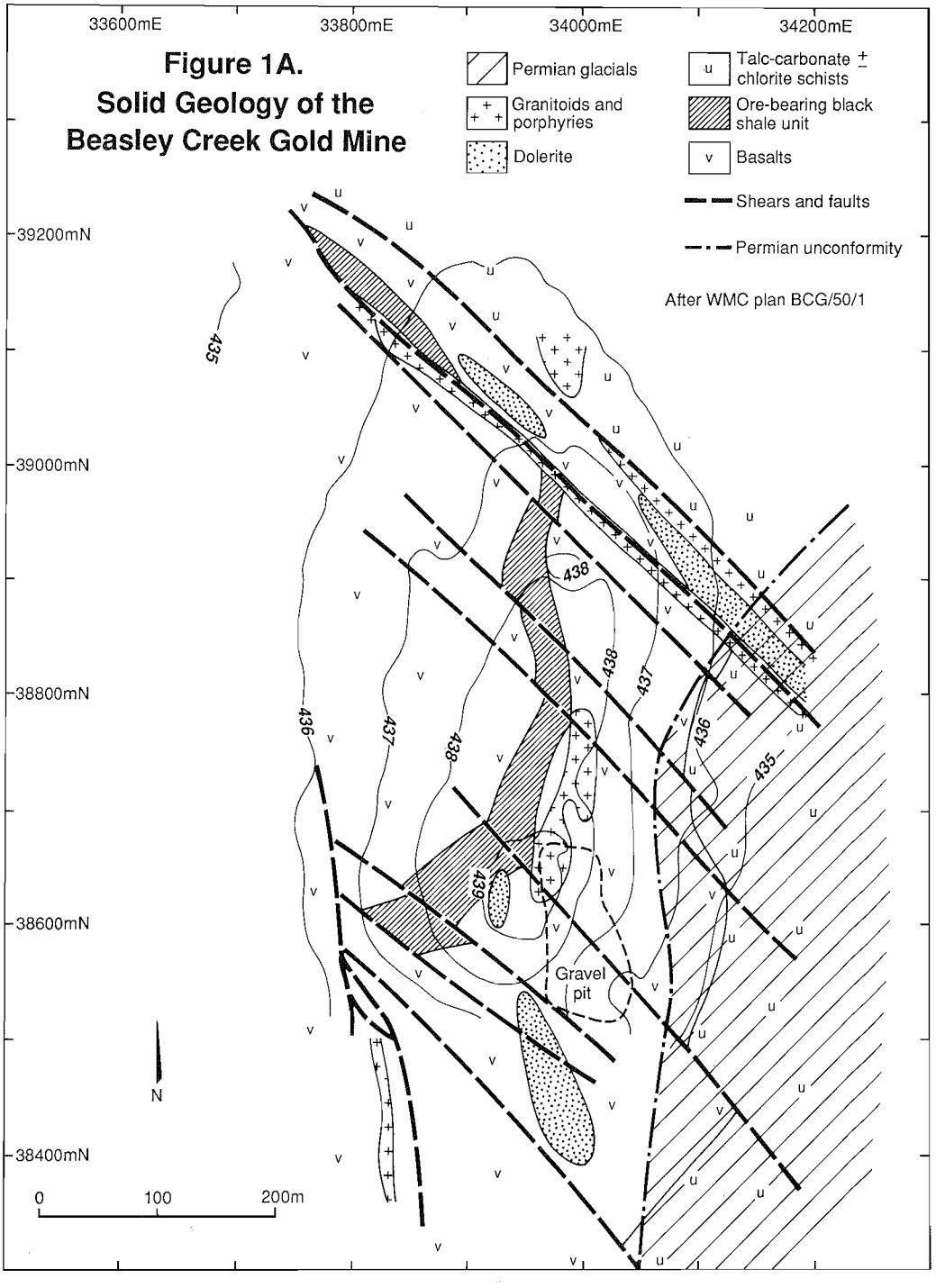
33600mE
33800mE
34000mE
34200mE
Figure 1A.
Solid Geology of the
Beasley Creek Gold Mine
Permian glacials
Granitoids and porphyries
Dolerite
Talc-carbonate ± chlorite schists
Ore-bearing black shale unit
Basalts
Shears and faults
Permian unconformity
After WMC plan BCG/50/1
39200mN
39000mN
38800mN
38600mN
38400mN
435
436
437
438
439
Gravel pit
N
0
100
200m

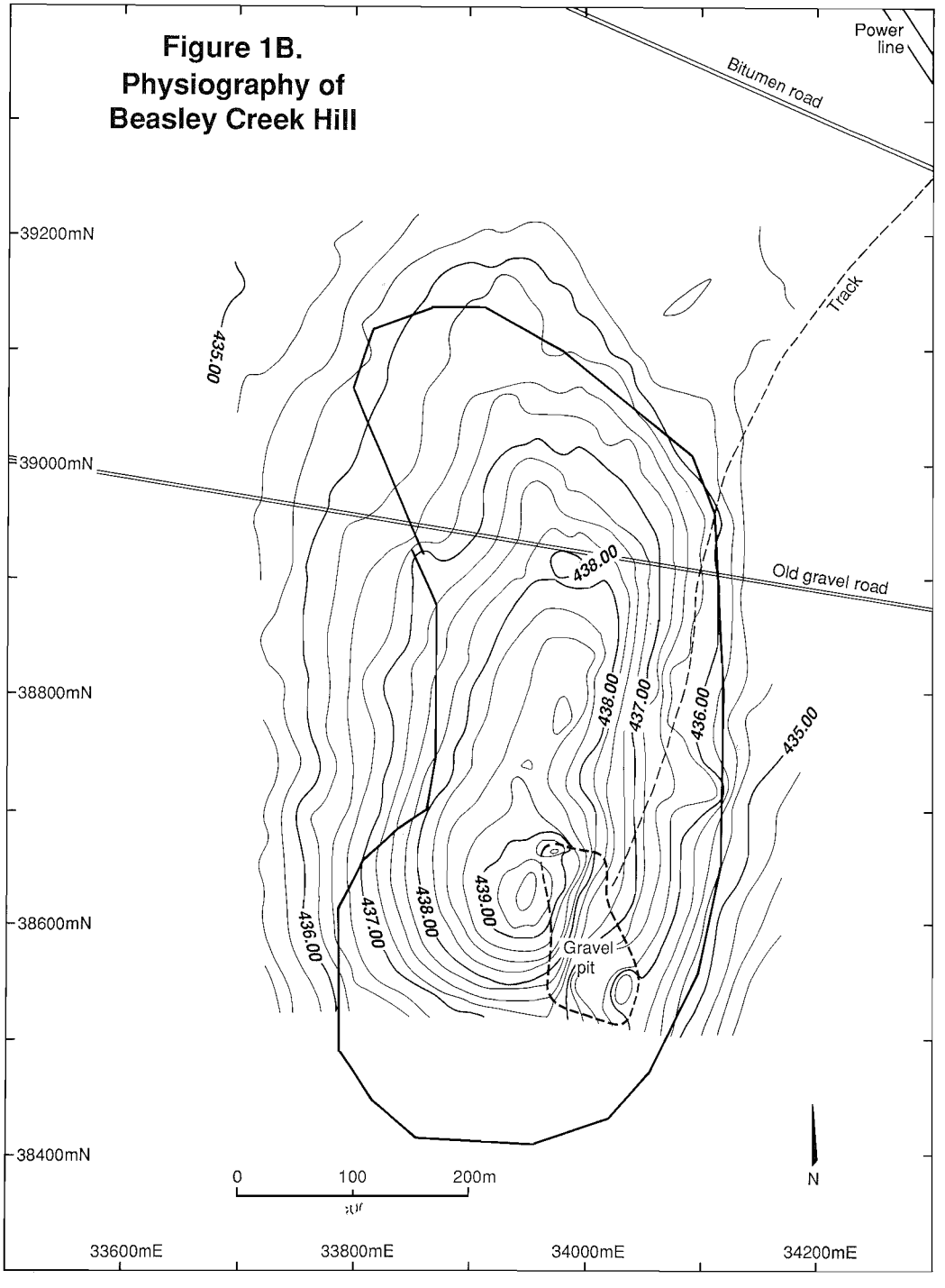
Figure 1B.
Physiography of
Beasley Creek Hill
Power line
Bitumen road
Track
Old gravel road
Gravel pit
435.00
436.00
437.00
438.00
439.00
0
100
200m
N
39200mN
39000mN
38800mN
38600mN
38400mN
33600mE
33800mE
34000mE
34200mE

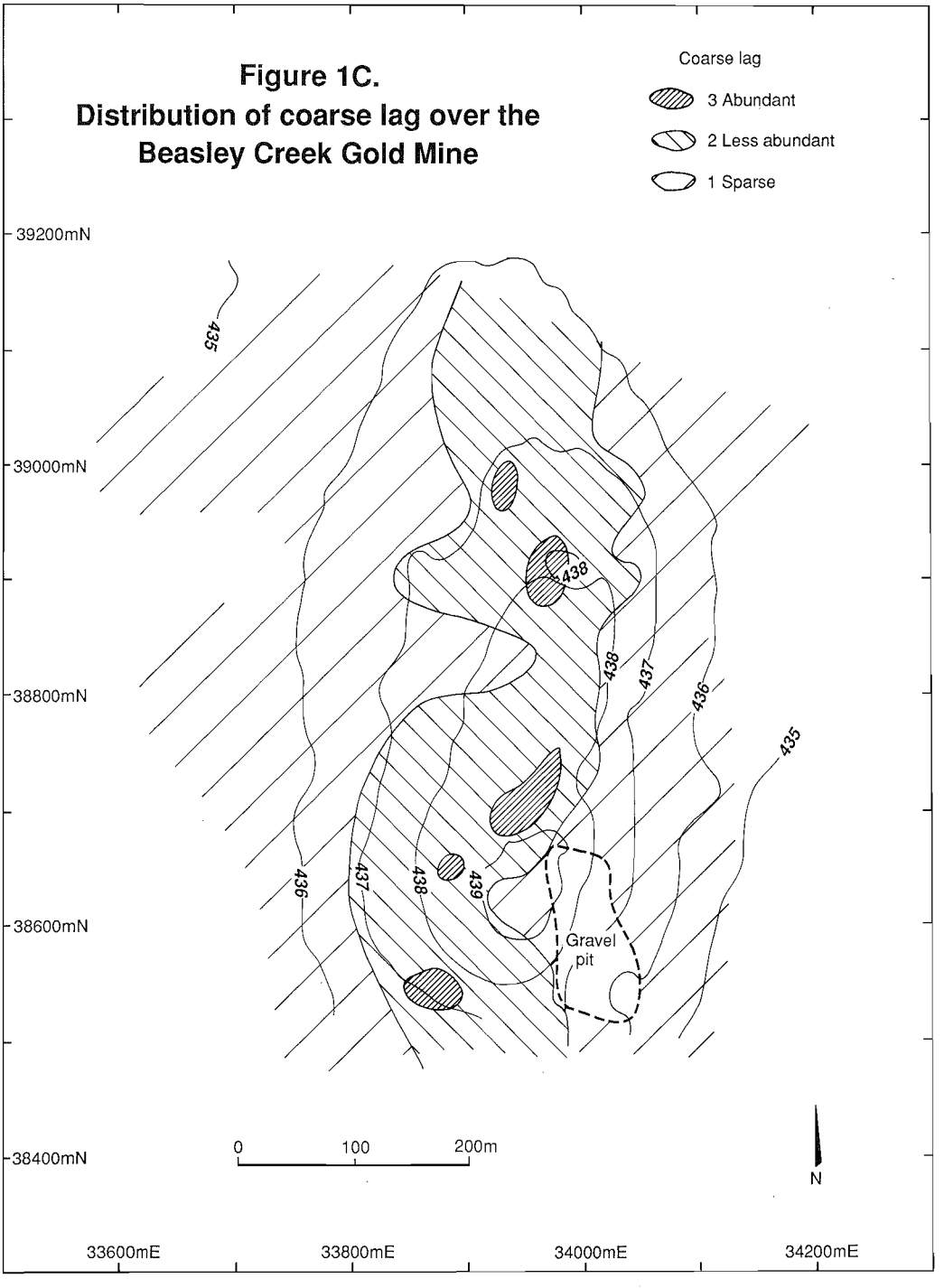
Figure 1C.
Distribution of coarse lag over the
Beasley Creek Gold Mine
Coarse lag
3 Abundant
2 Less abundant
1 Sparse
39200mN
39000mN
38800mN
38600mN
38400mN
435
436
437
438
439
Gravel
pit
0
100
200m
N
33600mE
33800mE
34000mE
34200mE

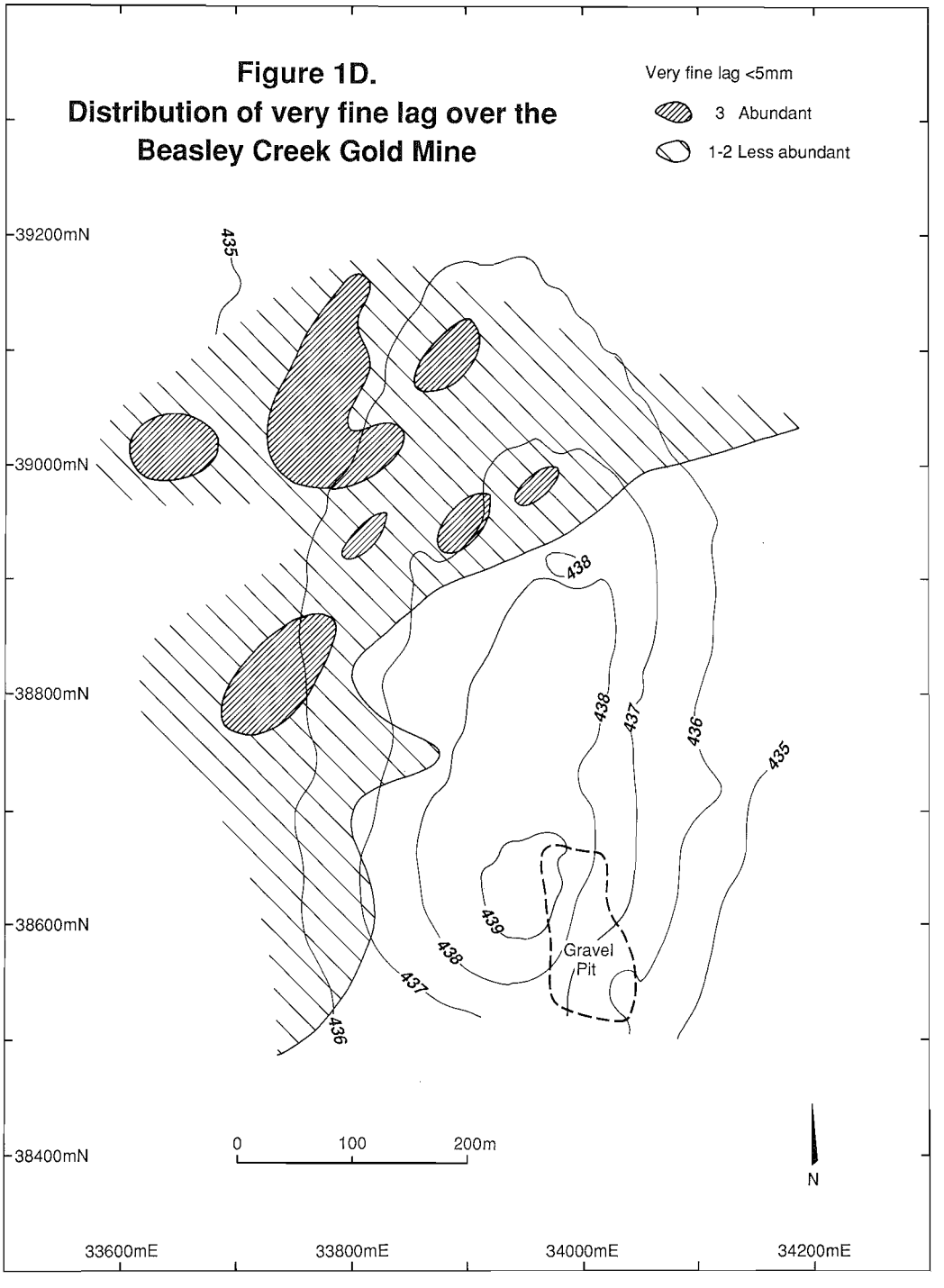
Figure 1D.
Distribution of very fine lag over the Beasley Creek Gold Mine
Very fine lag <5mm
3 Abundant
1-2 Less abundant
39200mN
39000mN
38800mN
38600mN
38400mN
435
438
438
437
436
435
439
438
437
436
Gravel Pit
0
100
200m
N
33600mE
33800mE
34000mE
34200mE

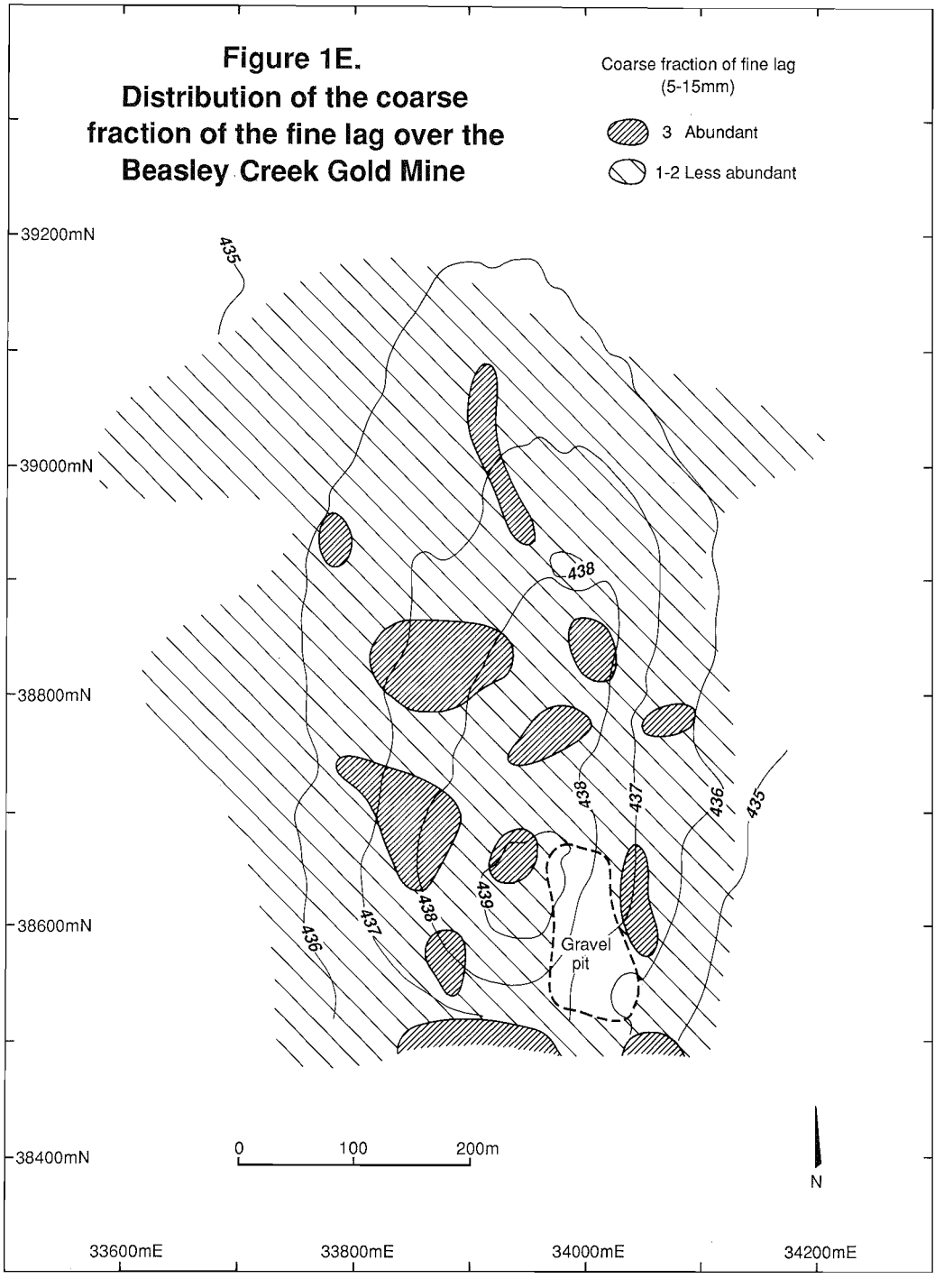
Figure 1E.
Distribution of the coarse fraction of the fine lag over the Beasley Creek Gold Mine
Coarse fraction of fine lag (5-15mm)
3 Abundant
1-2 Less abundant
39200mN
39000mN
38800mN
38600mN
38400mN
435
438
438
437
436
435
439
438
437
436
Gravel pit
0
100
200m
N
33600mE
33800mE
34000mE
34200mE

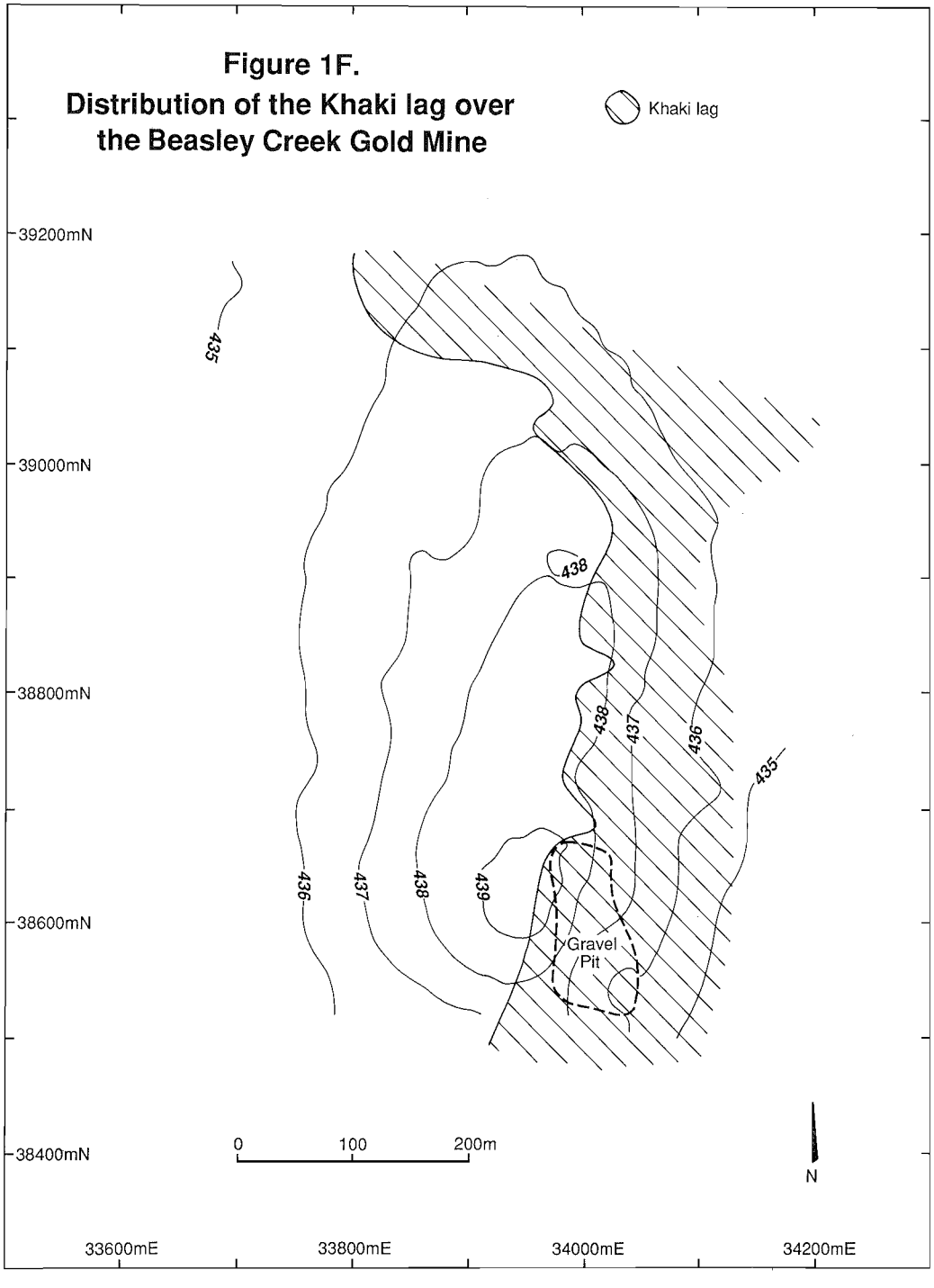
Figure 1F.
Distribution of the Khaki lag over the Beasley Creek Gold Mine
Khaki lag
39200mN
39000mN
38800mN
38600mN
38400mN
435
438
438
437
436
435
436
437
438
439
Gravel Pit
0
100
200m
N
33600mE
33800mE
34000mE
34200mE

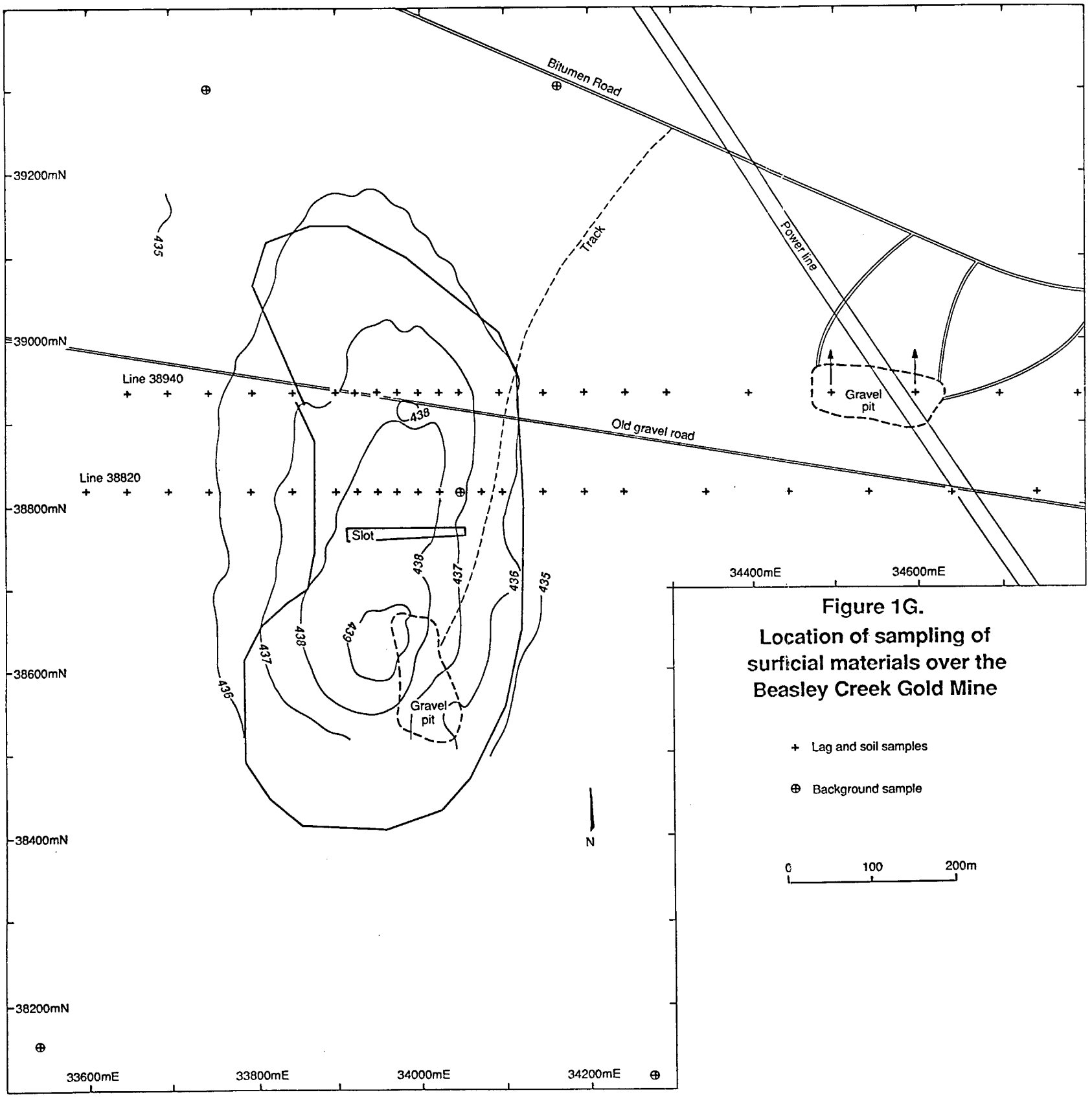

Figure 1G.
Location of sampling of surficial materials over the Beasley Creek Gold Mine

The regolith is overlain by a few tens of millimetres of colluvial soil. Mechanical analysis shows that the soil contains a wide range of size fractions. The finest is a clay (<5 μm, 2 - 5 wt %) with a larger proportion of fines (5 - 75 μm, 10%). The intermediate fraction (75 - 710 μm) consists of a large proportion of wind-blown sand. The coarse fraction (>710 μm) is largely ferruginous granules* and pebbles (defined by Anand *et al.* (1989) as LG201 and LG 203). Deflation of the soil, by wind and water, has left a lag of these granules and pebbles as a desert armour.

2.3 Geomorphology and Physiography

The geomorphology and surface geology of the orientation area were described by Robertson and Churchward (1989). The Beasley Creek Mine site is on a low hill, flanked by wash plains consisting of low broad rises or Wanderrie banks, and intervening flats. This tract of Wanderrie country forms a low tabular divide above broad drainage floors, in which the channels of ephemeral streams are incised.

A detailed contour map (0.25 m contour interval) was produced by Robertson and Churchward (1989) from WMC natural surface survey data. This is included (Figure 1B) to illustrate the physiography and to assist interpretation of lag dispersions. The hill at Beasley Creek is asymmetrical, with its steeper slope to the east. This steeper slope is preserved by an underlayer of hard lateritic duricrust and appears to be maintained by more active erosion at the foot of the hill, due to runoff from the gently undulating terrain to the east. The crest of the hill is partly protected by lateritic duricrust, calcrete and surficial ironstone. The phyllitic unit, which contains the orebody, follows the crest of the hill.

3.0 LAG GEOLOGY

The lag, or more specifically lag-gravel, forms a poorly-developed and uncemented desert armour over much of the surface underlain by mafic and ultramafic rocks near Laverton. It contains a variety of fragments, including ferruginous granules and pebbles and lesser amounts of ironstone, less abundant pieces of saprolite, lateritic duricrust and varying proportions of white vein quartz. The black ferruginous granules and pebbles are generally dominant and are mostly sub-rounded, though some are angular. A few adjacent fragments were found that could be fitted together and are thought to be the result of splitting by differential thermal expansion in the contrasting temperatures of day and night or summer sun and rain. Surface textures vary from glazed by desert varnish to mat or desert polished. Some show the classic dreikanter form (Holmes, 1944).

The lag forms a partial cover of residual stony fragments, from which the finer material is thought to have been removed by wind and water. Compacted or silica-indurated soil and less abundant patches of saprolite, calcrete, ironstone and lateritic duricrust show through this partial cover. The lag, together with the cover of mulga-eremophila scrub, performs a vital function in retarding soil erosion in this arid area (Figure 2A).

In general, the gold at Beasley Creek is related to zones of intense ferruginisation in the basement rocks, rather than to the occurrence of vein quartz. Ferruginous lag was considered to be a potentially useful geochemical sampling medium as it is almost ubiquitous at Beasley Creek. Key indicator-elements are readily adsorbed by goethite, which is its major component. It is also likely to have been derived from the underlying saprolite and lateritic duricrust and its high density would tend to retard

---

* The author regards the lower limit of 2 mm for the term granule and/or the lack of a term for smaller particles as restrictive. Similar particles extend into and possibly below sand sizes (<0.1 mm).

FIGURE 2

A. Typical scene on lower north-west flanks of the hill and onto the flats, showing Wanderrie Country, a sparse strew of lag, bare soil, grass tufts and mulga eremophila scrub.

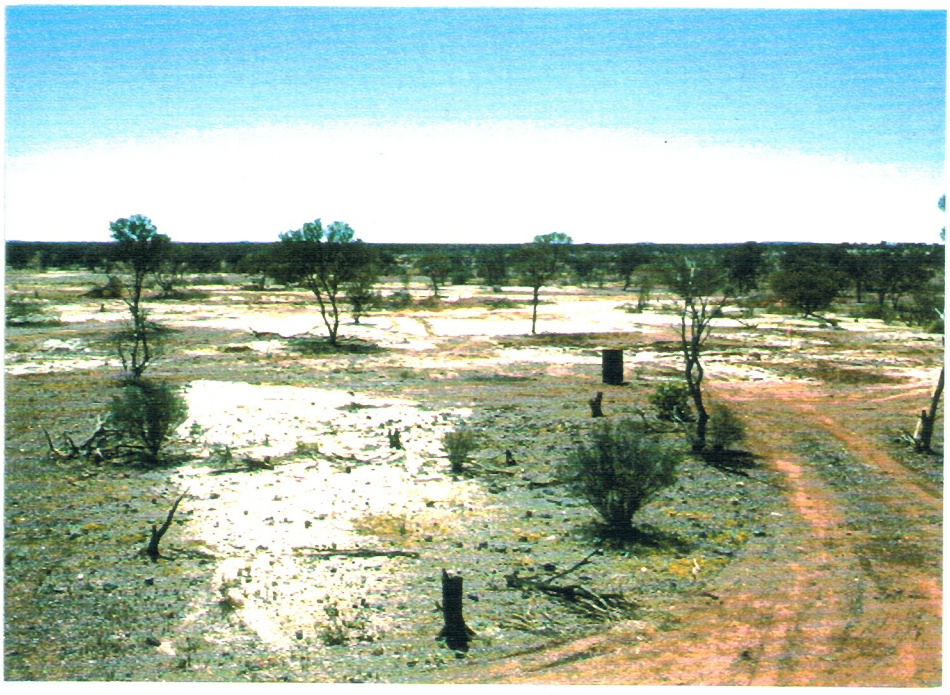

B Coarse black lag and ironstone lag strewn over the surface, underlain by the central part of the orebody. Note contamination of the surface by percussion drilling and vehicle tracks. Careful selection of sampling sites was, therefore, essential.

FIGURE 3

A Abundant very fine, brown, ferruginous lag (3), scarce, brown coarse lag (1) and moderately abundant, white quartz lag (3) strewn over compacted soil (north-east flank of hill).

B. Abundant, black coarse fraction of fine lag, some coarse, black, ferruginous lag, white quartz lag and cavernous ironstone lag, masking soil (overlying the central part of the orebody).

C. Khaki lag, partly set in soil, overlying the lateritic duricrust to the east of the orebody (approx 34050E, 38750N).

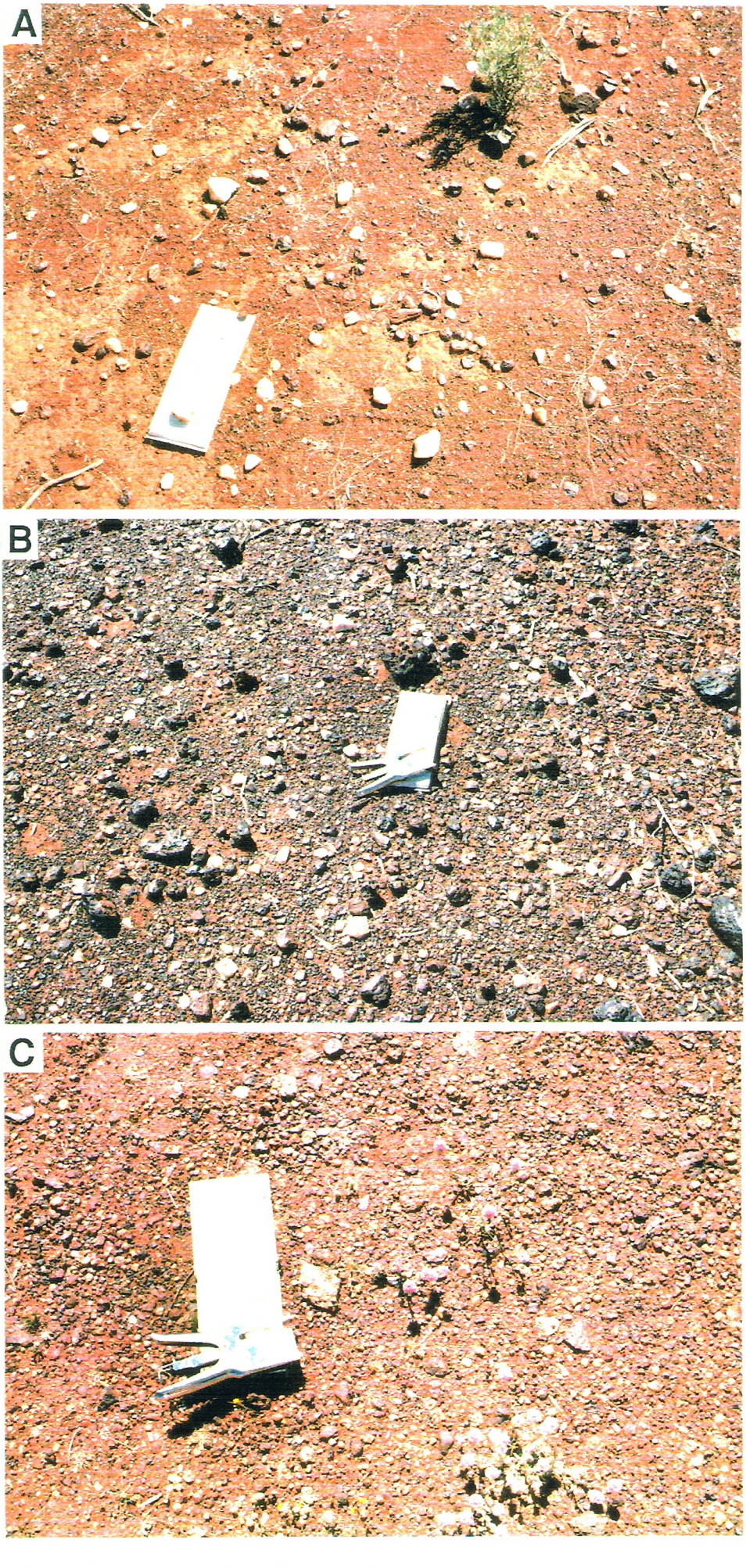
A
B
C

dispersion by wind or water. Lag geochemical surveys have been used extensively by WMC (Carver *et al.*, 1987) and this technique contributed to the discovery of Beasley Creek.

The size distribution of the lag is variable. In places the distribution is bimodal, showing distinct fine and coarse fractions (Figure 3), with one size fraction tending to dominate. The very fine subfraction of the fine lag is defined as having a size of generally <5 mm, the coarser subfraction of the fine lag ranges from 5 - 15 mm and coarse lag is >15 mm in size. In other places, the lag has a more continuous size-distribution and these size-fractions have a lesser use and validity. Both fine lag subfractions tend to be rounded to subrounded and the coarse lag subrounded to subangular. While, at first sight, these lag types seem to be quite distinct, they are generally intimately mixed.

3.1 Fine Lag (0.2 - 15 mm)

The finest subfraction of this granular lag (<5 mm) occurs largely on the flats to the north-west and blankets the lower slopes of the north-west and west of the hill (Figure 1D, 2A, 3A), where its abundance appears to be largely random. Elsewhere the very fine lag grades into the coarser, pebbly fine lag subfraction (5 - 15 mm) and this coarser subfraction is dominant (Figure 3B). This coarse subfraction of the fine lag is almost ubiquitous and its abundance does not seem to be linked to any underlying geological feature. The areas of its higher abundance seem to be centred on the hill in a general way (Figure 1E) and it seems to give way to the very fine lag subfraction in the north-west. Both fine lag subfractions are brown.

3.2 Coarse Lag (>10 mm)

The coarse pebbly fraction is relatively ubiquitous (Figure 1C) but it is best developed and is comparatively coarse near the crest of the hill. This lag is generally darker, often black to blue-black (Figure 3B). Fragments exceeding 50 mm (cobbles) are not uncommon and fragments of ironstone abound in places.

3.3 Khaki Lag

The slope to the east of the orebody, underlain by lateritic duricrust, is partly covered by a lag containing two and, in places, three components. The ubiquitous black to dark brown nodular material is generally dominant but this is accompanied by a lesser amount of yellow-brown to khaki coloured lag and in places by small amounts of a red-brown lag (Figure 3C). The last two lag types may be found attached in the same fragment. They appear to be derived from the underlying lateritic duricrust and may be classified as hardened mottles (LG105; Anand *et al.*, 1989), though some are pisoliths. Both the coarse and the fine lag fractions show these varieties but pisoliths and ooliths are more abundant in the fine lag. Varieties range from nodular hardened mottles, through pisoliths with nodular excrecences to true pisoliths.

4.0 STUDY METHODS

4.1 Mapping of Lag

The distribution of surficial materials was mapped by Robertson and Churchward (1989) before mining commenced. The comparatively scarce, larger outcrops of ironstone and calcrete, were mapped by conventional means at a scale of 1:1000. The various surface-lag types are inextricably mixed but their

distribution is nevertheless important. A visual impression of the relative abundance of these materials, on a scale of 1 to 3, was recorded at locatable points on the mine grid, compiled and rough contoured. Though the method is only semi-quantitative, the results show these distributions in a better than qualitative way. The relevant lag maps (coarse lag, fine and coarse fractions of the fine lag and khaki lag) are reproduced herein (Figures 1C-F).

4.2 Sample Site Selection

Two sample lines, separated by 120 m (Figure 1G), were selected, one which passes over the centre of the orebody (38820 N) and another which passes over its north end (38940 N). The lag samples were taken at 50-m intervals, where distant from the orebody, and at 25-m intervals over the orebody. As extensive drilling had been carried out and there was some disturbance to the natural surface by vehicle tracks, drill sumps, etc. (Figure 2B), care was taken in selecting undisturbed and uncontaminated sample sites. Where lag was scarce or where the sample site was disturbed or contaminated, the area of search was expanded up to 5 m along the sample line and up to 10 m across the line (along strike) in order to collect an adequate and clean sample.

Background sample sites were selected remote from the orebody, two to the north and two to the south. Their locations are shown on Figure 1G. When preliminary analytical results for Au became available for the two lag traverses, it was clear that background levels had not been reached laterally from the orebody. The lag sampling was extended, during August 1988, to the east, for 500 m on each line, to reach background. Here samples were collected at 100-m intervals. It was not possible to extend to the west, as mining had commenced and this area was occupied by the waste dump.

4.3 Sample Collection

The coarse lag samples were collected by hand (size 10 - 50 mm) until some 500 - 1000 g were bagged. Only dark, dense, shiny lag particles were collected, quartz as well as fragments of calcrete and saprolite were discarded. Where the yellow-brown to red-brown, nodular, khaki lag occurred in sufficient quantity, typically to the east of the orebody subcrop, it was sampled separately.

The fine lag samples were swept into a plastic dustpan, with a nylon bristled brush, from several randomly selected locations, covering a similar area to that used for the coarse lag sampling. The fine lag sample inevitably contained some organic litter, soil and sand. Some of this was winnowed out in the field, to reduce the sample size, and the remaining sample (1000 - 1500 g) bagged.

4.4 Preparation of Coarse Lag

The coarse lag samples were washed with tap-water on a 4-mm plastic sieve, to remove any dust or organic debris, and dried at $<50°$ C. Washing was essential in view of the extensive percussion drilling that had been carried out in the area (Figure 2B). A small, representative subsample was selected by hand for reference, and later petrographic examination, and the remainder jaw crushed to a nominal <12 mm. A 100 - 150-g aliquot was riffle split from the jaw crushed material and pulped to a nominal $<75\ \mu$m in a case hardened steel mill (Robertson and Crabb, 1988), using a double sand clean and alcohol wipe of the mill components between samples.

4.5 Preparation of Fine Lag

The fine lag samples were wet sieved to 0.2 - 4.0 mm in tap-water. Organic trash, sand and clay particles, adhering to the polished surfaces of the lag, were removed by agitation during sieving. The lag was dried at $<50°$ C. The result was a very clean product which was riffle split into three parts. One part was retained as a reference sample, one was pulped to $<75\,\mu$m for analysis of the whole fine lag and the third part was separated, using a Sepor Automagnet, into magnetic and non-magnetic components, which were each weighed and pulped to $<75\,\mu$m for analysis.

4.6 XRD Analysis

Each analysed coarse lag pulp was mineralogically examined semi-quantitatively by X-ray powder diffractometry, using LiF diffracted beam monochromated Cu Kα radiation at Floreat Park on a Sietronics automated Philips PW1050 diffractometer. Each sample was scanned over the range 5 - 65° 2θ, at a speed of 1° /min and data were collected at 0.02° 2θ intervals. The data were displayed and interpreted using Sietronics software.

4.6.1 Semi-quantitative estimation of mineral abundances

Semi-quantitative major mineral abundances were estimated using the height above background of a selected X-ray diffraction (XRD) peak for each mineral (Table 1). The peaks were chosen so as to avoid overlap by peaks of other minerals. The results are shown on Table 4 and graphed in Figure 10. It must be emphasised that these results are approximate and are influenced by the degree of crystallinity and mineral alignment as well as by abundance. They give a rough comparison of the relative abundances of *particular* minerals *between* samples; they do not indicate the relative abundances of the different minerals in each sample.

TABLE 1
DIFFRACTION PEAKS USED FOR
SEMI-QUANTITATIVE MINERALOGY

Mineral	Diffraction peak (hkl)	d-Spacing (Å)
Quartz	101	3.343
Goethite	111	2.450
Hematite	024	1.838
Kaolinite	100	7.10
Mica	001	10.0

4.6.2 Estimation of Al substitution in goethite and hematite

The goethite and, to a lesser extent, the hematite XRD peaks show a slight displacement, indicating some Al substitution for Fe. The extent of this substitution in both goethite and hematite was estimated by measuring the d[110] and d[111] for goethite and d[110] for hematite (Schulze, 1984). Shifts in these reflections, due to Al substitution, are small, and must be measured accurately. Study of

a quartz standard, using $Pb(NO_3)_2$, indicated that sample position error in the goniometer is significant but variable at 4 Å. It is negligible at 1 Å and that the error has a roughly linear distribution with d. The d[101] reflection of quartz, which occurs naturally in most samples, was used as an internal standard, measurement errors of the positions of the peaks were estimated and the positions of the diffraction peaks corrected. A synthetic internal standard would have improved confidence but this would have interfered with the semi-quantitative mineralogical investigation. Table 4 shows good correlation between the d[111] and the combined d[110] and d[111] methods for determining Al substitution in goethite. Though the data are satisfactory, they must be regarded as indicating trends rather than being correct in an absolute sense.

4.7 Microprobe Analysis

XRD investigation of Al substitution in goethite and hematite was carried out on the pulverised bulk sample, so it produces an "average" result. Mineral phases in known petrographic relationships needed major and minor element microprobe analysis. This analysis was a preliminary study both as a guide for further work and to develop the analytical schemes for a more detailed study.

Micas and specific goethite phases of three specimens were examined. This was to confirm the petrographic mineral determinations, to investigate briefly Al substitution in the goethites, the extent of dehydration of goethite to hematite, the stochiometry of the micas and the distribution of the more abundant key anomalous elements in the iron phases. The Cameca SX-50 microprobe at Floreat Park was used. The goethites were examined using a 100-nA beam, an accelerating voltage of 25 kV and a magnetite reference standard. A suite of minor elements was determined including As, Ba, Sr, Cu, Cr and Zn. Major elements in the mica relics were determined using a phlogopite reference standard, an accelerating voltage of 15 kV, and a beam current of 25 nA. In all 60 analyses were performed, exclusive of standards. Microprobe analysis was performed under the control of the WANU-SX geo-analytical package.

The mineral phases produced by weathering are very fine-grained and tend to be mixtures, even at the sub-micron scale. The area of emission of secondary X-rays produced, even by a finely focussed electron beam, is of the order of 2 μm in diameter, so it is inevitable that microprobe analysis of weathering minerals will be of mineral mixtures. Thus it was necessary to make numerous analyses to determine trends (see Section 7.2).

4.8 Geochemical Analysis, Sequencing and Standards

Detection limits and methods used for the analysis of each element are given in Table 2. Neutron activation analysis was by Becquerel Laboratories on 30-g aliquots. Minor and trace elements were determined on pressed discs, using a Philips PW1220C XRF at Floreat Park, by the methods of Norrish and Chappell (1977) and Hart (1989). Some particularly, low level elements were determined by long count XRF. Iron was determined on pressed disc, for matrix correction, and these approximate results are included. Major elements and some minor elements were also determined at Floreat Park by ICP analysis on a Hilger E-100, after Li-metaborate fusion. The INAA gold analyses were checked by AAS and Carbon Rod AAS analysis after cyanide and organic extraction and very good correlations were obtained. The geochemical data are tabulated in Appendices 1 and 2, displayed graphically in Appendix 3 and shown as frequency distribution plots in Appendix 4. Correlation matrices are given in Appendix 6 and r values of $> \pm 0.3$ are significant (95% confidence). A geochemical data disc, which includes all information given in Appendices 1 and 2, is included as Appendix 8.

The samples were analysed in random order and an in-house weathered rock standard (STD 9) was introduced into the analytical batches at a ratio of 1 : 10 to 1 : 15, to monitor both accuracy and precision. The performance of the analytical method in relation to this standard, together with its mean value, 95% confidence statistic and the currently accepted values for this standard are reported in Appendices 1 and 2. In general the results are satisfactory, though the values for Fe appear to be low (both ICP and XRF) and the ICP analyses show a poor precision compared to the INAA and XRF analyses. This is reflected in the geochemical profiles, where ICP data show a higher noise level.

It is interesting to note that STD 9, which is a fine lag, was collected from the Beasley Creek area, about 50 m north-west of the road bridge over Beasley Creek, so it is particularly relevant as a standard. It should not be construed as a background sample, as it is clearly anomalous in a number of elements, but this does not detract from its value as a standard.

Values below the detection limits have been reported without censorship, to make the graphs more natural and to aid mathematical treatment. It must be emphasised that values in this range are of suspect precision, are estimates and should be interpreted with caution. Reference should be made to Table 2 for the detection limits.

TABLE 2

TRACE ELEMENT
DETECTION LIMITS AND METHODS

Element	Det. Limit (ppm)	Method
Ag	5	XRF
As	2	INAA
Au	0.005	INAA
Ba	15, 100	XRF, ICP
Be	5	ICP
Bi	2	XRF (lc x 7)
Cd	2	XRF (lc x 7)
Ce	2	INAA
Co	1	INAA
Cr	5	INAA
Cu	5, 100	XRF, ICP
Ga	5	XRF
Ge	3	XRF
In	2	XRF (lc x 7)
La	0.5	INAA
Mn	20, 100	XRF, ICP
Mo	5	INAA
Nb	5	XRF
Ni	10, 50	XRF, ICP
Pb	5	XRF
Rb	5	XRF
Sb	0.2	INAA
Se	2	XRF (lc x 5)
Sn	2	XRF (lc x 7)
Sr	3	XRF
V	10, 100	XRF, ICP
W	5	INAA
Y	3	XRF
Zn	5	XRF
Zr	4, 100	XRF, ICP

INAA - Instrumental Neutron Activation Analysis - Becquerel Laboratories
XRF - X-ray Fluorescence Analysis - CSIRO, Floreat Park
ICP - Inductively Coupled Plasma Spectrophotometry - CSIRO, Floreat Park
lc - Long counting technique

FIGURE 4

SURFACE DETAIL OF COARSE AND FINE LAGS

Coarse Lag

A. Sample 08-090: Very dark brown lag pebbles, from very near the orebody: Co-ordinates 33950E 38820N. Sample 08-437: Deep red-brown lag pebbles some 600 m distant from the orebody: Co-ordinates 34600E 38940N. The lag pebbles from near the orebody have a slightly more porous fabric and are darker.

B. Sample 08-120. 'Regional background' black lag pebbles. Co-ordinates 34290E 38110N. Sample 08-131. Khaki lag pebbles from a point overlying the lateritic duricrust. Co-ordinates 34050E 38940N. Note the slightly dull appearance of the black 'background' lag pebbles, compared to that from near the ore in A (Specimen 08-090).

Fine Lag

C. Six components of the fine lag. 1. Red-brown, well rounded, clay-rich granules, probably related to the lateritic duricrust. 2. Yellow-brown, nodular lag granules, also related to the lateritic duricrust. 3. Rounded, porous granules of calcrete dotted with lag micro-pisoliths. 4. Various types of quartz granule, varying from white, through yellow to brown and iron-stained; also a small cluster of small quartz crystals. 5. Angular, cellular, gossanous granules which are rich in Mn. 6. Shiny, black, in part magnetic granules. These are the most common. Types 1,2 and 6 are major components in all lags; the others are generally scarse. These materials were hand-picked from Sample 08-217.

D. A comparison of a polished section of fine, ferruginous granular lag from over the orebody (Sample 08-216) with a more quartz-rich lag (Sample 08-453) from 650 m to the east of the orebody.

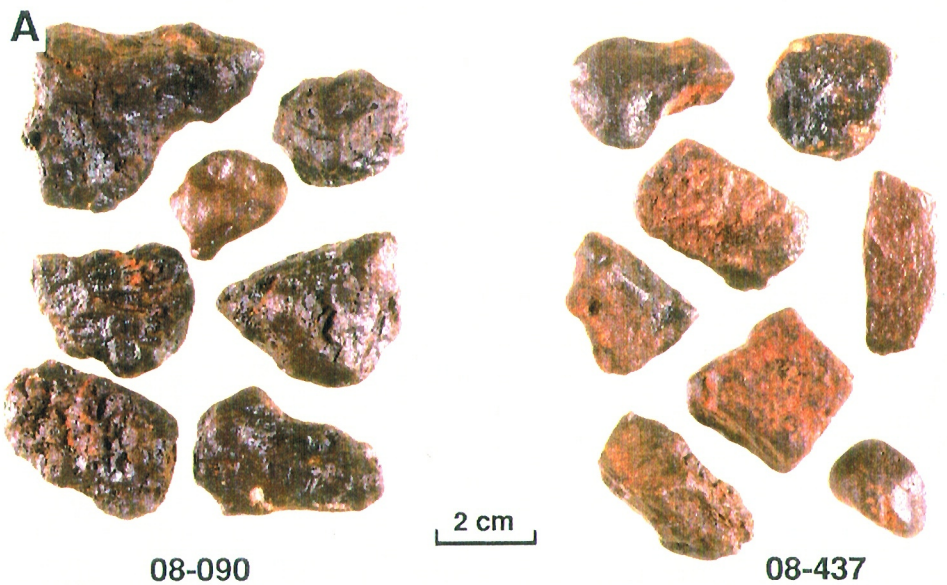
A
2 cm
08-090
08-437

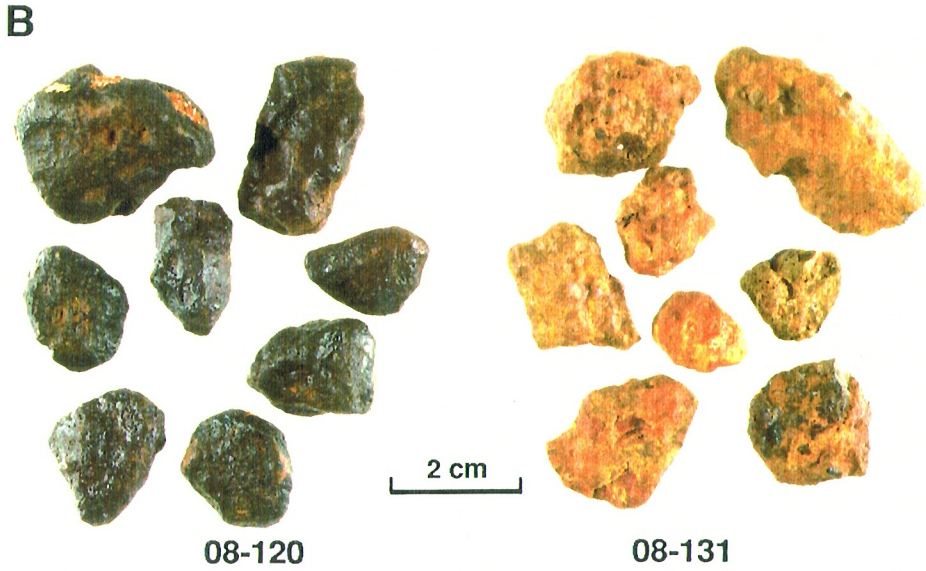
B
2 cm
08-120
08-131

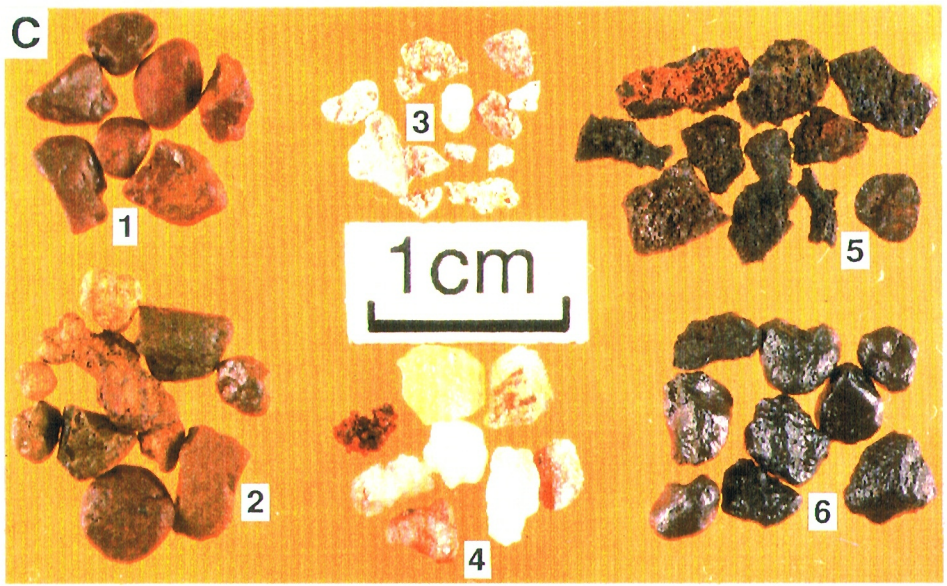
C
1
2
3
4
1cm
5
6

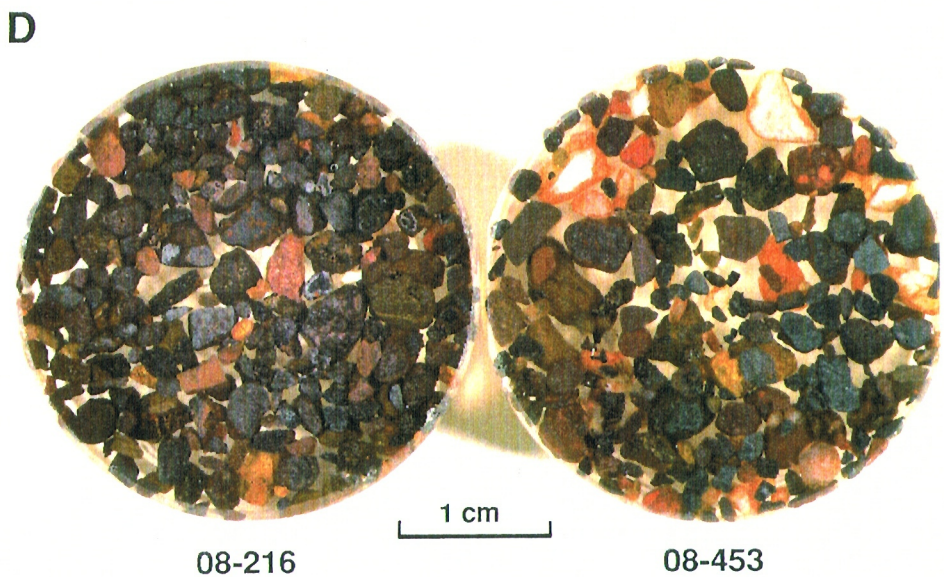
D
1 cm
08-216
08-453

4.9 Petrography

The polished sections, which are inexpensively and rapidly produced, were examined first under oblique reflected light with a binocular microscope and then under normally reflected light on a petrographic photomicroscope. Information gathered by both methods, one showing colour and fabric and the other detailed mineralogy and fabric, are complimentary. Density was measured by pycnometer.

Qualitative energy dispersive X-ray analysis of materials in the polished sections was carried out using a JEOL Geo SEM 1, to aid mineral identification where necessary. The results of such analyses are shown in the text so as to indicate approximate relative proportions, e.g. Fe>>Si=Al.

5.0 MORPHOLOGY AND COMPONENTS

This study provided a good opportunity to observe subtle variations in the appearance of the lag both near and distant from a known orebody. The external appearances of both the coarse and fine lag fractions are attributes that can be readily recorded in the field with the aid of a hand lens. Magnetic separation of this partly magnetic material is an obvious method of beneficiation of the sample and yields a more consistent product. An objective of this study is to determine if magnetic separation could improve the geochemical signal.

5.1 Coarse Lag

The external appearance of the coarse lag pebbles is very consistent, as they were selected by hand. They vary from subrounded to subangular. Some show a slight lamination, many are porous and most show a nodular form. Lag overlying the orebody is a very deep brown, in weak contrast to lag from the flats to the east of the orebody, which is a very slightly paler brown (Figure 4A). Lag from the regional background suite is dull and black (Figure 4B) and shows a higher proportion of laminated fragments. These differences are subtle. The khaki lag is yellow brown to red-brown (Figure 4B) and shows a marked nodular, and in places even a pisolitic, appearance. In contrast, cut surfaces of the lag show a wide variety of colours and fabrics and this is covered in Section 6.0.

5.2 Fine Lag

The fine lag is less consistent (see Frontispiece), as the samples were swept up from the surface and sizing was the only criterion. Its major components are red-brown, yellow-brown and shiny, black granules (Figure 4C). The red-brown and yellow to yellow-brown granules are subrounded and nodular in appearance. They are clay-rich, non-magnetic and are thought to be related to the duricrust. The black, glossy, goethite-rich, in part magnetic granules are similar to, but smaller than, the ferruginous, coarse lag fragments. Minor components are quartz, calcrete and ironstone. Also included in the lag, but having little geochemical input, are rare organic debris and small clusters of wind-blown quartz sand, bound by a lacey, siliceous cement (hardpan).

The quartz varies from being a minor to a trace component. It is diverse in appearance, from well-rounded grains, through glassy fragments, iron-stained fragments, white or yellowish opaque subangular shards of vein quartz and even small crystals (Figure 4C). It is particularly abundant in the lag on the flats (Figure 4D) to the east of the orebody. It forms only a trace component or is absent over the lateritic duricrust, where yellow-brown and red-brown, clay-rich fragments dominate the black, ferruginous fragments.

TABLE 3
RELATIVE ABUNDANCES OF FINE LAG COMPONENTS

Line 38820 N

Sample No	East (m)	Quartz	Iron-stone	Cal-crete	Au ppb	Mn ppm	Magnetic % Total
08-190	33600	M	-	-	5.3	363	16.4
08-191	33650	M	tr	tr	8.8	344	23.2
08-192	33700	M	-	-	12.5	314	23.2
08-193	33750	M	-	tr	66.8	340	26.7
08-194	33800	M	-	tr	6.3	367	32.4
08-195	33850	M	str	tr	81.3	384	36.3
08-196	33900	M	str	tr	93.9	396	38.0
08-197	33925	M	str	tr	2.1	389	34.9
08-198	33950	M	str	-	12.0	591	33.5
08-199	33975	M	-	-	66.4	1357	31.5
08-200	34000	M	tr	tr	77.1	1785	31.2
08-201	34025	tr	M	-	52.5	2374	19.4
08-202	34050	tr	-	-	146.3	966	34.5
08-203	34075	tr	tr	-	149.7	767	39.8
08-204	34100	tr	tr	-	342.0	817	30.7
08-205	34150	tr	-	-	160.7	915	24.1
08-206	34200	tr	-	-	618.6	959	21.1
08-207	34250	tr	-	-	244.0	995	17.3
08-450	34350	M	-	-	128.9	618	10.9
08-451	34450	M	-	-	11.5	472	13.2
08-452	34550	M	-	-	34.8	475	14.2
08-453	34650	M	-	-	5.1	401	17.9
08-454	34750	M	-	-	5.3	367	17.5

X Major Component
M Minor Component
str Significant trace
tr Trace
- None

Line 38940 N

Sample No	East (m)	Quartz	Iron-stone	Cal-crete	Au ppb	Mn ppm	Magnetic % Total
08-208	33650	M	tr	-	8.0	313	26.5
08-209	33700	M	-	-	7.3	312	20.3
08-210	33750	M	tr	tr	13.7	313	22.5
08-211	33800	M	tr	tr	6.1	344	26.6
08-212	33850	tr	str	tr	31.7	402	27.2
08-213	33900	M	str	tr	7.1	568	22.1
08-214	33925	M	str	-	15.5	877	22.7
08-215	33950	M	str	tr	886.5	826	27.6
08-216	33975	M	M	tr	85.8	1138	23.9
08-217	34000	M	M	str	288.2	895	9.4
08-218	34025	M	M	tr	117.1	723	12.3
08-219	34050	tr	str	-	217.3	795	16.2
08-220	34100	tr	tr	-	314.2	558	14.7
08-221	34150	tr	-	-	371.5	561	17.0
08-222	34200	-	-	-	260.2	650	17.5
08-223	34250	tr	-	-	45.2	614	19.8
08-224	34300	M	tr	-	43.6	540	15.0
08-445	34400	M	tr	-	15.4	407	21.0
08-446	34500	M	-	-	5.5	395	15.3
08-447	34600	M	-	-	8.1	358	26.6
08-449	34800	M	-	-	5.5	301	15.5

BACKGROUND DATA

Sample No	East (m)	Quartz	Iron-stone	Cal-crete	Au ppb	Mn ppm	Magnetic % Total
08 - 225	33747	M	-	-	5.9	318	21.4
08 - 226	34172	M	-	-	7.0	333	20.0
08 - 227	33545	M	-	-	2.0	361	12.4
08 - 228	34290	M	-	-	7.5	436	30.4

FIGURE 5

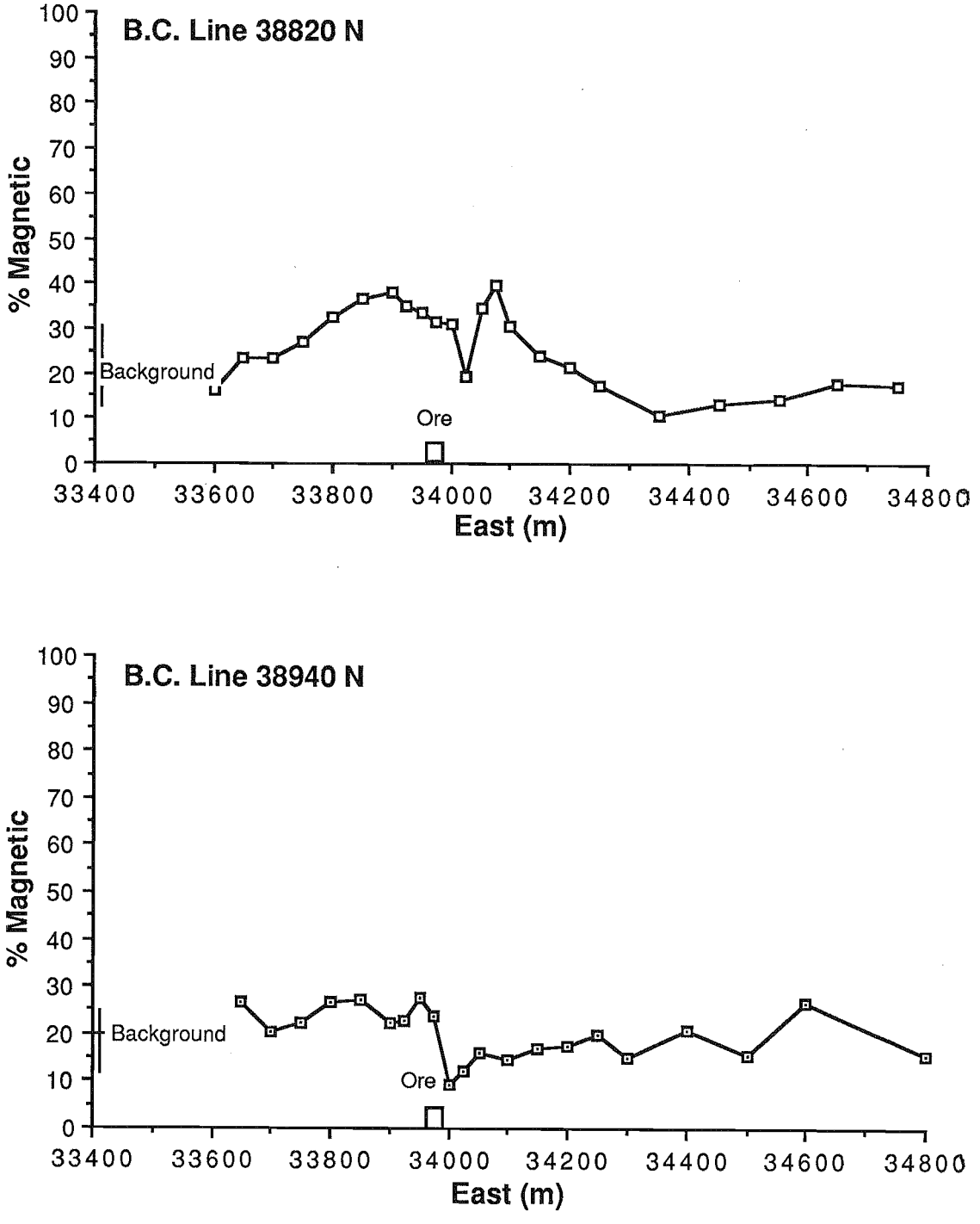

Proportion of Magnetic Component in Fine Lag

Calcrete varies from white to pink and is massive or cellular and contains minute inclusions of quartz and ferruginous lag (Figure 4C). Some grains are well rounded, others subrounded. The angular grains of generally non-magnetic ironstone have a cellular to granular appearance (Figure 4C) and they vary in colour from black and blue-black through mauve to brown. They are particularly abundant near the orebody, where they form a significant trace or even a minor component of the fine lag.

The distribution of these minor lag components is illustrated in Table 3. The calcrete fragments relate to nearby calcrete outcrops and subcrop (Robertson and Churchward, 1989: Figure 2J) and there is little significant mechanical dispersion (max. 100 m). The cellular ironstone component of the fine lag appears to depict the shale host to the orebody and some of the footwall rocks and its appearance correlates with high gold values and particularly well with high Mn (Table 3). This ironstone component is relatively non-magnetic and the Mn anomaly (see Section 8.0), associated with the orebody, is restricted to the non-magnetic component of the fine lag. The cellular ironstone component also shows limited dispersion (<150 m) down slope to the east over hangingwall rocks. The lack of dispersion of these two minor lag components, calcrete and ironstone, seems related to their fragility. The calcrete, cellular ironstone and red-brown clay components were separated and their geochemistry has been studied in detail (Appendix 7). The cellular ironstone appears to be a gossan.

5.3 Magnetic and Non-magnetic Components

The coarse lag pebbles are too large for effective magnetic separation. The magnetic and non-magnetic components of the fine lag were separated and each weighed (Section 4.0). Magnetic separation yields a small, very clean and consistent material, consisting of black, glossy granules. The larger, non-magnetic component contains a small proportion of similar granules, which are in many instances slightly magnetic but not sufficiently so to be removed by the Automagnet, together with granules of quartz, calcrete, ferruginous clay and ironstone.

The results of weighing these components are presented in Table 3 and the magnetic component is expressed as a percentage of the total. Graphs of these data (Figure 5) show that the fine lag has a larger proportion of its magnetic component over the orebody and to the west. There seems to be an inverse relationship between the proportion of magnetic to non-magnetic components and soil depth (see Robertson and Churchward, 1989; Figure 3), i.e., thin soils have a higher proportion of magnetic component in the overlying lag.

XRD has shown that the magnetic properties of the lag are caused by small quantities of maghemite in the black shiny granules. The exact site of this mineral awaits further and detailed examination. Maghemite has a spinel structure and is ferromagnetic. It may be produced either from supergene alteration of magnetite, which does not appear in the lag in any appreciable quantities, or by dehydration of lepidocrocite (γ.FeO.OH) to maghemite ($\gamma.Fe_2O_3$) (Deer, Howie and Zussman, 1967). The latter route seems most likely. This dehydration is paralleled by the dimorph of lepidocrocite, goethite (α.FeO.OH), which dehydrates to paramagnetic hematite ($\alpha.Fe_2O_3$). It seems feasible that lepidocrocite could be altered to maghemite in surface lag and lag enclosed in the soil, by heating from bush fires. A higher proportion of the lag enclosed in a thin soil would reach the dehydration temperature than that enclosed in a deeper soil. Alternatively the soils near the top of the hill would be better drained than those further down slope, so aiding dehydration.

A study of ferromagnetic materials in the lateritic duricrust has still to be carried out. The zone of intense, short wavelength, magnetic noise, found by WMC at Beasley Creek, seems associated with the lateritic duricrust to the east of the orebody and not with the higher proportion of magnetic lag component found over the orebody and to the west. It seems the contribution from the ferromagnetic component of the lateritic duricrust to the total magnetic field is far greater than that from the lag.

5.4 Density

The shiny black lag has an s.g. of about 3.97, i.e. between hematite (4.9 - 5.3) and goethite (3.3 - 3.5). The red-brown and yellow-brown, clay-rich component has an s.g. in the range 3.15 - 3.22, falling between goethite and kaolinite (2.6). The Mn-rich, cellular ironstone has an s.g. of 3.36.

5.5 Beneficiation of the Fine Lag

Improvement of the geochemical signal from a multi-component material, such as the fine lag, can be achieved by separation and analysis of the component providing the signal. It seems that the best geochemical signals are shown by the black lag, which may or may not be magnetic, and from the cellular ironstone which is generally non-magnetic. It seems likely that heavy medium beneficiation of the fine lag would remove the minor quartz and calcrete with little difficulty but this would add little improvement. Parting the goethite-rich, in part magnetic, lag from the remainder would be easy, as the s.g. contrast is significant, but the cellular ironstone is also an important component. Parting the abundant clay-rich lag from the far less abundant cellular ironstone would help but separation may not be complete in view of the probable variations in the s.g. of these materials. This is an avenue for further research.

6.0 PETROGRAPHY

The objectives of the petrography were to provide a better understanding of the history of this geochemical medium and to determine if fabrics have been preserved, which could be used to indicate underlying lithologies. Specimen sites were selected so as to ensure that lags overlying all known rock types, as well as the orebody, the local background (to the east of the orebody) and the regional background were included. For details of each studied specimen, the reader is referred to Appendix 5. A summary and interpretation of the main fabric elements follow. Fabrics visible by binocular examination are illustrated in Figure 6. Those visible under the petrographic microscope are shown in Figures 7 and 8.

6.0.1 Specimen representivity

Inhomogeneity of the coarse lag (compare Figure 6A with Figure 6G and Figure 6B with Figure 6F), due to inherent bedrock variation, differing degrees of iron replacement and lateral dispersion, made it necessary to cut four sections from each location. Though the fine lag is even more inhomogeneous, sufficient fine lag grains (100 - 200) were included in each section to provide a representative specimen.

6.0.2 Relics and Pseudomorphs

Many of the fragments in the lag are lithorelics (Figures 6A-E). Iron minerals, principally goethite with some hematite, have almost completely replaced the original mineralogy, though some older fabrics may still be recognised. Where mineral preservation has occurred, these are relics; where iron replacement is complete and only the mineral fabric is preserved, these are pseudomorphs.

The relics are invariably iron-stained mica (Si=Al>K, Fe). The pseudomorphs are more difficult to determine. They appear to be layer silicates and some may be after kaolinite, kaolinite interlaminated with illite and even smectite. Examination of the goethite of the layer silicate pseudomorphs by SEM shows Fe>>Si, Al. This suggests either that some of the silicate minerals are preserved on a sub-

FIGURE 6

INTERNAL STRUCTURES OF LAG FRAGMENTS

Primary Fabrics

A. A honey-brown, ferruginised lithorelic of mafic schist, showing preserved schistosity along which some secondary goethite has penetrated. The granular fabric contains island-like pseudomorphs of layer silicate, set in goethite. Co-ordinates 33850E 38940N. Specimen 08-104A.

B. A deep red-brown ferruginised lithorelic of ore-zone phyllite, showing a preserved and folded schistosity with a high proportion of mica relics. Co-ordinates 33975E 38940N. Specimen 08-108D.

C. Islands of yellow-brown goethite, with a very fine-scale preserved schistosity, contain very fine-grained layer silicate pseudomorphs after probable ultramafic saprolite. This is veined with dark brown goethite. Co-ordinates 33747E 39311N. Specimen 08-117B.

D. A clearly distinguishable and probably exotic silicified lithorelic of banded iron formation, showing an iron-stained quartz-rich layer separating two goethite- and hematite-rich layers. Co-ordinates 34172E 39314N. Specimen 08-118A.

E. A lithorelic showing possible polymictic fragments set in an arenaceous matrix. Overlying Permian glacials. Co-ordinates 34290E 38110N. Specimen 08-120B.

Secondary Fabrics

F. A very fine-grained, ferruginised lithorelic of ore-zone phyllite. Though some schistosity is preserved, much of the original fabric has been replaced by dark brown, secondary goethite. Co-ordinates 33975E 38940N. Specimen 08-108C.

G. A fine-grained flinty lithorelic, largely replaced by cauliflower-like secondary goethite. This is cut by later stylolitic veins of black goethite. Co-ordinates 33850E 38940N. Specimen 08-104B.

H. Khaki lag showing dark goethite nodules, containing some preserved saprolite micro-fabrics and secondary goethite, set in a yellow-brown ferruginous clay. Co-ordinates 34025E 38820N. Specimen 08-124A.

I. Khaki lag showing a red hematitic clay fragment, containing ferruginous clay pisoliths and pisolith fragments. This is set in a mass of oolitic yellow clay which was precipitated chemically in a solution cavity. Co-ordinates 34025E 38940N. Specimen 08-130D.

J. A schistose lithorelic containing numerous vermiform vesicles. These have been filled with a breccia of angular goethitic fragments, cemented by clay and hardpan. This cementation probably occurred in the soil. Co-ordinates 34150E 38940N. Specimen 08-113D.

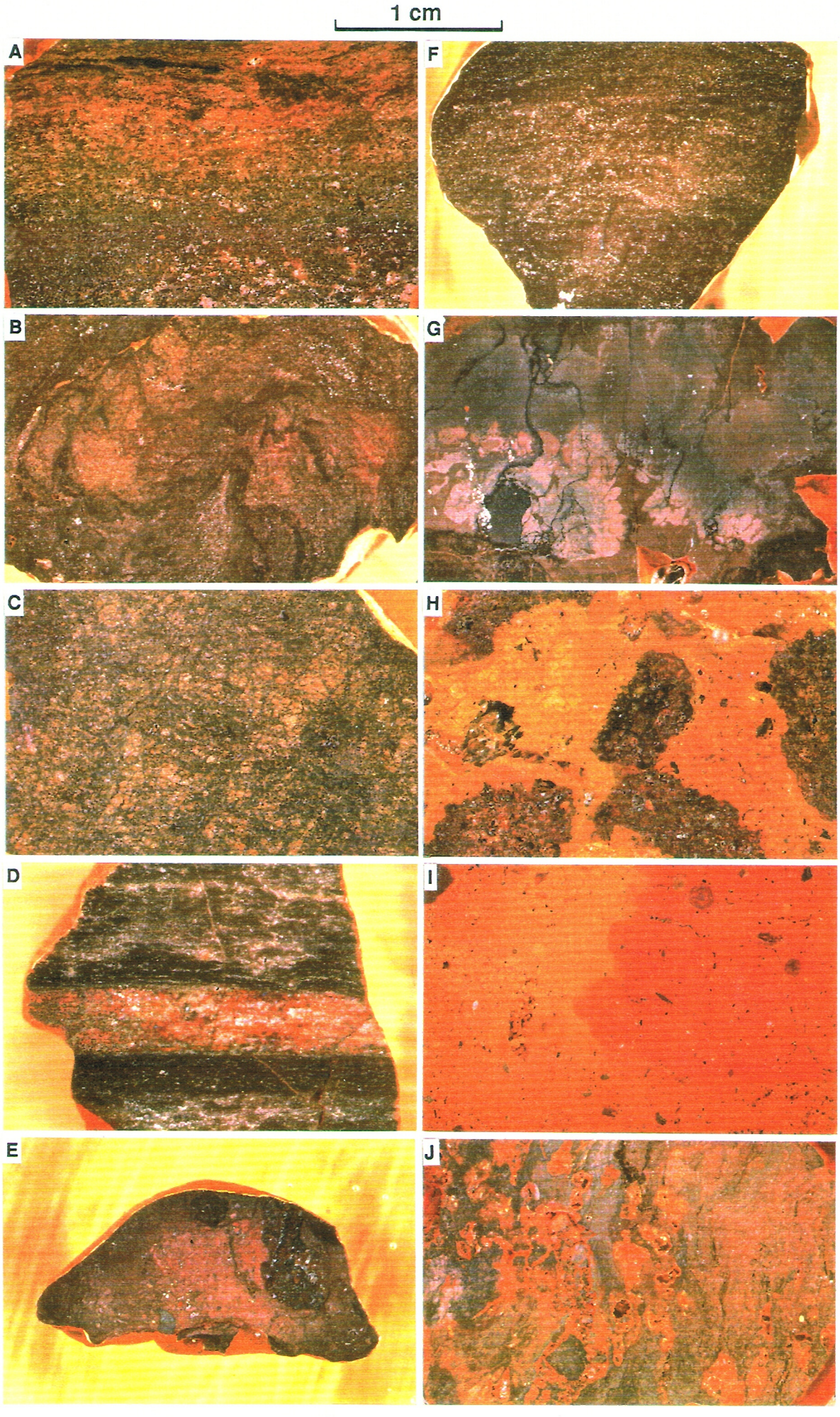
1 cm
A
F
B
G
C
H
D
I
E
J

FIGURE 7

PETROGRAPHY OF COARSE LAG

Primary fabrics

A. Coarse black ferruginous lag, located over orebody. Mica relics (M) set in spongey goethite (G) with small vesicles. Goethite has in part wedged the mica cleavages apart. Specimen 08-108B. Co-ordinates 33975E 38940N.

B. Coarse black ferruginous lag, located over orebody. Fine-scale layer silicate pseudomorphs (Ls), apparently after kaolinite and interstratified kaolinite and mica, set in goethite (G). A small lens of gold (Au) appears in the place of a small mica sheet. Specimen 08-108D. Co-ordinates 33975E 38940N.

C. Coarse black ferruginous lag, located over mafic footwall rocks. A matted layer silicate pseudomorph (Ls) with a globular fingerprint structure, set in dull grey, spongey goethite (G).

D. Coarse black ferruginous lag, located over ultramafic rocks. A confused fingerprint structure of layer silicate pseudomorphs, set in bright goethite. Specimen 08-113C. Co-ordinates 34150E 38940N.

E. Coarse black ferruginous lag, located over Permian glacial sediments. Possible matrix-supported polymictic lithorelics, including one which is sub-angular and consists of bright goethite (G) with a few small layer silicate pseudomorphs, others which are angular, rather shaddowy and goethitic (S) and angular fragments of quartz (Q), all set in a fine-grained goethitic groundmass. This has been cut by fractures and secondary goethite has permeated the matrix. Specimen 08-120B. Co-ordinates 34290E 38110N.

Secondary Layer Silicate Fabrics

F. Coarse black ferruginous lag, located distant from the orebody over either Permian glacial sediments or ultramafics. Two layer silicate pseudomorphs with an 'accordion' structure (A). These appear to have formed after kaolinite which recrystallised in the saprolite. Compare these structures to similar structures in Figure 9, which formed diagenetically in a fireclay. These are set in spongey, bright goethite (G) with numerous irregular vesicles (V). Specimen 08-438B. Co-ordinates 34700E 38940N.

Gold

G. Coarse black ferruginous lag, located over footwall basaltic rocks but seems to have been relocated by lateral dispersion from the ore zone. A lens of gold (Au) partly infills a small vesicle (v) in bright secondary goethite (G). SEM examination showed no Ag. A few small crystals of hematite (H) are scattered in the goethite. Specimen 08-104A. Co-ordinates 33850E 38940N.

H. Coarse black ferruginous lag, located over ore zone. A small gold grain (Au) is attached to the edge of a vesicle (V). SEM examination showed no Ag. Specimen 08-108D. Co-ordinates 33975E 38940N.

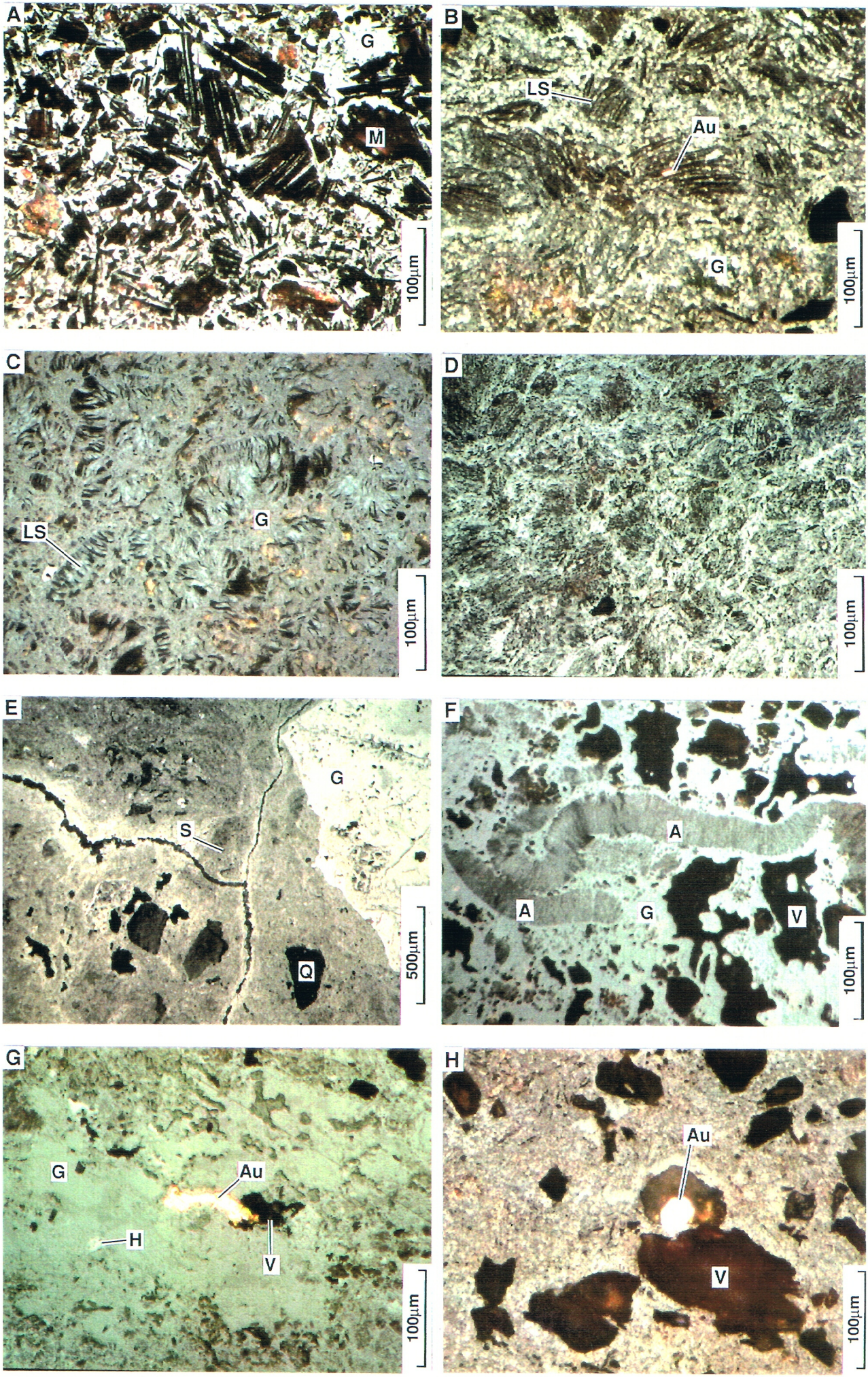
A
G
M
100µm
B
LS
Au
G
100µm
C
LS
G
100µm
D
100µm
E
G
S
Q
500µm
F
A
A
G
V
100µm
G
G
Au
H
V
100µm
H
Au
V
100µm

FIGURE 8

PETROGRAPHY OF COARSE AND FINE LAGS

Secondary goethite structures

A. Coarse black ferruginous lag, located over footwall basaltic rocks. Islands of layer silicate pseudomorphs and a few mica remnants, set in dull goethite (G1), invaded by and now set in bright goethite (G2). A few lozenge-shaped hematite crystals (H) are scattered in the fabric. Specimen 08-104A. Co-ordinates 33850E 38940N.

B. Khaki lag, located over lateritic duricrust. Colloform goethite (G) lining a vesicle. The brightest goethite phase has been partly altered to hematite (GH) and shows a network of dehydration cracks which have been filled with a later and darker goethite phase. Specimen 08-124C. Co-ordinates 34025E 38820N.

C. Coarse black ferruginous lag, located over lateritic duricrust. Fibrous colloform goethite (GF) filling voids (V). Specimen 08-93C. Co-ordinates 34025E 38820N.

D. Coarse black ferruginous lag, located over mafic footwall rocks. Coarse fibrous goethite (GF) lining voids (V) in spongey secondary goethite (G). Specimem 08-104D. Co-ordinates 33850E 38940N.

E. Fine ferruginous lag, located over the orebody. Delicately banded botryoidal structures in alternating layers of goethite (G) and hematite (H) on the edge of a lag granule. Specimen 08-216. Co-ordinates 33975E 38940N.

Clay structures

F. Khaki lag, located over lateritic duricrust. Dark, concentrically zoned, red clay pisiliths (P), set in a red clay (RC) nodule. The zonation is due to goethite in the clay. Small crystals of hematite (H) are scattered in the clay matrix. Specimen 08-130D. Co-ordinates 34025E 38940N.

G. Khaki lag, located over lateritic duricrust. Ooliths of yellow clay (YC) which surround the red clay of F. These are set with small crystals of hematite (H). A pisolith fragment with attached cutan (PF) is set in this oolithic matrix. Specimen 08-130D. Co-ordinates 34025E 38940N.

H. Khaki lag, located over lateritic duricrust. Red clay, containing solution cracks and interlinked vesicles. Goethite has penetrated the clay around these vesicles. Specimem 08-133B. Co-ordinates 34025E 38940N.

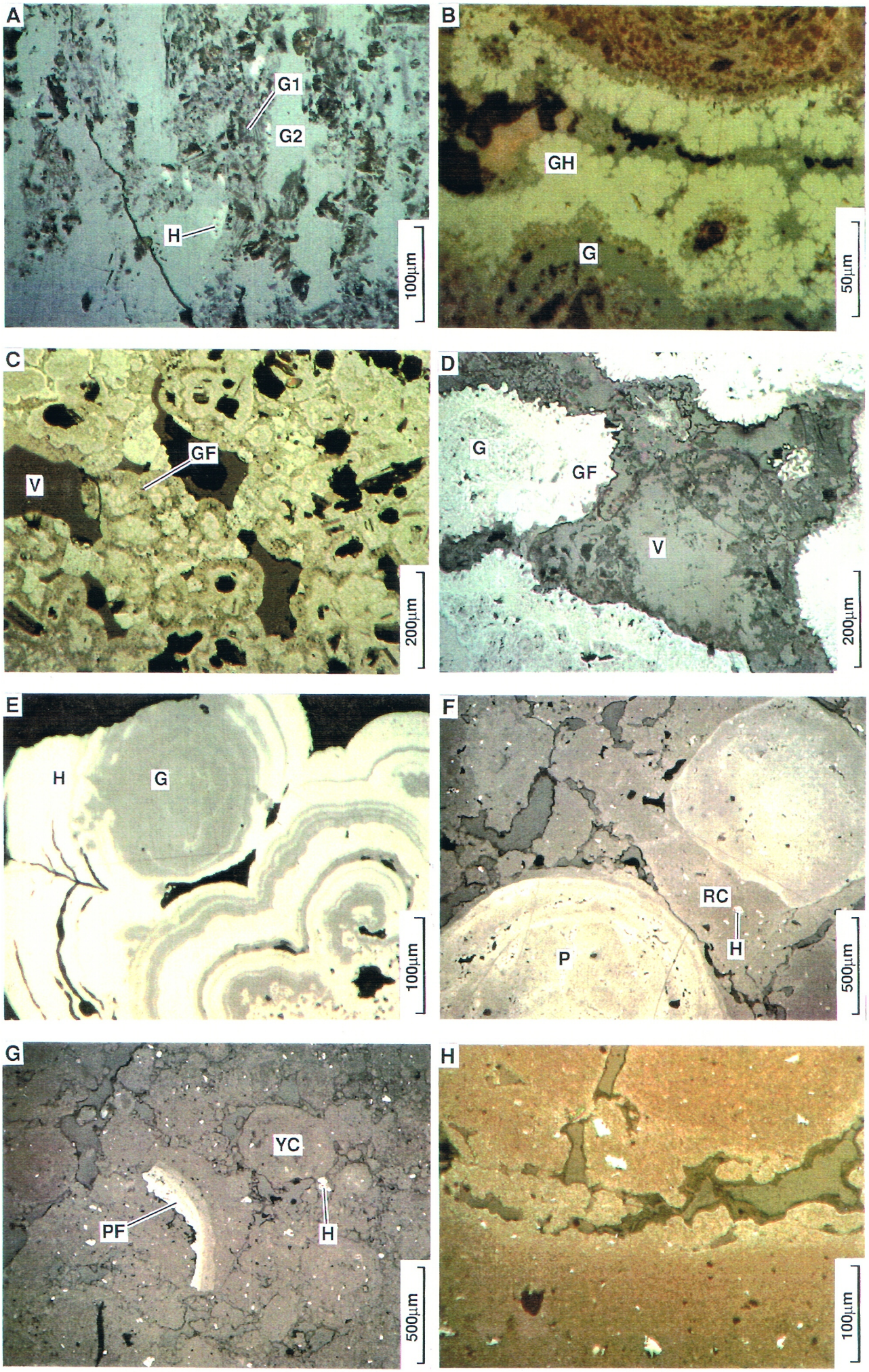
A
G1
G2
H
100μm
B
GH
G
50μm
C
GF
V
200μm
D
G
GF
V
200μm
E
H
G
100μm
F
RC
H
P
500μm
G
YC
PF
H
500μm
H
100μm

micron scale or that the goethite of the pseudomorph has absorbed some of the Si and Al into its lattice. It may be possible to resolve this with a TEM, but this is beyond the scope of this study.

6.0.3 Secondary Goethite and Hematite

Where pseudomorphed mineral fabrics have been destroyed, only secondary iron oxide structures are left (Figures 6F, G). In places, there is evidence for several cycles of iron dissolution and precipitation. Some goethite forms colloform, delicately banded structures as a sequence of linings on the walls of open spaces which, in places, have been completely or almost completely filled.

Hematite occurs overtly as small lozenge-shaped crystals and as poikiloblasts but it also occurs covertly, with goethite, as an ultra fine-grained product of goethite dehydration. This has lead to a wide variety of goethite colours and reflectances, from dull brownish-grey, through lead grey to goethites of increasing brightness as dehydration progresses. This has lead to a greater hematite content in the specimens than is immediately apparent from a polished section study. The dehydration process is accompanied by a volume change, leading to dehydration cracking or to a spongy appearance. This process has been discussed by Morris (1985), who described the process as selective, in that goethite pseudomorphs after quartz were the most easily transformed, followed by silicate and then carbonate pseudomorphs. In the iron ores of the Hamersleys, this dehydration appears to be due to long exposure of the goethite above the water-table and is most prevalent near the surface. This process is equally applicable to a lag accumulation.

6.1 Coarse Lag

Petrographic investigation of the coarse lag found recognisable remnant, original, saprolitic fabrics which may be used to identify the bedrock. A complex series of iron solution and precipitation events partly overlap with a generally later sequence of clay precipitations. Small gold grains were seen in a few instances.

6.1.1 Saprolitic Fabrics

The lag overlying the orebody and its black shale host (Specimens 08-108 A - D, 08-104 D, 08-93 C) show preserved schistose fabrics which are clearly visible under the binocular microscope (Figures 6 A-E). The polished sections show islands of preserved original, saprolitic fabric, now largely taken over by goethite, set in bright, massive, to spongy goethite which contains open vesicles. The secondary goethite is fibrous to colloform where it lines vesicles.

The preserved saprolitic fabrics contain mica relics (10 - 100 μm), some of which have been split along their cleavages by the enclosing goethite (Figure 7A). The mica of these relics is poorly crystalline but still contains potassium (Section 7.2). There are also some fine-textured layer silicate pseudomorphs, probably after kaolinite and interstratified kaolinite and mica (Figure 7B). These mica relics may be compared to identical relics and to unferruginised saprolitic, phyllitic mica and kaolinite fabrics from the Beasley Creek orebody, intersected in drillhole BCD1 (Robertson and Gall, 1988; Figures 2G, H).

Preserved schistose fabrics are shown by lag fragments which overlie the footwall mafic schists (Specimens 08-104 C - D). The polished sections show numerous very fine-grained layer silicate pseudomorphs, with a matted fabric, forming a confused fingerprint structure (Figure 7C). This structure appears to be metamorphic, though the metamorphic minerals (feldspar and uralitic amphibole) have since been replaced by kaolinite and smectite and these in turn by goethite. This

FIGURE 9

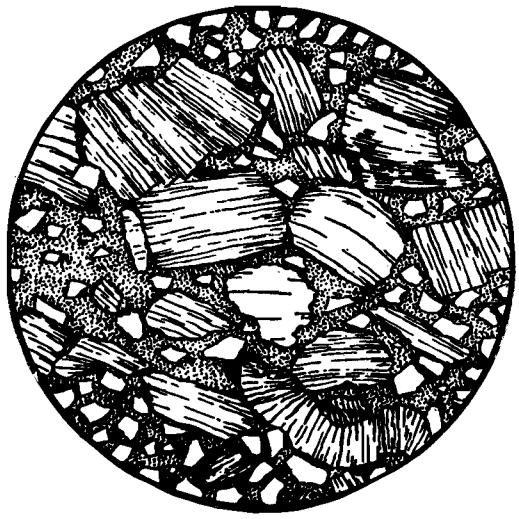

Sandy fire clay (Eocene), Ione, California. Diam. 3 mm. Angular detrital quartz grains in a kaolin matrix (stippled). Abundant vermicular kaolinite crystals developed authigenically after deposition, as shown by their elongation normal to the cleavage (lower right and top). Note displacements along cleavage in some crystals and "accordion" structure. (After Williams, Turner & Gilbert, 1955).

fabric can be compared with the similar but less ferruginised fabric of the saprolitic footwall amphibolite in DDH BCD1 (Robertson and Gall, 1988).

Although the interior of the lag fragments overlying the lateritic duricrust vary widely in colour from blue-grey, through dark red-brown to mottled yellow and honey-brown (Specimens 08-93 A, B, D), they all show patches of a preserved confused fingerprint structure, containing matted layer silicate pseudomorphs in various stages of distortion. These remnants of the original saprolitic fabric are set in varying proportions of several generations of secondary goethite, some of which are fibrous, and bright polygonal grains of hematite. It appears that some of the ferruginous, nodular material from the lateritic duricrust contains preserved saprolitic fabrics, despite extensive replacement by iron.

Schistose fabrics are preserved in some of the lag fragments found overlying ultramafic schists. Their colours vary from yellowish brown or red-brown, mottled with blue-black (Specimens 08-113 C, D: 08-118 B, D). The fabric of the underlying ultramafic saprolite is difficult to determine, from a study of the lag, for it appears also to consist of a matted pseudomorphed layer silicate fabric, in a few places showing a confused fingerprint structure (Figure 7D), similar to that of the mafic rocks, but characterised by a very fine scale.

The Permian glacials, exposed in the pit wall at Beasley Creek and at the Telegraph pit, Lancefield area, are arenaceous to rudaceous rocks. They have been converted to clay-rich saprolites, which show all the characteristics of lateritic weathering. Polymictic fragments (Figure 7E), several mm in size, were seen in two brown to mauve coloured sections (08-120 B, C) of the lag. Some of these fragments show faint saprolitic fabrics. They form a breccia-like structure, set in what appears to be an arenaceous matrix. The lag fragments, overlying the glacial rocks, would be expected to be particularly diverse and this is so. It is tempting to suggest that these are sedimentary breccias and the fabric of the lag reflects the underlying tillites and arenites. Alternatively, the complex nature of the ferruginisation process could mimic such a structure.

Accordion-like layer silicate pseudomorphs are very evident in some sections. These form vermicular structures and generally lie within, or on, the outside of preserved silicate relics, close to, and intimately associated with, secondary goethite structures (Figure 7F). Very similar accordion-like structures (Figure 9) are described in authigenic kaolinite of argillaceous rocks (Williams *et al.*, 1955) and in kaolinites derived from granite weathering (Robertson and Eggleton, in prep). It is suggested that these pseudomorphs represent authigenic recrystallisation of kaolinite in the saprolite, that have since suffered iron replacement, preserving them from saprolite re-texturing and collapse.

6.1.2 Secondary Goethite and Hematite Structures

The interstices between layer silicate relics and pseudomorphs are filled with grey goethite, which generally has a massive or a spongy appearance (Figure 8A). In places a remnant schistosity is found, penetrated by parallel bands of secondary goethite. Its reflectivity is variable and this seems linked to dehydration to microcrystalline hematite. Where dehydration to hematite has been particularly intense, dehydration cracks (Figure 8B) are found in the hematite. In places the hematite forms bright discrete grains which may be irregular, poikiloblastic or lozenge-shaped, that lie in the secondary goethite (Figures 8A and 7C). XRD examination of these rocks indicates more hematite than is seen as a separate phase in the polished sections. In places the secondary goethite is permeated with one or more younger goethite phases of subtly different reflectivity, which in places are fibrous or form delicate colloform structures. Fibrous and colloform structures are prevalent among the last stages of goethite deposition and fill what were once open spaces (Figures 8B - E). These goethite phases indicate successive solution and re-deposition of iron oxide. Gold is found commonly associated with the last phases of secondary goethite.

6.1.3 Clay Structures - Khaki Lag

Sections of the khaki lag (08-124, 08-130, 08-133) illustrate the complex later history of the lag, where it has become enclosed in the lateritic duricrust, to which it is undoubtedly related. The sections contain several types of fragment, both nodular and pisolitic, as well as fragments of angular quartz, set in several generations of red-brown to yellow-brown clay (Figure 6H). These clays are in part gibbsitic in the duricrust but they are kaolinitic in the lag. The nodules contain predominant saprolitic pseudomorphs, indicative of mafic rocks and minor mica relics, related to the ore host. Goethite cutans and partial cutans on the ferruginous nodules suggest precipitation and re-solution of goethite before the clays were precipitated.

The clays show a wide variety in colour, from red to yellow, indicating a range in hematite content (Figure 6I). The outer parts generally tend to be yellow or goethitic and the inner parts red or hematitic. This could be related to water access, which would either influence the equilibrium between goethite and hematite precipitation or the solid state hydration of hematite to goethite. In some, a history of at least two clay phases is shown by the presence of fragmentary or complete clay pisoliths, some with yellow clay cutans, now set in a clay matrix (Figures 8F, G). Some of these pisoliths contain dark goethite nodules. Small crystals of hematite occur scattered in the clay (Figures 8F - H). Solution cavities in the khaki lag are filled with ooliths of yellow clay, indicating chemical precipitation of clay (Figures 6I and 8G).

In places goethite is found filling channelways, which link vesicles in the clay, and which has permeated outwards from the channel into the clay for a short distance (Figure 8H).

6.1.4 Vesicles, Hardpan- and Agate-filled Voids

Voids in the rock vary from round and cavernous to vermiform and some form channelways, which are linked by hairline fractures, now either still open or filled with clay or goethite. Some voids are lined with thin goethite cutans, which are in places colloform, fibrous or both. Some solution cavities are filled with brown ferruginous clay, with numerous, small, angular fragments of goethitic, nodular material and angular quartz, set in brown hardpan (Figure 6J), or with white, banded, opaline silica.

6.1.5 Gold

Petrographic discovery of gold grains, which have a concentration in the rock of 0.1 - 10 ppm, is very much a matter of chance. It would be necessary to search an area 70 mm square in order to find one 30 μm grain at a concentration of 1 ppm, which is considerably more than the 15 mm square of most polished sections. It is therefore only possible to gain an impression of the site and petrographic relationships of gold. Nevertheless a few gold grains were found and, in almost all instances, they were associated with voids in the rock.

One lag fragment (08-104A), which appears to have been derived from the orebody host shale, but which is now located over footwall basaltic rocks, by down-hill mechanical dispersion, contains a lenticular particle of gold 100 μm long and 10 μm wide (Figure 7G). This is set in secondary goethite and is attached to the edge of a small vesicle. A small spherical grain of gold, about 5 μm in diameter, was found attached to the clay lining of an irregular vesicle about 60 μm across. This vesicle is set in the hardpan filling of a solution cavity in specimen 08-113D. Other gold grains were found attached to the linings of vesicles in specimens 08-113A and 08-108D (Figure 7H). These suggest very late gold mobility. Specimen 08-108D contains a small flake of gold (10 x 1 μm), in a whispy layer silicate relic (Figure 7B), but the timing of gold deposition is difficult to determine.

6.2 Fine Lag

The fine lag is a very heterogeneous material, containing a wide variety of granule fabrics and colours (Figure 4D and Frontispiece). The fine lag has all the components and features of the coarse lag, though in a very fragmentary way, which is inherent in the small size of the granules. The wide variety of lithorelic fabrics, found in any one specimen site, demonstrates a greater degree of lateral dispersion than in the coarse lag. In spite of this, fabrics related to underlying lithologies can be seen in a general way.

Lithorelics vary from honey brown to deep mauve-brown and show preserved schistosities and islands of preserved fabric, cut by secondary goethite. Relics of included platy mica and layer silicate pseudomorphs are preserved. Some show confused fingerprint structures but, in some, replacement by secondary goethite is almost complete and a very weak, swirled fabric is all that remains. Accordion-like goethite pseudomorphs after kaolinite are also found.

Where secondary goethite is abundant, the granules are a deep brown. The goethite can be massive or porous, as in the coarse lag, and veins of secondary goethite are common. A few colloform or botryoidal structures of alternating goethite and hematite are to be seen (Figure 8E). Some granules show cutans or partial cutans of grey goethite. A late goethite phase is identified, where it is found permeating ferruginous clay from small cracks and solution channels.

Granules related to the lateritic duricrust (khaki lag) vary from yellow-brown to red-brown. They consist of ferruginous clay (kaolinite, goethite, varying amounts of hematite and minor quartz) and many have an oolitic structure. Some cutans of ferruginous clay are found on dark, goethitic granules and colloform goethite was found cementing yellow ferruginous clay.

Quartz fragments are more abundant in lag from the flats to the east of the hill than from over the orebody. The proportion of ferruginous clay granules to goethitic granules is also higher on the flats.

7.0 MINERALOGY

7.1 XRD Analysis

7.1.1 The Coarse Lags

All the analysed samples of coarse lag were examined by powder diffractometry. They consist largely of goethite, with lesser quantities of hematite and kaolinite, some mica and quartz. Semi-quantitative mineral abundances were also estimated and are presented in Table 4 and graphed in Figure 10. Goethite and hematite are complementary, there being significantly more goethite and less hematite over footwall rocks, the orebody and the lateritic duricrust than over the ultramafics and Permian rocks to the east. Kaolin and quartz are variable but there is a slight tendency for there to be a higher kaolin, hematite and particularly a higher quartz content in the background rocks and where goethite is low.

The khaki lag is richer in hematite and poorer in goethite than corresponding ferruginous lag samples. It is also richer in kaolin and poorer in quartz.

TABLE 4
MINERALOGY OF COARSE LAG

BLACK LAG

Field No	Lab Seq	Lib No	Co-ordinates East	Co-ordinates North	Peak Heights in mm Kaolin 7.1Å	Goeth 2.45Å	Quartz 3.343Å	Hematite 1.838Å	Mica 10Å	hump 8-12Å	% Al Substitution Goethite Schulz	Goethite d(111)	Hematite d(110)
BC 001	L08-120	08-082	33600	38820	2	50	10	3	8	3	4	4	0
BC 002	L08-112	08-083	33650	38820	3	56	10	5	5	2	0	0	0
BC 003	L08-117	08-084	33700	38820	3	52	12	4	5	3	3	4	4
BC 004	L08-097	08-085	33750	38820	7	52	8	3	3	3	6	5	4
BC 005	L08-093	08-086	33800	38820	2	54	6	5	10	3	6	5	4
BC 006	L08-116	08-087	33850	38820	4	55	11	6	12	3	5	5	3
BC 007	L08-087	08-088	33900	38820	6	62	21	3	9	4	5	4	6
BC 008	L08-099	08-089	33925	38820	5	61	34	3	5	3	3	3	2
BC 009	L08-091	08-090	33950	38820	2	62	13	6	10	3	6	5	9
BC 010	L08-115	08-091	33975	38820	3	54	9	3	6	3	5	5	7
BC 011	L08-089	08-092	34000	38820	1	49	5	8	9	4	10	9	6
BC 012	L08-113	08-093	34025	38820	3	52	12	4	8	3	4	5	5
BC 013	L08-084	08-094	34050	38820	6	56	6	6	6	3	6	4	5
BC 014	L08-109	08-095	34075	38820	6	45	10	6	5	3	7	7	1
BC 015	L08-094	08-096	34100	38820	6	54	7	5	8	2	4	5	7
BC 016	L08-123	08-097	34150	38820	5	55	5	10	3	3	1	0	0
BC 017	L08-086	08-098	34200	38820	3	63	10	4	5	3	5	6	7
BC 018	L08-082	08-099	34250	38820	5	69	16	6	7	4	3	3	3
BC 706	L08-474	08-440	34350	38820	19	26	6	12	0	0	10	8	6
BC 707	L08-440	08-441	34450	38820	10	10	6	20	2	0	8	9	7
BC 708	L08-466	08-442	34550	38820	3	7	11	22	0	0	12	10	10
BC 709	L08-452	08-443	34650	38820	4	18	40	16	0	0	2	4	13
BC 710	L08-475	08-444	34750	38820	17	27	29	13	6	1	8	5	9
Min	-	-	33600	38820	1	7	5	3	0	0	-	-	-
Max	-	-	34750	38820	19	69	40	22	12	4	-	-	-

TABLE 4 (contd)

Field No	Lab Seq	Lib No	Co-ordinates East	Co-ordinates North	Peak Heights in mm Kaolin 7.1Å	Goeth 2.45Å	Quartz 3.343Å	Hematite 1.838Å	Mica 10Å	hump 8-12Å	% Al Substitution Goethite Schulz	Goethite d(111)	Hematite d(110)
BC 021	L08-119	08-100	33650	38940	5	43	45	14	8	3	5	4	5
BC 022	L08-090	08-101	33700	38940	6	55	17	11	5	4	6	6	7
BC 023	L08-105	08-102	33750	38940	4	32	18	21	4	3	0	0	0
BC 024	L08-103	08-103	33800	38940	7	61	19	7	5	3	7	4	-1
BC 025	L08-110	08-104	33850	38940	5	62	21	4	5	2	6	5	0
BC 026	L08-083	08-105	33900	38940	4	67	10	4	8	3	6	6	3
BC 027	L08-098	08-106	33925	38940	6	65	13	3	3	4	6	8	7
BC 028	L08-114	08-107	33950	38940	6	39	16	12	9	4	6	5	2
BC 029	L08-118	08-108	33975	38940	5	44	12	14	6	4	6	6	8
BC 030	L08-107	08-109	34000	38940	6	53	18	15	4	4	7	7	10
BC 031	L08-108	08-110	34025	38940	6	52	6	7	5	2	7	8	9
BC 032	L08-122	08-111	34050	38940	7	27	8	15	3	2	8	6	5
BC 033	L08-102	08-112	34100	38940	13	11	4	23	7	3	7	10	10
BC 034	L08-100	08-113	34150	38940	10	14	5	17	5	3	9	8	2
BC 035	L08-095	08-114	34200	38940	9	15	5	19	11	3	10	13	14
BC 036	L08-121	08-115	34250	38940	10	13	6	21	5	3	7	10	10
BC 037	L08-101	08-116	34300	38940	4	21	6	19	2	3	0	3	3
BC 701	L08-460	08-435	34400	38940	23	9	2	24	3	0	7	5	8
BC 702	L08-471	08-436	34500	38940	23	33	34	9	2	0	4	5	6
BC 703	L08-453	08-437	34600	38940	4	36	80	7	2	0	4	4	9
BC 704	L08-469	08-438	34700	38940	17	45	99	6	2	0	2	2	7
BC 705	L08-439	08-439	34800	38940	18	35	68	8	0	0	1	2	3
Min	-	-	33650	38940	4	9	2	3	0	0	-	-	-
Max	-	-	34800	38940	23	67	99	24	11	4	-	-	-

TABLE 4 (contd)

KHAKI LAG

Field No	Lab Seq	Lib No	Co-ordinates East	North	Peak Heights in mm Kaolin 7.1Å	Goeth 2.45Å	Quartz 3.343Å	Hematite 1.838Å	Mica 10Å	hump 8-12Å	% Al Substitution Goethite Schulz	Goethite d(111)	Hematite d(110)
BC 112	L08-126	08-124	34025	38820	12	26	6	8	3	3	11	15	10
BC 113	L08-132	08-125	34050	38820	12	24	2	8	5	3	11	13	10
BC 114	L08-125	08-126	34075	38820	6	19	5	11	10	4	12	15	13
BC 116	L08-129	08-127	34150	38820	11	41	5	9	3	2	2	3	0
BC 117	L08-128	08-128	34200	38820	10	58	2	3	3	3	4	4	0
BC 118	L08-133	08-129	34250	38820	16	62	4	2	3	2	8	7	6
BC 131	L08-127	08-130	34025	38940	12	16	2	13	0	3	11	18	8
BC 132	L08-134	08-131	34050	38940	5	18	2	19	3	3	8	13	7
BC 133	L08-124	08-132	34100	38940	8	14	2	15	2	3	16	19	10
BC 231	L08-130	08-133	34025	38940	15	12	7	31	6	2	16	17	5
Min	-	-	34025	38820	5	12	2	2	0	2	-	-	-
Max	-	-	34250	38940	16	62	7	31	10	4	-	-	-

BACKGROUND DATA SET

Field No	Lab Seq	Lib No	Co-ordinates East	North	Peak Heights in mm Kaolin 7.1Å	Goeth 2.45Å	Quartz 3.343Å	Hematite 1.838Å	Mica 10Å	hump 8-12Å	% Al Substitution Goethite Schulz	Goethite d(111)	Hematite d(110)
BC 041	L08-085	08-117	33747	39311	9	31	82	14	7	3	5	5	5
BC 042	L08-106	08-118	34172	39314	4	15	57	21	9	3	0	1	8
BC 043	L08-104	08-119	33545	38146	5	28	74	16	3	3	8	6	4
BC 044	L08-088	08-120	34290	38110	5	8	23	32	0	3	7	4	10
G.Mean	-	-	-	-	5.5	17.9	53.1	19.7	2.1	3	2	3	6
Max	-	-	-	-	9	31	82	32	9	3	8	6	10
Min	-	-	-	-	4	8	23	14	0	3	0	1	4

FIGURE 10

Graphed Mineralogy

Black Ferruginous Lag

Khaki Lag

Ore Body

Range and geometric mean of background data set

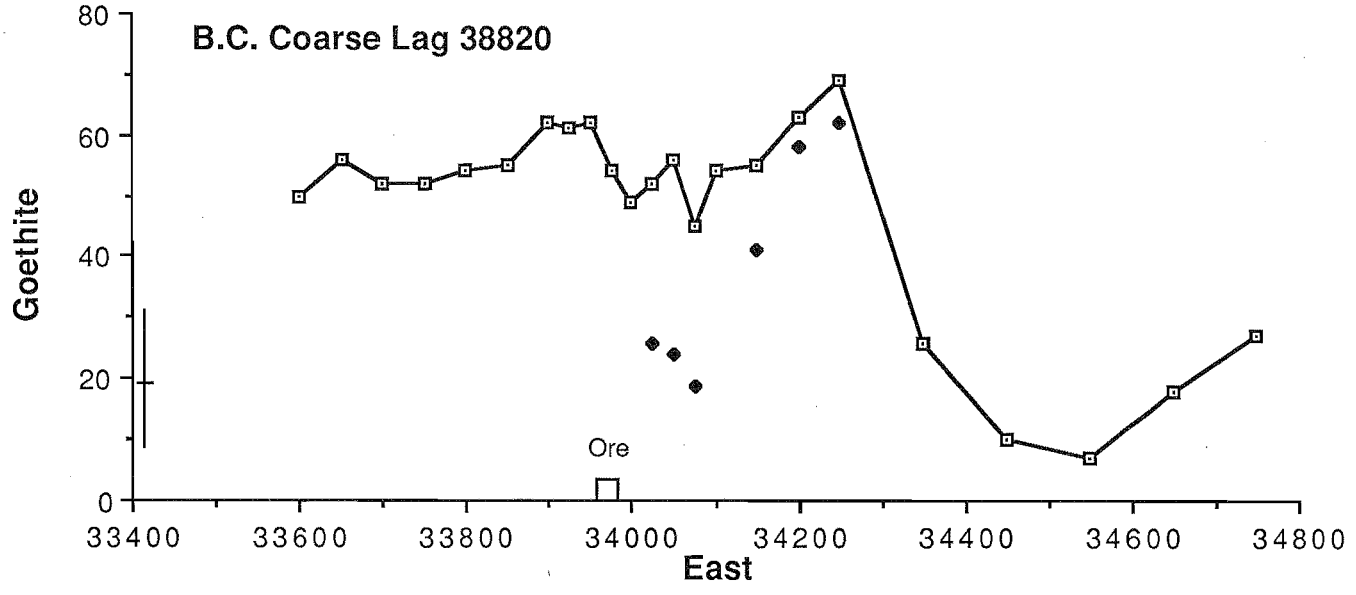
B.C. Coarse Lag 38820
Goethite
80
60
40
20
0
Ore
33400
33600
33800
34000
34200
34400
34600
34800
East

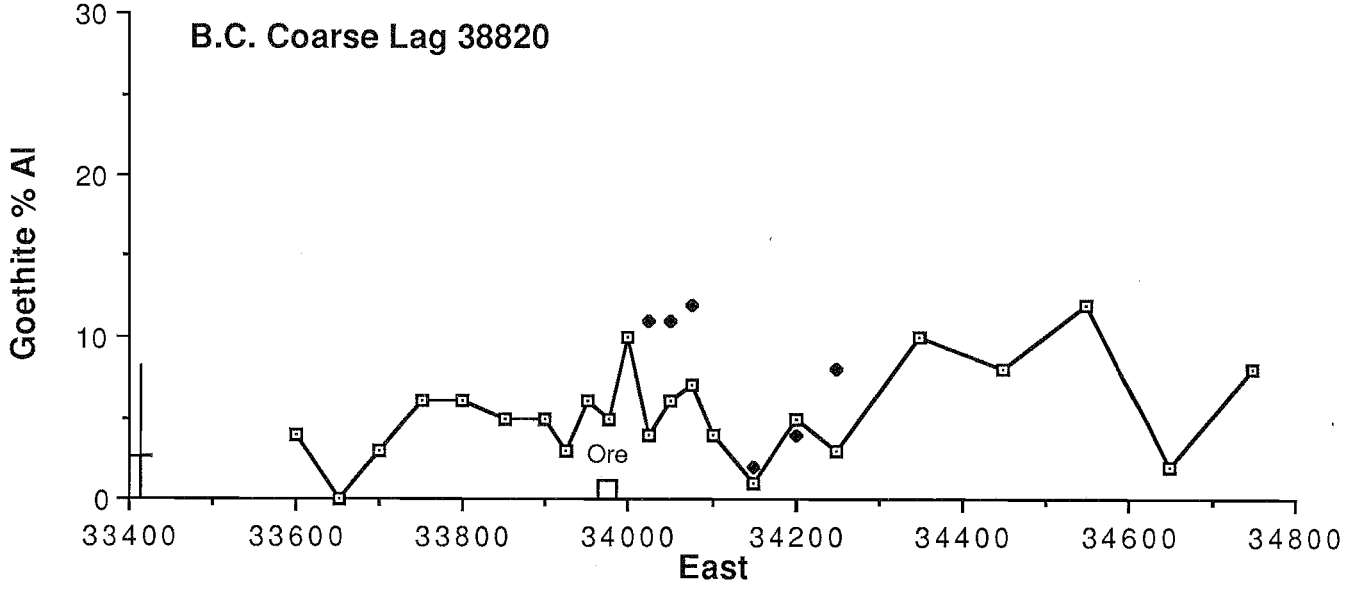
B.C. Coarse Lag 38820
Goethite % Al
30
20
10
0
Ore
33400
33600
33800
34000
34200
34400
34600
34800
East

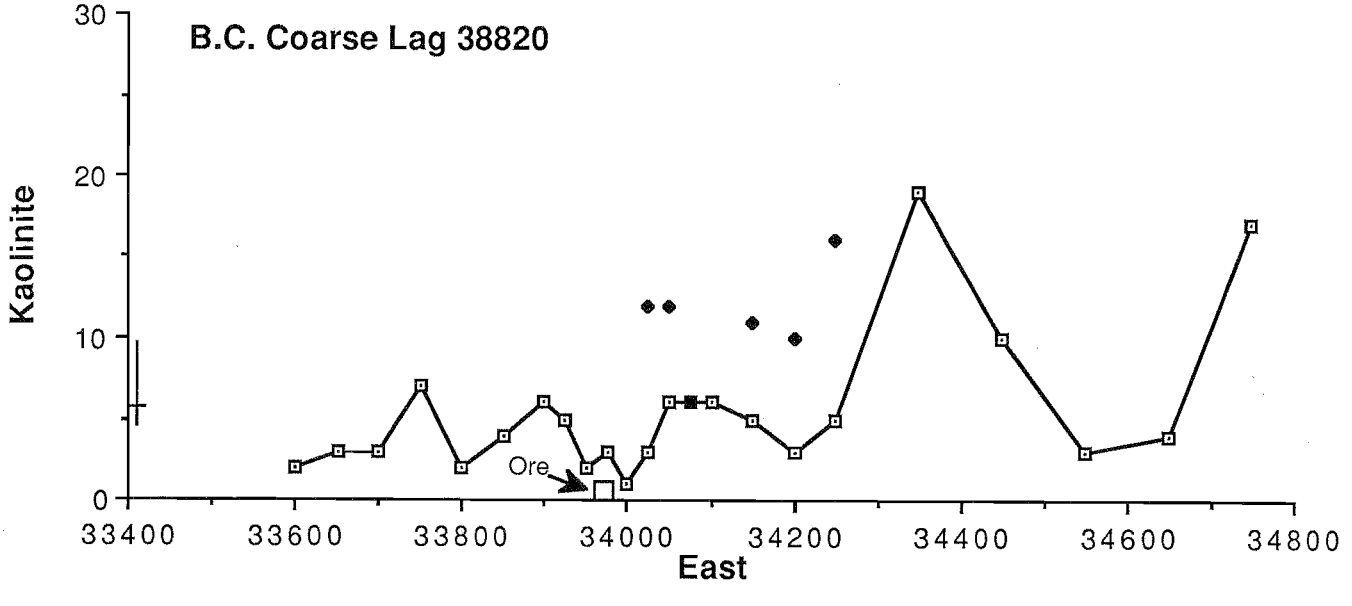
B.C. Coarse Lag 38820
Kaolinite
30
20
10
0
Ore
33400
33600
33800
34000
34200
34400
34600
34800
East

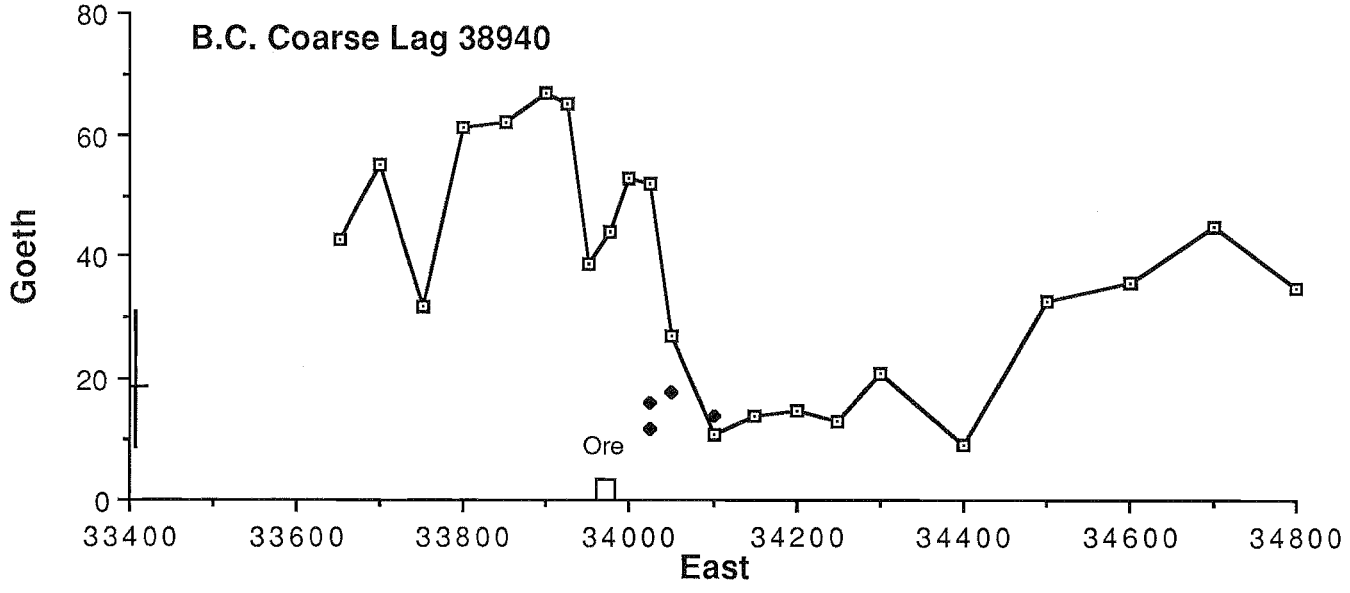
B.C. Coarse Lag 38940
Goeth
80
60
40
20
0
Ore
33400
33600
33800
34000
34200
34400
34600
34800
East

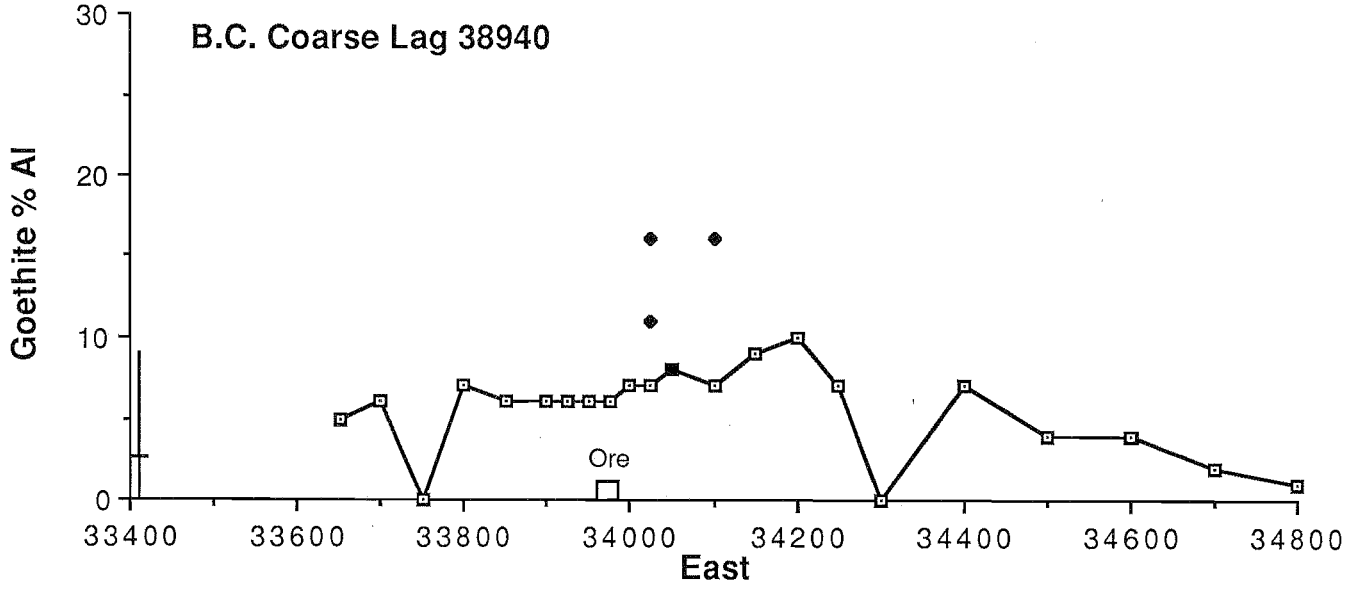
B.C. Coarse Lag 38940
Goethite % Al
30
20
10
0
Ore
33400
33600
33800
34000
34200
34400
34600
34800
East

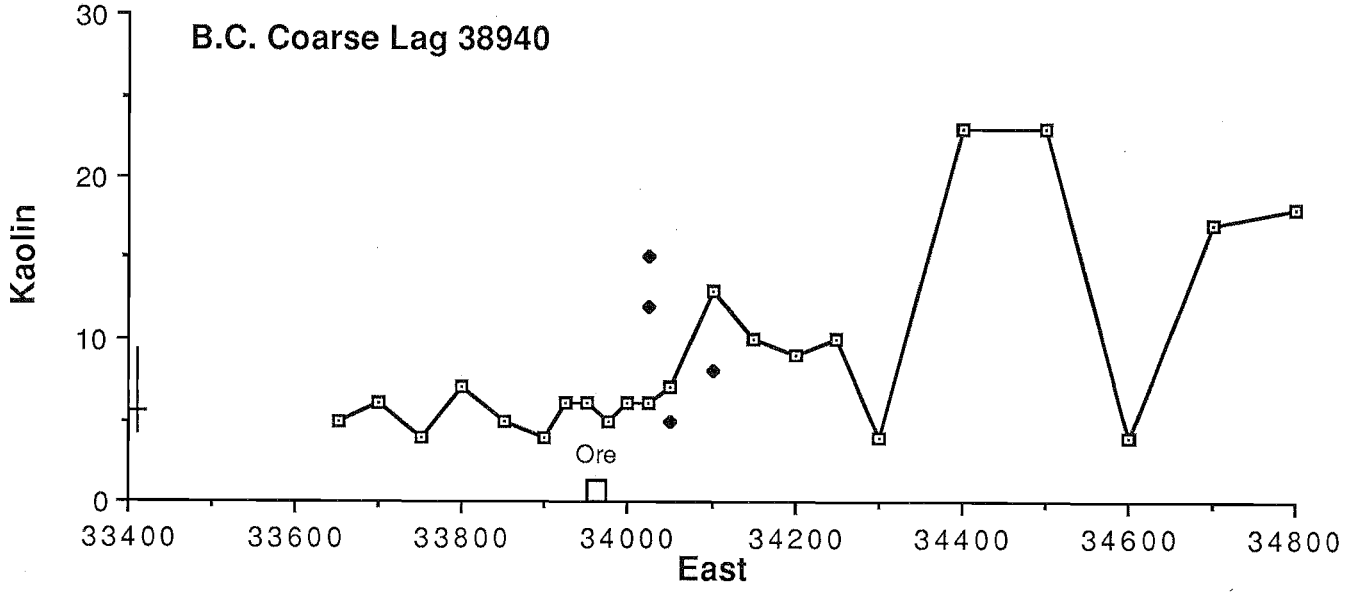
B.C. Coarse Lag 38940
Kaolin
30
20
10
0
Ore
33400
33600
33800
34000
34200
34400
34600
34800
East

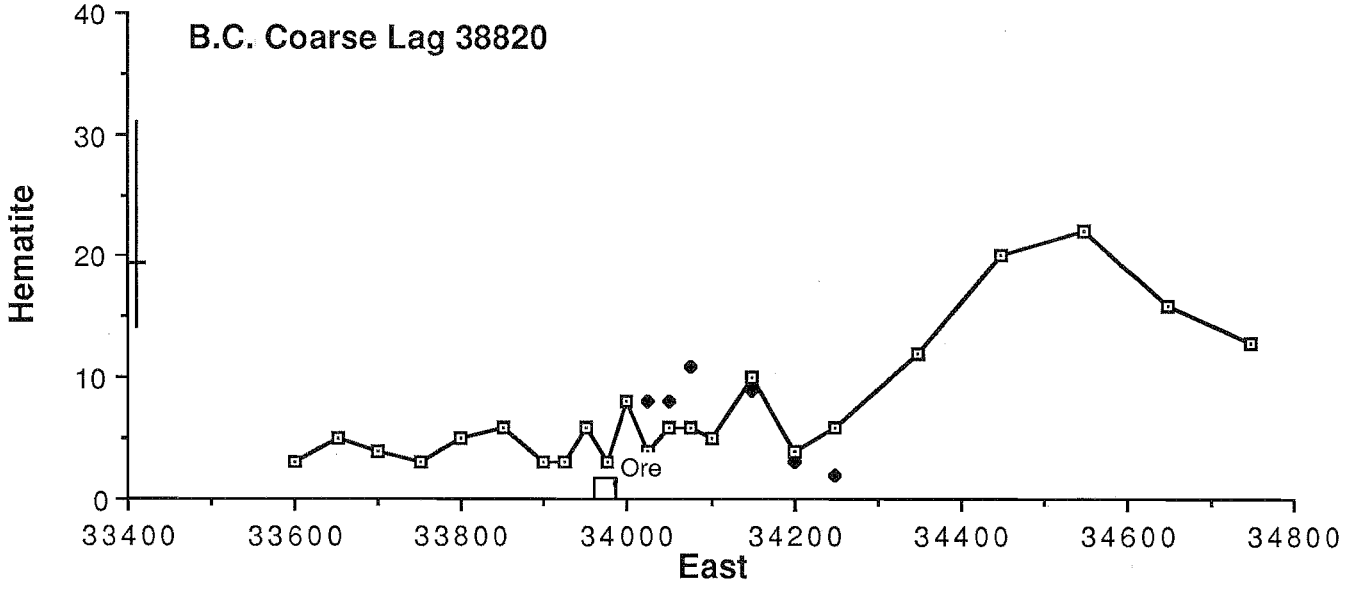
B.C. Coarse Lag 38820
Hematite
40
30
20
10
0
Ore
33400
33600
33800
34000
34200
34400
34600
34800
East

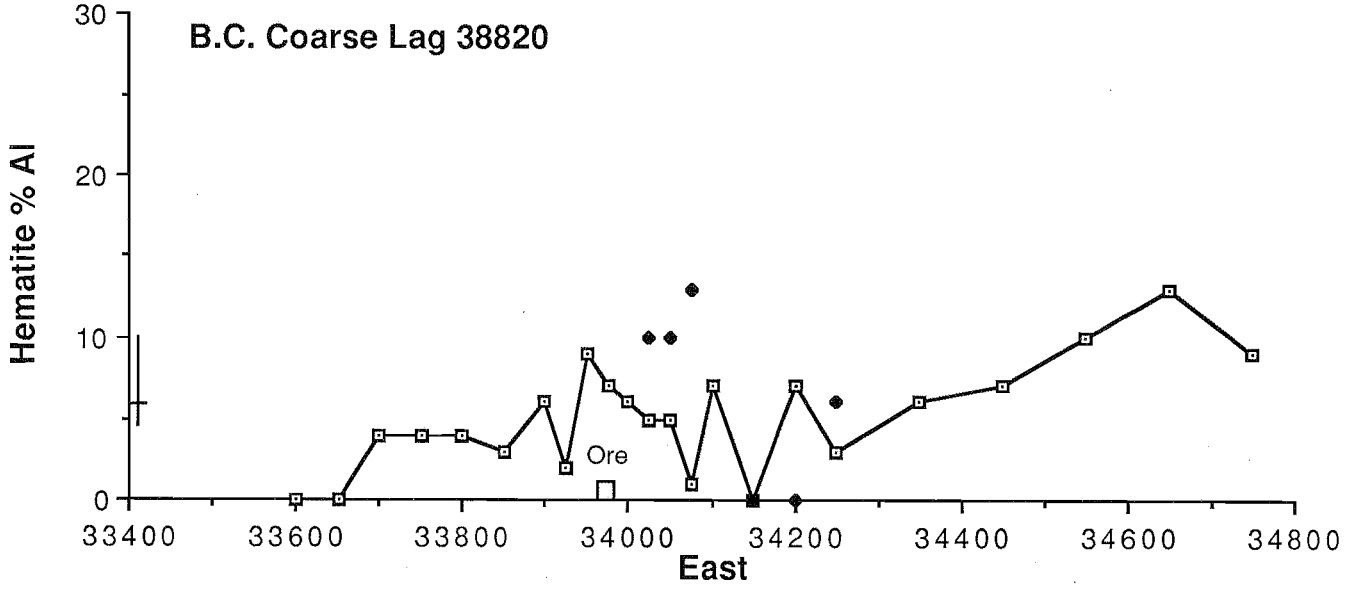
B.C. Coarse Lag 38820
Hematite % Al
30
20
10
0
Ore
33400
33600
33800
34000
34200
34400
34600
34800
East

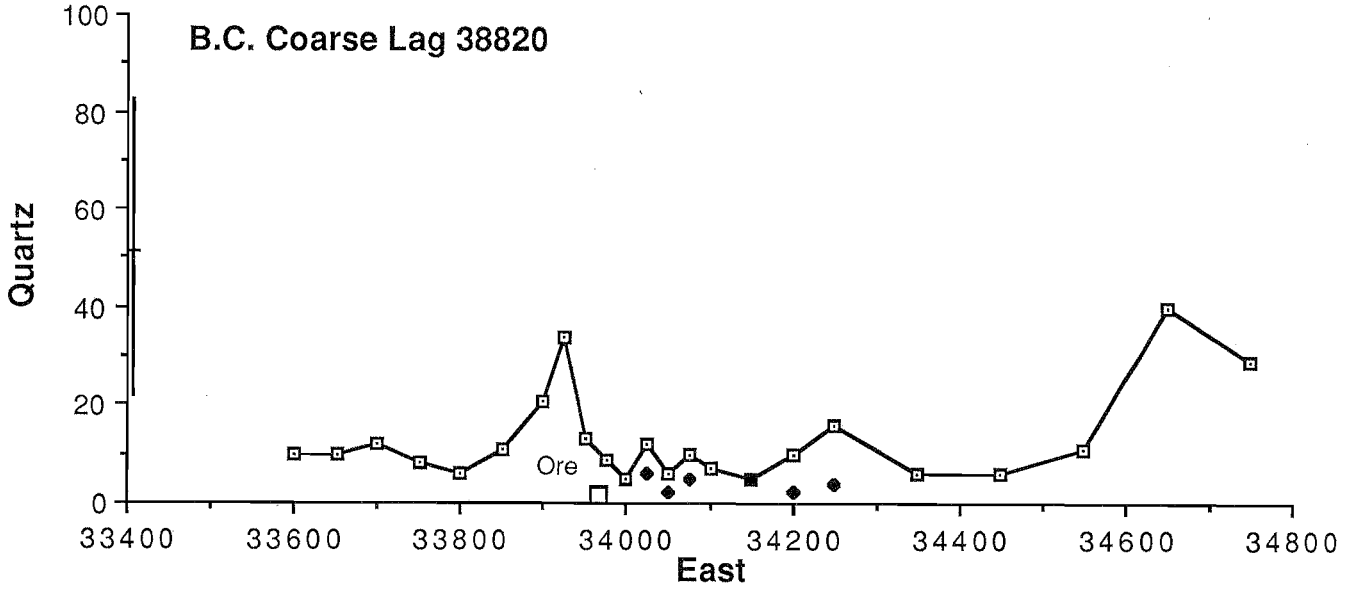
B.C. Coarse Lag 38820
Quartz
100
80
60
40
20
0
Ore
33400
33600
33800
34000
34200
34400
34600
34800
East

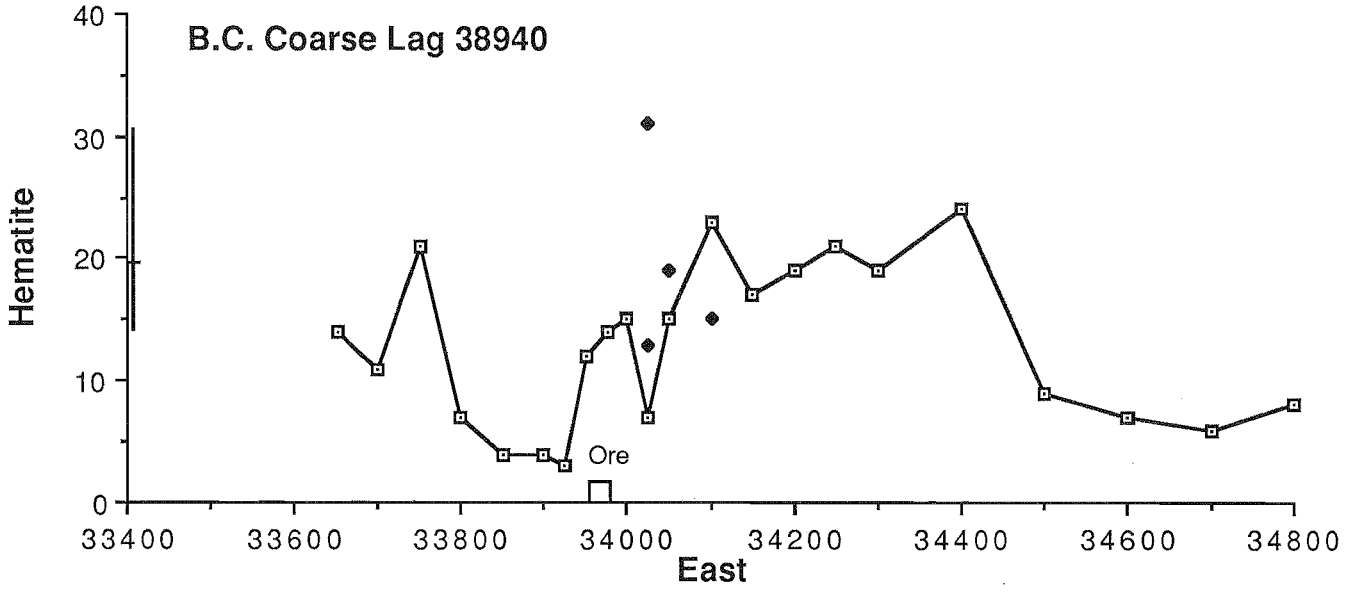
B.C. Coarse Lag 38940
Hematite
40
30
20
10
0
Ore
33400
33600
33800
34000
34200
34400
34600
34800
East

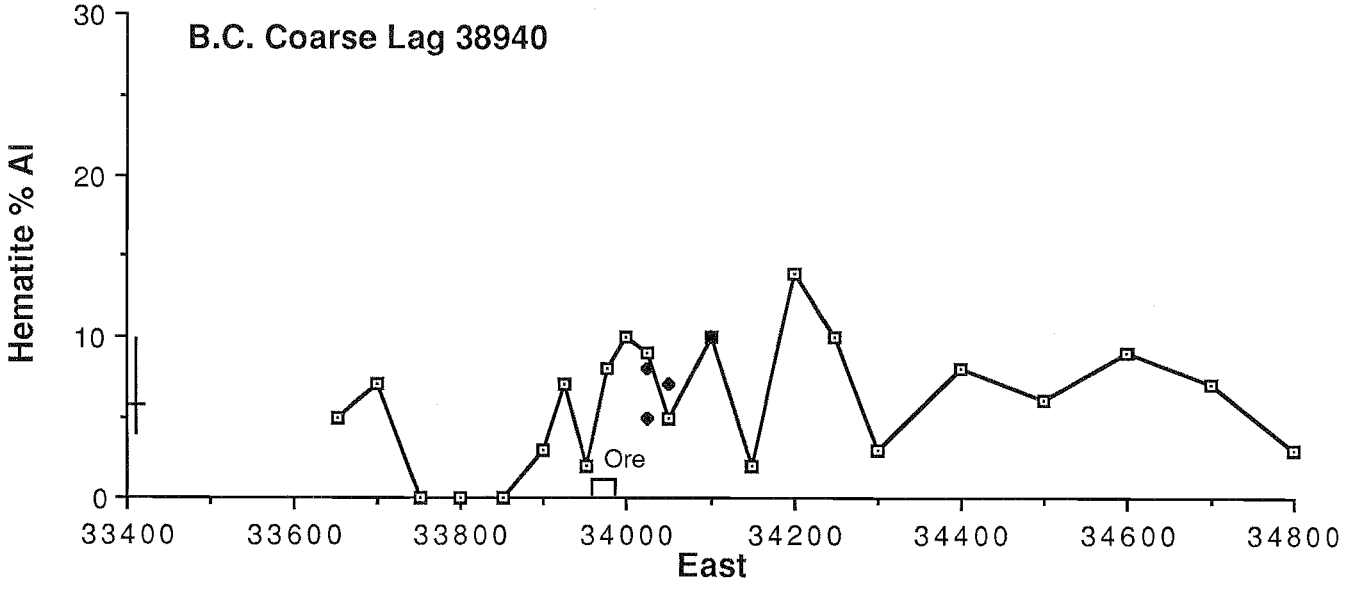
B.C. Coarse Lag 38940
Hematite % Al
30
20
10
0
Ore
33400
33600
33800
34000
34200
34400
34600
34800
East

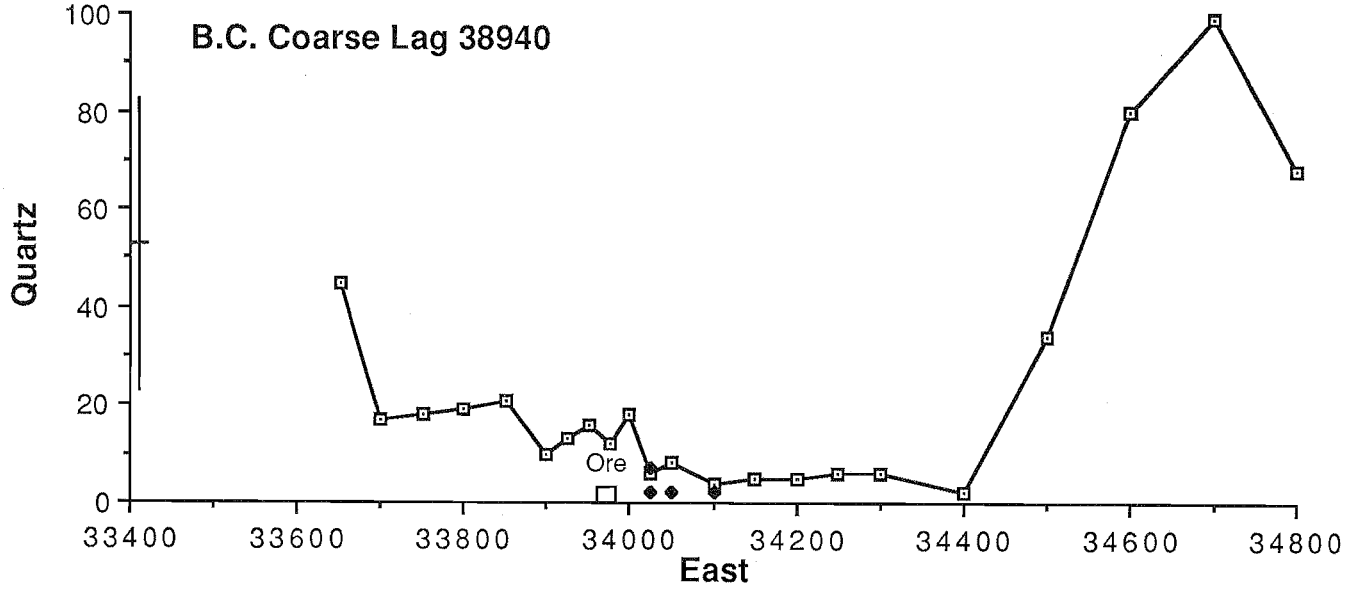
B.C. Coarse Lag 38940
Quartz
100
80
60
40
20
0
Ore
33400
33600
33800
34000
34200
34400
34600
34800
East

FIGURE 11

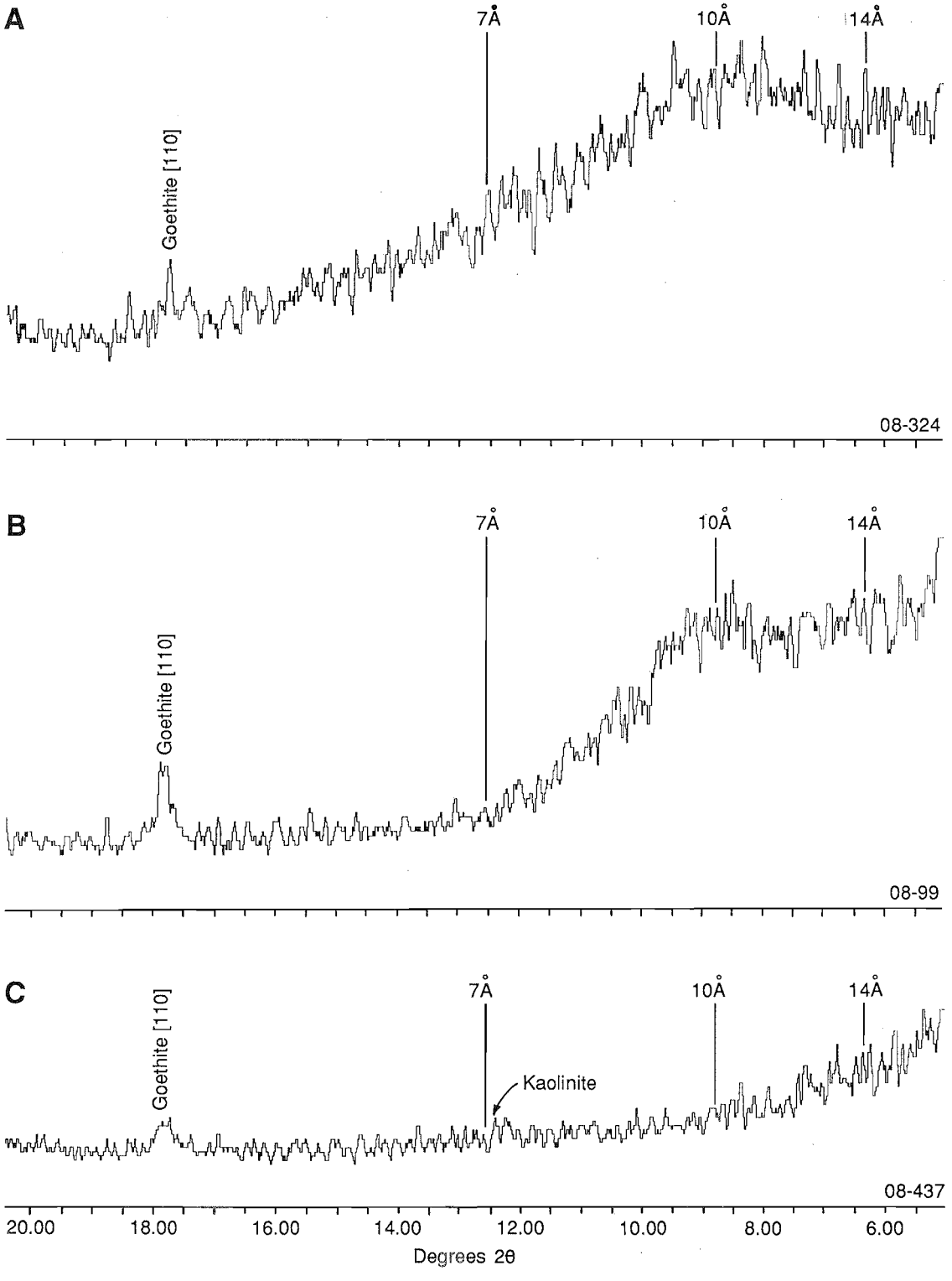

X-ray diffraction traces, illustrating the broad hump in the 8-12 Å range (A and B). The normal asymptotic background is shown in C. The hump appears to be due to interstratified clays.

The results of the estimation of Al substitution in the goethite and hematite are given in Table 4 and graphed in Figure 10. The extent of Al substitution in both goethite and hematite is well-correlated. Though there is a weak anomaly near the ore, the region over the lateritic duricrust is also elevated. The khaki lag shows more extensive Al substitution in goethite than in hematite.

The petrographic study showed some mica relics, set in goethite, and the presence of a potassium-bearing mineral in these relics was confirmed by SEM and microprobe analysis. Mica would generally be expected to be a trace component of the lag. Careful examination of the XRD traces showed only a little well-crystalline mica at 10 Å and this has been recorded in Table 4.

Many XRD traces showed a broad hump on the background in the 8 - 12 Å range (Figure 11A and B). An XRD trace that is typical of the area further east of 34300E (Figure 11C) shows the normal asymptotic background curve. Each XRD trace was examined and the extent of this background hump was estimated on a scale of 0 - 4. This semi-quantitative information has been included in Table 4. The hump is particularly evident in XRD traces of samples from over the orebody and to the west of it on line 38940N. There is a significant hump in the XRD traces of all regional background samples and it is absent in traces from samples from east of 34350E on both lag sample lines. The hump is not due to muscovite or illite, both of which normally give well-defined 10 Å peaks. It is probably due to interstratified clays, which would require detailed investigation, beyond the scope of this report.

7.1.2 Yellow-brown and red-brown clays of the lateritic duricrust and the fine lag

The red-brown and yellow-brown materials, found surrounding ferruginous nodules in the lateritic duricrust, underlying the lag and exposed in the gravel pit, were examined by powder diffractometry using a NaCl internal standard. Both consist essentially of gibbsite, with a lesser quantity of goethite. Hematite occurs as a minor component in the red-brown material (responsible for its colour) and as a trace component in the yellow material. The goethite from both materials is strongly Al substituted (29 - 32% for the red-brown material and 27 - 32% for the yellow-brown material). The hematite of the red-brown material is 9% Al substituted but the hematite in the yellow material was too scarce for meaningful estimation.

The yellow and reddish-brown, generally pisolitic, granular component of the fine lag (taken from samples 08-212, 08-216, 08-255 and 08-453) looks very similar to that binding the lateritic duricrust, so it and the khaki lag were also examined for comparison. They all consist of a mixture of goethite and kaolinite with lesser amounts of hematite and a trace of quartz and possibly a trace of gibbsite. This is markedly different from the lateritic duricrust and demonstrates how field similarities can be deceptive.

7.2 Microprobe Analysis

7.2.1 Mica Relics

The microprobe analyses and the structural formula of the average mica together with the two most potassium-rich micas are given in Table 5. The range in K (1.53 - 6.68%) is lower than would be expected for muscovite and so is the sum of the larger cations (Na, K, Ca) which link the tetrahedral sheets. Some hydronium ions would have to be present to maintain the charge balance. The microprobe totals are low. If the difference (100-Total) is assumed to be H_2O, then hydronium is high, suggesting an illite (hydromica) composition. This is to be expected as loss of K is a common preliminary step in the weathering of mica (Banfield and Eggleton, 1988; Wang, 1988).

TABLE 5

MICROPROBE ANALYSES OF MICAS FROM SAMPLE 08-108A

Analysis No	SiO2 %	TiO2 %	Al2O3 %	FeO %	MgO %	CaO %	K2O %	Na2O %	Cr2O3 ppm	Total %
11939	45.23	0.51	31.75	5.33	1.94	0.07	4.79	0.09	278	89.71
11940	47.74	1.19	31.87	2.84	1.86	0.05	2.78	0.07	1464	88.39
11941	34.56	0.57	25.19	23.26	1.27	0.15	5.76	0.19	765	90.95
11942	46.64	0.81	32.98	2.43	1.58	0.07	3.49	0.04	199	88.05
11943	49.96	0.94	34.27	2.21	1.78	0.02	2.60	0.05	331	91.83
11944	48.35	0.51	33.84	3.12	2.19	0.77	3.09	0.06	364	91.93
11945	39.16	0.46	27.37	12.87	1.82	0.49	6.68	0.09	196	88.95
11946	49.96	0.92	34.26	2.57	1.89	0.03	2.68	0.05	881	92.37
11948	49.62	0.55	35.20	2.49	1.91	0.00	3.32	0.06	510	93.16
11949	52.29	0.89	35.64	2.05	1.84	0.00	2.03	0.03	251	94.77
11950	52.78	0.96	36.14	2.16	1.81	0.02	1.53	0.03	0	95.44
11951	45.68	0.38	30.55	3.64	2.04	0.12	3.73	0.08	734	86.21
11952	47.18	0.60	33.08	3.44	1.82	0.04	3.74	0.06	0	89.97
Mean	46.86	0.72	32.47	5.26	1.83	0.14	3.56	0.07	459	90.90

TABLE 5 (contd)

MICA STRUCTURAL FORMULA

Analysis	11941	11945	Mean
	Tetrahedral Site		
Si	5.431	5.910	6.368
Al	2.569	2.090	1.632
	Octahedral Site		
Al	2.096	2.778	3.568
Ti	0.067	0.052	0.074
Cr	0.014	0.004	0.007
Mg	0.298	0.409	0.371
Fe+2	3.057	1.624	0.598
	Large Cation Site		
Ca	0.025	0.079	0.020
Na	0.058	0.026	0.018
K	1.155	1.286	0.617

Corresponds to an Illite with admixture of iron (goethite)

TABLE 5 (contd)

SAMPLE 08-108A
GOETHITE SURROUNDING MICA RELICS

Analy No	SiO2 %	Al2O3 %	FeO %	TiO2 %	MnO %	MgO %	CaO %	Na2O %	K2O %	As ppm	Ba ppm	Sr ppm	Cu ppm	Cr ppm	Zn ppm	Total %
11840	1.56	1.04	81.12	0.25	0.00	0.07	0.24	0.12	0.09	296	464	0	0	339	0	84.49
11841	1.37	0.99	81.76	0.64	0.00	0.03	0.25	0.14	0.08	307	258	107	101	243	0	85.26
11842	2.70	1.60	76.85	0.13	0.02	0.18	0.80	0.13	0.50	221	243	140	164	389	0	82.91
11843	1.53	0.88	82.03	0.04	0.00	0.06	0.21	0.10	0.10	452	180	116	92	341	149	84.95
11845	1.40	0.90	81.66	0.00	0.00	0.03	0.19	0.10	0.08	371	3505	181	127	292	0	84.36
11846	1.59	0.93	81.99	0.05	0.00	0.05	0.23	0.11	0.13	221	322	0	87	255	114	85.08
11847	1.42	1.04	81.56	0.42	0.00	0.03	0.22	0.10	0.08	155	294	116	100	305	0	84.87
11848	1.42	0.87	82.15	0.17	0.00	0.04	0.18	0.11	0.07	0	157	123	0	287	0	85.01
11854	1.70	1.06	82.40	0.06	0.01	0.04	0.20	0.02	0.09	261	368	93	96	289	0	85.58
11855	2.22	1.67	75.65	0.06	0.02	0.20	0.27	0.10	0.08	194	0	245	0	306	0	80.27
11857	1.50	0.94	82.43	0.04	0.00	0.04	0.18	0.05	0.04	202	237	154	0	314	0	85.22
11858	1.50	1.05	82.86	0.05	0.00	0.03	0.23	0.07	0.06	386	239	147	111	372	0	85.85
Mean	1.66	1.08	81.04	0.16	0.00	0.07	0.27	0.10	0.12	256	522	119	73	311	22	84.49
Sd.Dev	0.40	0.27	2.30	0.19	0.01	0.06	0.17	0.03	0.12	120	946	68	58	43	52	3.55

AS ABOVE BUT MIXED WITH MICA

Analy No	SiO2 %	Al2O3 %	FeO %	TiO2 %	MnO %	MgO %	CaO %	Na2O %	K2O %	As ppm	Ba ppm	Sr ppm	Cu ppm	Cr ppm	Zn ppm	Total %
11839	21.22	17.72	41.35	0.37	0.01	1.39	0.45	0.09	4.34	0	963	0	150	275	0	86.94
11844	8.90	6.39	67.03	0.20	0.04	0.36	0.42	0.10	2.03	172	310	0	0	278	0	85.47

TABLE 5 (contd)

VEIN GOETHITE - SAMPLE 08-108A

Analy No	SiO2 %	Al2O3 %	FeO %	TiO2 %	MnO %	MgO %	CaO %	Na2O %	K2O %	As ppm	Ba ppm	Sr ppm	Cu ppm	Cr ppm	Zn ppm	Total %
11860	1.34	0.70	81.37	0.00	0.00	0.02	0.09	0.16	0.01	0	151	0	0	288	0	83.69
11861	1.24	0.60	81.35	0.00	0.00	0.00	0.07	0.06	0.01	0	0	155	0	359	0	83.33
11862	1.30	0.91	81.83	0.00	0.00	0.03	0.15	0.18	0.02	179	186	0	0	488	0	84.42
11863	1.28	1.09	82.10	0.00	0.00	0.05	0.23	0.11	0.02	230	300	190	0	466	0	84.88
Mean	1.29	0.83	81.66	0.00	0.00	0.03	0.14	0.13	0.02	102	159	86	0	400	0	84.08
Sd.Dev	0.04	0.22	0.37	0.00	0.00	0.02	0.07	0.05	0.01	120	124	101	0	94	0	0.78

TABLE 5 (contd)

MATTED GOETHITE - SAMPLE 08-104A

Analy No	SiO2 %	Al2O3 %	FeO %	TiO2 %	MnO %	MgO %	CaO %	Na2O %	K2O %	As ppm	Ba ppm	Sr ppm	Cu ppm	Cr ppm	Zn ppm	Total %
11865	3.84	2.77	75.18	0.05	0.08	0.23	0.20	0.00	0.01	0	109	0	235	119	746	82.36
11866	3.35	2.30	73.79	0.06	0.08	0.20	0.06	0.00	0.01	163	184	0	161	79	1042	79.85
11867	6.65	5.20	67.95	0.04	0.07	0.19	0.22	0.02	0.01	0	233	0	129	0	924	80.35
11868	5.02	3.20	74.24	0.06	0.08	0.25	0.24	0.01	0.01	161	156	0	196	0	1090	83.11
11869	3.88	2.44	74.50	0.15	0.07	0.21	0.14	0.02	0.01	202	179	197	181	140	1173	81.42
11870	5.59	3.96	72.10	0.10	0.08	0.17	0.18	0.00	0.01	0	262	0	178	78	924	82.19
11871	5.00	3.78	70.83	0.03	0.09	0.14	0.13	0.03	0.01	0	338	189	302	0	1029	80.04
11872	3.54	2.48	74.54	0.03	0.08	0.19	0.10	0.00	0.00	0	204	114	276	0	1168	80.96
11873	3.59	2.50	74.85	0.05	0.08	0.26	0.09	0.00	0.00	0	163	0	290	99	1124	81.42
Mean	4.50	3.18	73.11	0.06	0.08	0.20	0.15	0.01	0.01	58	203	56	216	57	1024	81.30
Sd.Dev	1.13	0.97	2.39	0.04	0.01	0.04	0.06	0.01	0.00	88	67	86	62	57	139	4.65

SECONDARY GOETHITE - SAMPLE 104A(1)

Analy No	SiO2 %	Al2O3 %	FeO %	TiO2 %	MnO %	MgO %	CaO %	Na2O %	K2O %	As ppm	Ba ppm	Sr ppm	Cu ppm	Cr ppm	Zn ppm	Total %
11874	9.64	1.83	69.04	0.02	0.08	0.31	0.17	0.02	0.05	0	214	145	215	0	469	81.16
11875	10.20	1.65	69.73	0.02	0.07	0.35	0.17	0.00	0.05	0	239	0	198	72	440	82.24
11876	18.44	1.18	59.60	0.02	0.07	0.17	0.18	0.05	0.13	0	0	0	86	0	668	79.84
11877	17.66	1.36	62.11	0.01	0.07	0.18	0.18	0.04	0.16	0	90	0	156	0	400	81.77
11878	27.44	1.18	52.10	0.00	0.06	0.15	0.14	0.05	0.14	0	102	0	0	0	525	81.26
11879	1.35	1.24	50.26	0.01	0.13	0.14	0.32	0.00	0.02	0	143	91	0	0	683	53.47
11880	1.71	1.38	62.27	0.02	0.13	0.12	0.29	0.02	0.02	230	163	0	92	75	800	65.96
Mean	12.35	1.40	60.73	0.01	0.09	0.20	0.21	0.03	0.08	33	136	34	107	21	569	75.10
Sd.Dev	9.48	0.25	7.52	0.01	0.03	0.09	0.07	0.02	0.06	87	81	60	87	36	149	17.53

TABLE 5 (contd)

SECONDARY COLLOFORM GOETHITE - SAMPLE 104A

Analy No	SiO2 %	Al2O3 %	FeO %	TiO2 %	MnO %	MgO %	CaO %	Na2O %	K2O %	As ppm	Ba ppm	Sr ppm	Cu ppm	Cr ppm	Zn ppm	Total %
11881	4.27	2.92	73.81	0.01	0.12	0.17	0.62	0.02	0.02	0	177	164	402	83	476	81.96
11882	6.03	2.83	72.14	0.01	0.10	0.22	0.72	0.00	0.03	0	249	0	321	0	477	82.08
11883	6.11	2.57	71.59	0.02	0.16	0.26	1.01	0.03	0.05	0	432	0	360	0	296	81.80
Mean	5.47	2.77	72.51	0.01	0.13	0.22	0.78	0.02	0.03	0	286	55	361	28	416	81.95
Sd.Dev	1.04	0.18	1.16	0.01	0.03	0.05	0.20	0.02	0.02	0	131	95	41	48	104	2.69

TABLE 5 (contd)

GOETHITE SURROUNDING MICA RELICS - SAMPLE 443A

Analy No	SiO2 %	Al2O3 %	FeO %	TiO2 %	MnO %	MgO %	CaO %	Na2O %	K2O %	As ppm	Ba ppm	Sr ppm	Cu ppm	Cr ppm	Zn ppm	Total %
11912	5.97	3.83	69.77	0.03	0.05	0.30	0.06	0.02	0.27	0	144	0	148	205	423	80.30
11915	3.72	2.45	75.34	0.02	0.03	0.29	0.05	0.02	0.13	0	334	147	195	217	510	82.05
11916	9.46	6.45	66.49	0.05	0.06	0.24	0.10	0.03	0.26	188	174	0	216	376	345	83.14
11918	3.66	2.46	74.03	0.01	0.03	0.22	0.03	0.00	0.05	0	0	0	262	669	514	80.49
Mean	5.70	3.80	71.41	0.03	0.04	0.26	0.06	0.02	0.18	47	163	37	205	367	448	81.49
Sd.Dev	2.73	1.88	4.05	0.02	0.02	0.04	0.03	0.01	0.11	94	137	74	47	216	80	8.88

AS ABOVE BUT MIXED WITH MICA

Analy No	SiO2 %	Al2O3 %	FeO %	TiO2 %	MnO %	MgO %	CaO %	Na2O %	K2O %	As ppm	Ba ppm	Sr ppm	Cu ppm	Cr ppm	Zn ppm	Total %
11910	7.57	5.39	67.39	0.04	0.03	0.34	0.04	0.00	1.34	0	188	0	0	112	347	82.14
11911	8.33	5.70	65.43	0.02	0.05	0.28	0.05	0.04	1.34	0	269	99	84	166	507	81.24
11913	14.29	10.16	54.49	0.04	0.04	0.36	0.07	0.03	2.62	0	343	210	143	340	318	82.10
11914	7.88	5.59	68.77	0.03	0.03	0.35	0.04	0.00	1.34	0	134	0	0	69	351	84.03
11917	13.09	9.71	56.54	0.03	0.04	0.40	0.07	0.04	1.85	0	311	109	0	235	348	81.77
Mean	10.23	7.31	62.52	0.03	0.04	0.35	0.05	0.02	1.70	0	249	84	45	184	374	82.26
Sd.Dev	3.20	2.40	6.55	0.01	0.01	0.04	0.02	0.02	0.56	0	87	88	66	107	75	12.81

7.2.2 Goethites

Microprobe analyses of the goethites are given in Table 5. The goethites of three specimens, 08-108A, 08-104A and 08-443A were examined. They have been subdivided according to their petrographic relationships.

Analyses of two goethites surrounding mica relics (Specimen 08-108A, from above the orebody) showed significant quantities of Si, Al and K. This indicates admixture of goethite with mica on a sub-micron scale and these have been segregated. The remainder (12) did not. Four microprobe analyses of vein goethite were carried out for comparison. The goethite of the vein is not significantly different (95% confidence) from the goethite surrounding the mica relics in any elements except for Cu and Cr; the goethite surrounding the mica is richer in these elements.

The average structural formulae of these two materials, which were calculated by summing Fe and Al to unity are illustrated in Table 6. There is 1.4 - 1.8% Al substitution in the goethite molecule. Water has been estimated from the probe analysis total and this implies that the goethite could be partly dehydrated to hematite (40%). However, this assumes that porosity plays little part, which may not be entirely true.

Three phases of goethite were analysed in specimen 08-104A, from above mafic schists on line 38940N, a matted goethite with layer silicate pseudomorphs, a secondary goethite and a secondary colloform goethite. The matted goethite is a relatively homogenous material. In contrast, the secondary goethite is rather inhomogeneous in its Si content (1.3 - 27.0%). Both K and Al are minor constituents, so it seems that silica is the contaminant rather than clay or mica. The secondary colloform goethite appears homogenous. It is quite similar in composition to the matted goethite, but it is slightly richer in Mn, Ca, K and Cu and slightly poorer in As and Zn. The matted goethite, which pseudomorphs layer silicates, is however significantly richer in Si, Al, Mn, Mg, Cu and Zn and poorer in Fe, Na, K and Cr than the goethite surrounding the micas in 08-108A. The Si/Al ratio is close to unity, suggesting the presence of sub-micron quantities of clay (kaolinite).

The structural formulae of the matted goethite and the colloform goethite of specimen 08-104 A may be compared in Table 7. These goethites show 5% Al substitution and the estimated water content suggests that they may approximate true goethites with little dehydration to hematite, however the effect of porosity cannot be discounted.

The goethites surrounding mica relics in specimen 08-443A were analysed. They fall into two distinct groups, ordinary goethites and goethites containing sub-micron scale mica. The former goethites are richer in Si, Al, Mn, Mg, Cu and Zn and poorer in Fe, Ca and As than the equivalent goethites in specimen 08-108A. The goethites surrounding the micas of 08-443A show 7% Al substitution and do not seem to be dehydrated (Table 8). Again the presence of significant quantities of Si, Al and K indicate remnant sub-micron scale mica.

TABLE 6
SPECIMEN 08-108 A
GOETHITE STRUCTURAL FORMULAE

	1	2
Si	0.024	0.019
Al	0.018	0.014
Fe	0.982	0.986
Ti	0.002	0.000
Mg	0.002	0.001
Ca	0.004	0.002
Na	0.003	0.004
K	0.002	0.000
H	0.629	0.659
Total	1.874	1.872

1 Goethite surrounding micas

2 Goethite from vein material

TABLE 7
SPECIMEN 08-104 A
GOETHITE STRUCTURAL FORMULAE

	3	4
Si	0.069	0.086
Al	0.058	0.051
Fe	0.942	0.949
Ti	0.001	0.000
Mn	0.001	0.002
Mg	0.005	0.005
Ca	0.002	0.013
Na	0.000	0.001
K	0.000	0.001
H	1.088	1.045
Total	2.192	2.215

3 Matted goethite

4 Colloform goethite

TABLE 8
SPECIMEN 08-443 A
GOETHITE STRUCTURAL FORMULA

Si	0.089
Al	0.070
Fe	0.930
Ti	0.000
Mn	0.001
Mg	0.006
Ca	0.001
Na	0.001
K	0.004
H	1.099
Total	2.237

Goethite surrounding micas

8.0 GEOCHEMISTRY

8.1 Geochemical Background

As in any geochemical exercise of this type, establishing geochemical background is of crucial importance. The data provided by the comparatively small database of four samples collected remote from ore (Figure 1G) are referred to as "regional" background. In addition, at least some of the eastern parts of the lag survey lines may be in "local" background (>34400 E). The ranges of the regional background data, together with their geometric mean, have been calculated (Appendices 1 and 2) and are plotted with the data from the survey lines (Appendix 3), allowing the regional and local backgrounds to be compared to the concentrations encountered near the ore.

The geological map of the immediate surroundings of the deposit shows the variety of lithologies that underlie the regional and local background areas; this includes Archaean mafic, and ultramafic rocks as well as Permian glacial sediments. If the geochemistry of the lag reflects these underlying rocks, then variation in background is to be expected. In spite of this, the "regional" background lag samples are all, as well as can be determined, distant from ore.

8.2 Major Oxides

The geochemistry of the lag materials is discussed systematically, by elements, so that the performance of each fraction can be compared and the signal produced by the centrally located sample line (38820 N) can be compared to that located across the north end of the orebody (38940 N). It will be necessary to refer repeatedly to Appendix 3.

Most of the major oxides were determined by ICP spectrophotometry and their precision is not as good as that which may be expected from XRF analysis. The iron values are probably a little low but the trends which these oxides show are considered satisfactory. Iron and Ti were also measured by XRF in the pressed powder. These XRF iron values are also approximate and were determined primarily for matrix correction.

8.2.1 SiO_2

The coarse lags on each line show silica levels of 6 - 10% near the ore and into the hanging wall but the silica background away from ore is significantly higher (11 - 18%). This is particularly apparent in the eastern extensions to the lag survey (>34300 E). The fine lag and the non-magnetic component of the fine lag both show high silica (15 - 35%) distant from ore and low silica over ore. The magnetic component has a very consistent silica level of 5 - 10%. The khaki lag has a similar to significantly higher Si content than the corresponding black lag, reflecting its kaolinite content.

8.2.2 Al_2O_3

The coarse black lags near the ore are slightly depleted in Al relative to background. All the khaki lag is very Al-rich, reflecting both its elevated clay content and significant goethite Al substitution (Section 7.1.1, Figure 10). On the other hand, all components of the fine lags have Al ranges which correspond closely to background. In general, the Al content of the fine lag is significantly higher than that of the coarse lag, reflecting the numerous clay granules included in this sample medium. The fine lag and its non-magnetic component show a weak depletion in the vicinity of the ore, similar to that shown by the coarse lag. The magnetic component of the fine lag is slightly depleted in Al in relation to the non-magnetic component and its Al level is more consistent than in the others, showing no visible depletion near ore.

8.2.3 Fe_2O_3

The XRF data and the ICP data are consistent, though the XRF data show less scatter and are preferable. Though the coarse lags over the ore correspond in range to regional background (XRF), there seems to be a slight increase in Fe content over the ore within this range. This is better shown by the fine lag and its non-magnetic component (45 - 70% Fe_2O_3). The magnetic component of the fine lag shows the expected iron enrichment (70 - 76% Fe_2O_3), but the iron anomaly has been removed. The khaki lag shows iron depletion relative to the black lag. The cellular ironstone (Section 5.2) has a similar Fe content to the magnetic component of the fine lag (Appendix 7).

Strong correlations (Table 9) of Fe occur with As, Pb, Se, W and Zn, particularly in the non-magnetic component of the fine lag. Significant quantitites of As, Cu, Mn, and Zn are concentrated in the cellular ironstone component (Appendix 7). This illustrates the well-known adsorption of trace elements, notably Zn and As, on goethite. In view of these high correlations of key target elements with Fe in the non-magnetic component, it seems that use of the magnetic component of the fine lag on its own is a poor choice. This will be discussed further in Sections 8.3.3 and 9.7.

TABLE 9
CORRELATION MATRIX FOR IRON

Fraction	Coarse	Fine	Magnetic	Non-Mag
n	49	48	48	48
TiO_2	-0.460	0.670	0.337	0.676
As	0.333	0.310	0.019	0.412
Au	0.266	0.391	0.191	0.311
Ba	-0.316	0.373	0.060	0.381
Cu	-0.411	0.236	-0.326	0.375
Ga	-0.407	0.546	0.336	0.492
Mn	0.047	0.399	0.464	0.440
Pb	-0.181	0.721	0.098	0.804
Se	-0.441	0.440	0.089	0.418
V	-0.399	0.862	0.592	0.862
W	-0.101	0.392	0.562	0.527
Zn	0.332	0.302	-0.011	0.501

Correlations of > $\pm$ 0.3 are significant (95% confidence)
See Appendix 6 for a complete matrix

8.2.4 *Si, Al and Fe Relationship*

The oxides SiO_2, Al_2O_3 and Fe_2O_3, together with water, comprise over 90% of the lags, so these three oxides are inter-dependent. Where Fe increases, there are corresponding decreases in Si and Al. The ternary distributions in both lag fractions is illustrated in Figure 12. The larger range in the Si content of the fine lag is in part due to dilution of the lag by chips of quartz and in part due to clay granules. The relationship between Fe and Au in both fractions and the Al-rich nature of the duricrust-related khaki lag are clearly illustrated. The fine lag is generally more Al rich than the coarse lag, indicating the presence of a small component of fine khaki lag.

FIGURE 12

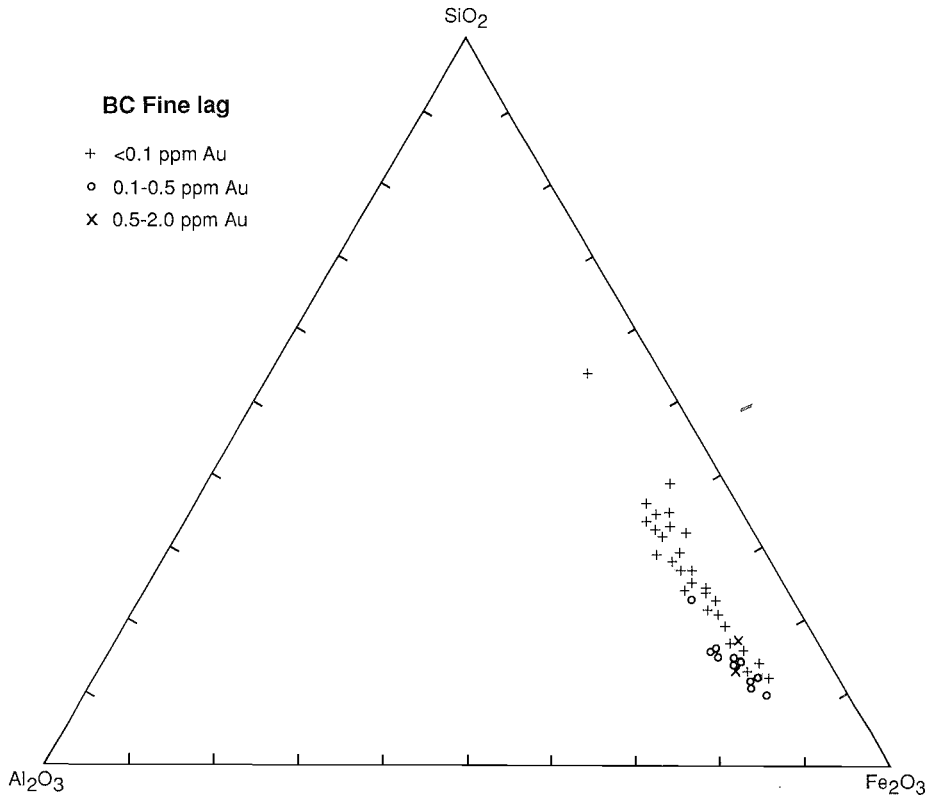
SiO2
BC Fine lag
+ <0.1 ppm Au
o 0.1-0.5 ppm Au
x 0.5-2.0 ppm Au
Al2O3
Fe2O3

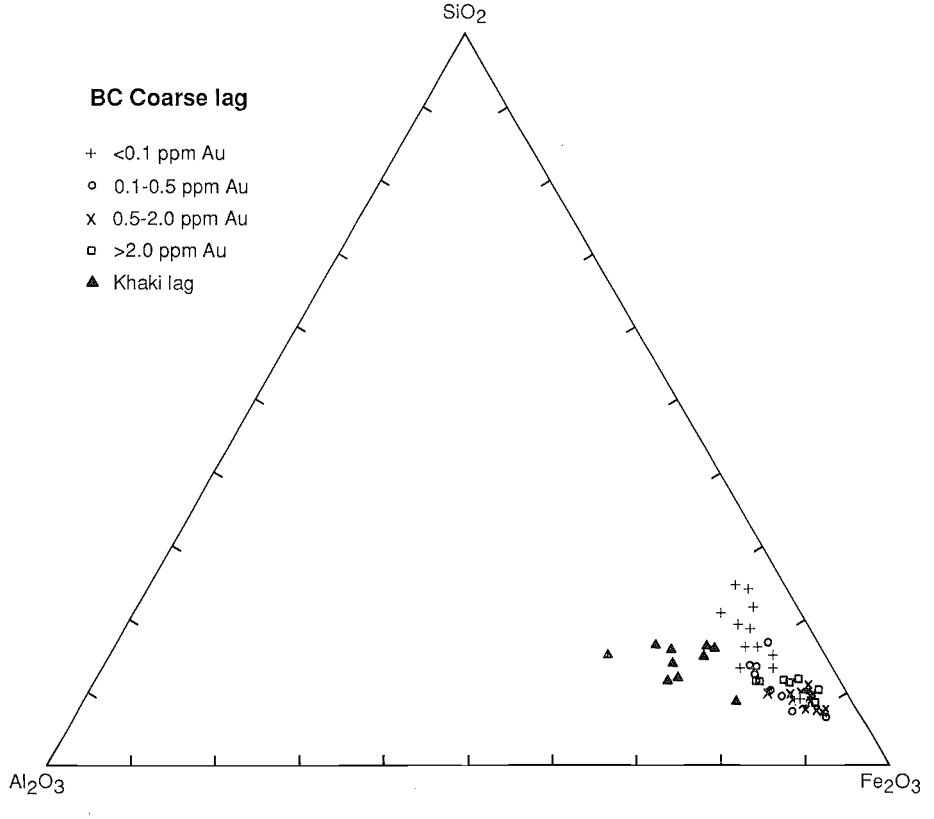
SiO2
BC Coarse lag
+ <0.1 ppm Au
o 0.1-0.5 ppm Au
x 0.5-2.0 ppm Au
□ >2.0 ppm Au
▲ Khaki lag
Al2O3
Fe2O3

FIGURE 13

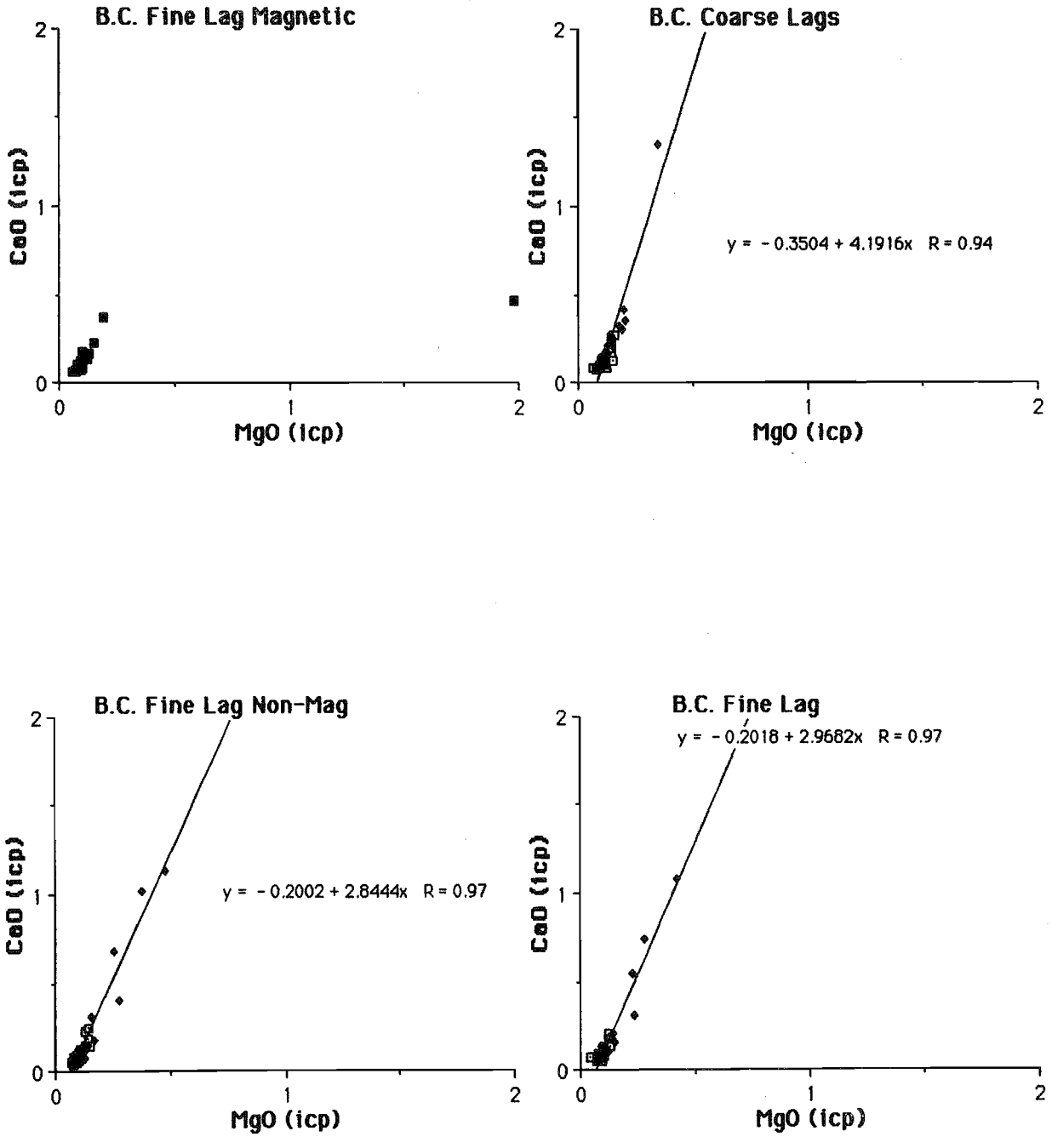
B.C. Fine Lag Magnetic
CaO (icp)
MgO (icp)
B.C. Coarse Lags
y = -0.3504 + 4.1916x R = 0.94
B.C. Fine Lag Non-Mag
y = -0.2002 + 2.8444x R = 0.97
B.C. Fine Lag
y = -0.2018 + 2.9682x R = 0.97

FIGURE 14

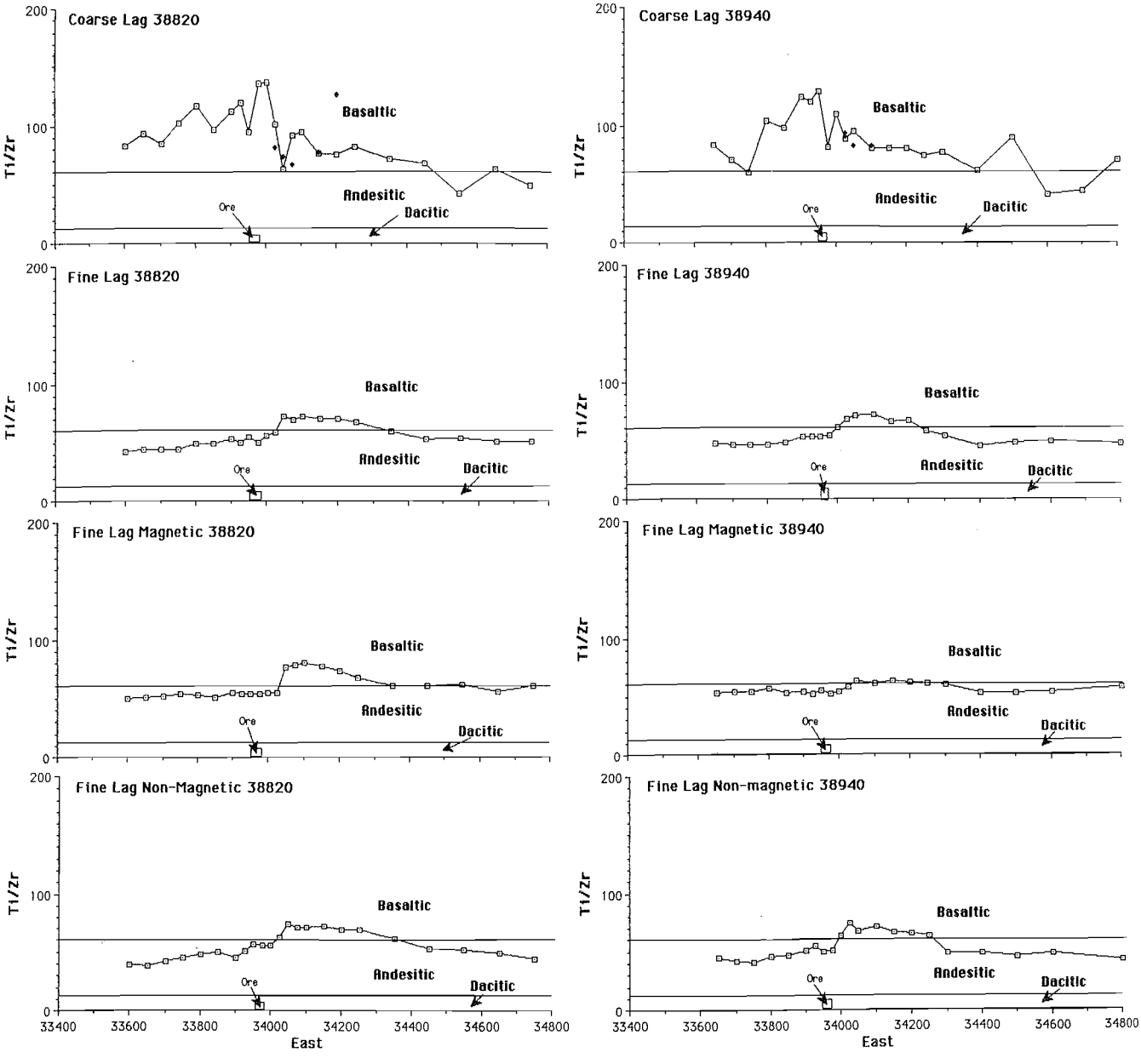
Coarse Lag 38820
Coarse Lag 38940
Fine Lag 38820
Fine Lag 38940
Fine Lag Magnetic 38820
Fine Lag Magnetic 38940
Fine Lag Non-Magnetic 38820
Fine Lag Non-magnetic 38940
Ti/Zr
200
100
0
Basaltic
Andesitic
Dacitic
Ore
33400
33600
33800
34000
34200
34400
34600
34800
East

8.2.5 MgO and CaO

Both these oxides are highly correlated (r=0.94 for the coarse lag and 0.97 for the fine lag). Both lag fractions show anomalies associated with the ore position. Line 38820 shows a low dispersion for 100 - 200 m on either side of the ore but line 38940 shows a gentle build up to the west and a very strong peak immediately to the east of the ore position. This strong anomaly in MgO and CaO is associated with outcrops of calcrete (Robertson and Churchward, 1989). There is little difference between the behaviour of MgO and CaO in any of the fine lag components (total, magnetic and non-magnetic), all show co-incident peaks in the vicinity of the ore. Examination of scattergrams for these two elements (Figure 13) shows that the CaO : MgO ratio is remarkably consistent (3 - 4) for both survey lines and for all lag fractions. Initially it was suspected that this was a reflection of the underlying calcrete, however the only calcrete analysed to date is Standard 10, from the south-east edge of the pit (34100E, 38620N), with a CaO : MgO ratio of 20.99 : 0.75 or 28. This will need detailed interpretation when analytical data from other calcretes become available. The calcrete component of the fine lag has a CaO : MgO ratio of 12.86. Nevertheless, the Mg, Ca and Sr anomalies are clearly a calcrete signature and cannot be used as indictors of ore (Appendix 7).

8.2.6 TiO_2

The coarse lag overlying the ore is poor in Ti relative to background and the duricrust-related khaki lag is very Ti-rich. Thus all components of the fine lag show a Ti anomaly over the subcrop of the lateritic duricrust and show levels which correspond to background over the ore.

The Ti/Zr ratio (Hallberg, 1984) was used by Robertson and Gall (1988) as an indicator of the parent rock types in the weathered profile at Beasley Creek, which are predominantly basaltic. The coarse lags show a similar predominantly basaltic Ti/Zr ratio (Figure 14). The fine lag, on the other hand, shows a typical basaltic signature only over the zone underlain by duricrust; the remainder, particularly over the ore, has an andesitic Ti/Zr ratio. It seems that Ti is diminished relative to Zr in the fine lag. The red and yellow clay component shows no appreciable Ti lowering relative to Zr (Ti/Zr = 72) in the fine lag but the magnetic component (Ti/Zr = 53), the cellular ironstone (Ti/Zr = 51) and particularly the calcrete (38) show strong lowering of the Ti/Zr ratio (Appendix 7).

8.3 Trace Elements

8.3.1 Ag

Almost all the XRF Ag data are at or below the detection limit, so an improved method (ICP/MS with a detection limit of 0.1 ppm) would be desirable for further work. The khaki lag appears to be richer in Ag than the corresponding coarse black lag. Silver is highly mobile in the weathering environment and its precipitation conditions are different from that of gold, from which it is readily parted. It is said to be adsorbed by Mn and Fe oxides and by organic matter but it shows no strong correlations with any other element in any of the lag fractions.

8.3.2 As

There is a significant As anomaly associated with the ore host saprolite at Beasley Creek (average 42 ppm, reaching 226 ppm; Robertson and Gall, 1988). In contrast, a mean value of 3.5 ppm has been reported from the footwall rocks, which corresponds closely with the expected background for mafic rocks.

The best As anomaly over the ore occurrs in the coarse lags, particularly on line 38940, where it reaches 1040 ppm and exceeds 200 ppm over a width of 200 m. The fine lag shows similar, more consistent but weaker anomalies. Though As tends to co-precipitate with iron hydroxides, there is virtually no As response in the magnetic component of the fine lag on either line but As is significantly enhanced in the non-magnetic component. Scatter plots of Fe and As (not shown) indicate a relationship but calculation of an As residual only marginally improved the anomaly to background relationship. Arsenic in the khaki lag tends to be lower than in the corresponding coarse black lag. Arsenic lies in the cellular ironstone component of the fine lag rather than in the clay-rich component (Appendix 7).

8.3.3 Au

Gold has a wide abundance range (four orders of magnitude), so both the normal and the more useful logarithmic plots in Appendix 3 should be examined. Gold lies above a very consistent background (2 - 10 ppb) over a very wide area. Though isolated samples show over 10 000 ppb in the coarse lags on both lines, an anomalous zone 600 - 900 m wide is over 1000 ppb. This extended beyond the limit of the original sampling, which necessitated extending the survey to the east. The khaki lag is poorer in gold than the corresponding black lag.

The fine lag shows a lower (100 - 1000 ppb) and generally more restricted (200 - 600 m) gold anomaly than the coarse lags. The magnetic component of the fine lag shows an even lower and less dispersed gold anomaly. Here the gold anomaly lies on either side of the ore and has reached background over the ore.

The magnetic component of the fine lag is the least effective Au sampling medium. There is little difference in the width of dispersion of the anomalous Au in the coarse and the fine lag fractions, but in the coarse lag fraction, Au appears to pinpoint the orebody more accurately with some very high values. The fine lag gives more consistent results, probably reflecting its greater dispersion and its finer particle size and thus it is more suitable as a practical sampling medium. Carver *et al* (1987) used the 2.0 - 6.0 mm size fraction probably for this reason. The cellular ironstone component of the fine lag contains significantly more Au than the calcrete and the calcrete significiantly more than the red-brown clays (Appendix 7). Fine lag appears to be a good regional tool and coarse lag could be used for follow-up work.

Elements which show a significant correlation with Au are Fe, Mg, Ca and As in all lag fractions, except for the magnetic component of the fine lag. There are also less pronounced correlations with W, V and Ti.

8.3.4 Ba

A distinct saprolitic Ba anomaly of 1000 - 2000 ppm is associated with the ore host. This reaches 1% in one phyllitic saprolite sample. In contrast, the saprolitic mafic footwall rocks have a range of 60 - 470 ppm (Robertson and Gall, 1988). Barium shows similar distinct lag anomalies, centred on the orebody, particularly in all the fine lag components. Levels of 2000 ppm are common on a background of 100 - 200 ppm. The coarse lags show a higher background range and some very high values on the flats to the east. The high background on the flats to the east is weakly reflected in the fine lag components. Backscatter electron microscopy of some samples shows that Ba is present as $BaSO_4$, filling fractures. It was not possible to distinguish barite from the gangue in the polished section study. The Ba is strongly enriched both in the cellular ironstone component and in the red and yellow clays, relative to the calcrete component (Appendix 7). The Ba anomaly is therefore not associated with the calcrete.

8.3.5 Bi

Most of the XRF Bi data lie close to the detection limit and there is no detectable Bi anomaly. Results may have been improved using ICP/MS, with a detection limit of 0.1 ppm.

8.3.6 Cd

All the Cd data are close to the detection limit, as are the data from the saprolitic ore host rocks (Robertson and Gall, 1988). There is no recognisable Cd anomaly in either.

8.3.7 Ce

The Ce levels in general fall gradually from west to east, suggesting that it is largely influenced by lithology. The eroded basaltic saprolites have a higher Ce level than the duricrust. The background variance in the coarse lags is higher than in the fine lags.

8.3.8 Co

Cobalt concentrations increase slightly over the orebody in all lag fractions except the magnetic component of the fine lag. Again the coarse lag shows a higher background variance than the fine fractions. Cobalt correlates with Cu and Ni in all lag fractions, with Ba in the fine lag , with Cr in the magnetic component of the fine lag and with Ca in the non-magnetic component of the fine lag. It does not show a significant correlation with Fe, Au or Mn. A two-point Co anomaly is recorded in the ore host saprolite (Robertson and Gall, 1988) and both of these samples are relatively Ni-rich. It is either adsorbed on Mn oxides or it could be associated with carbonates. The former is probable as Co is strongly enriched in the Mn-rich cellular ironstone component, relative to the calcrete component (Appendix 7).

8.3.9 Cr

The behaviour of Cr in the coarse and the fine lags is markedly different. The coarse lags to the west of the orebody have a low Cr content, significantly below regional background. A short distance to the east of the ore (100 - 200 m) the Cr levels rise sharply and this corresponds closely with the change from basaltic to ultramafic lithology. The high regional background suggests that the background samples were collected from areas underlain by ultramafic rocks. The fine lag samples, in contrast, show high levels of Cr, both to the east and to the west, but the Cr levels over the orebody and just to the east of the ore, over the lateritic duricrust, show a trough-like depression. Again the regional background has an ultramafic signature.

The chemical properties and ionic radius of Cr^{3+} closely resembles Al^{3+} and Fe^{3+}, so, where it is mobile, it readily concentrates in laterites and clays; however, where it occurs as chromite, it is not readily mobilised and is a resistate element. A trough-like depression in the Cr level, apparent on both sample lines, is present in both the magnetic and the non-magnetic components. The coarse lag shows a high correlation between Al and Cr (0.865) but this is much lower for all the fine lag components (0.298 - 0.349). In contrast, Cr shows a high correlation with Si as well as Ce, La, and Ni in the fine lag components (0.333 - 0.793). Correlations with Sb and Zr are common to both lag fractions. The signal from Cr seems to reflect lithology in the coarse lag, where it is probably immobile (chromite), but the very different pattern shown by the fine lag may be related to Cr in a more mobile form. Neither the XRD nor the petrography revealed the site of Cr in either lag fractions. Chromium is enriched in the red-brown clays relative to the cellular ironstone (Appendix 7).

8.3.10 Cu

There is a distinct Cu anomaly of 200 - 300 ppm in the fine lag over the orebody compared to a background of 100 - 150 ppm. This is enhanced in the non-magnetic component and is not shown by the magnetic component. The regional background fits with the local background. The coarse lag has a Cu anomaly only on line 38940N.

Copper shows particularly strong correlations with the alkaline earth elements Mg, Ca , Sr and, to some extent, with Ba in all lag fractions, except in the magnetic component of the fine lag, suggesting co-precipitation with carbonates. However, Cu is strongly enriched in the cellular ironstone component relative to calcrete (Appendix 7). There is also some correlation with As, Co, Mn, Se, Y and Zn. Copper appears to be a useful indicator element.

The single point 600 ppm Cu ICP anomaly on line 38820 should be ignored. Though the ICP data are systematically slightly higher than the XRF data they are essentially similar. The ICP data show a wider variance than the XRF data so the XRF data are regarded as superior.

8.3.11 Ga

The coarse lags show a broad response of 40 ppm in Ga over the ultramafics but the fine lags show a more localised response over the lateritic duricrust. The area to the west of and over the orebody are slightly lower in Ga. The regional background seems atypical of ultramafic rocks. The magnetic component of the fine lag is more Ga-rich than the non-magnetic component which implies that Ga is associated more with Fe than with Al. A strong correlation of Al with Ga was found in the deeper saprolite at Beasley Creek (Robertson and Gall, 1988) and the Ga levels are similar. This reflects the higher mobility of Ga over Al in the weathering environment. Gallium is also correlated with Fe, Al, Ti, V and Zr. The fine lags show additional correlations with Au, As, Pb and W.

8.3.12 Ge

Almost all the data lie below the detection limit (3 ppm) so the graphs reflect statistical noise. Clearly Ge needs to be analysed to a lower detection limit (1.0 - 0.1) for the results to be meaningful.

8.3.13 In

All the In data are close to the detection limit of 2 ppm, so this element could be more successfully determined by ICP/MS.

8.3.14 La

Like Ce, the La data for the fine lags show a gradual decrease from west to east but the coarse lags show a trough-like distribution, with a localised low to the east of the orebody, over the lateritic duricrust.

8.3.15 Mn

The ICP and the XRF data are closely comparable and there is a wide range in values (2 - 3 orders of magnitude) so a logarithmic plot is particularly appropriate. Both the regional and local backgrounds are closely matched at 500 - 1000 ppm for the coarse lag and 400 - 500 ppm for the fine lag. The coarse lag on line 38820N shows a very marked anomaly over the ore, reaching 20 000 - 45 000 ppm (2.0 - 4.5% Mn) at two points. The anomaly on line 38940N reaches 8000 ppm (0.8% Mn). The fine lag also

shows Mn anomalies but these reach only 1000 - 2000 ppm. All are centred on the orebody or tend slightly towards the hangingwall but they are unmistakable and are 100 - 150 m in width.

The MnO content of some of the ore zone rocks at Beasley Creek reach 12.5% and several exceed 6%. The minerals, cryptomelane and lithiophorite, have been reported from a colloform goethite-hematite rock, enclosed in ferruginised phyllitic saprolite (Robertson and Gall, 1988). Manganese is commonly strongly concentrated in weathered rocks and particularly in laterites and in this case the underlying phyllite was probably enriched in Mn. A large number of trace elements are reputed to be adsorbed onto manganese minerals or co-precipitated with them. An extract of the correlation matrices for the various fractions is presented in Table 10. Manganese correlates well with Fe and the fine lags show a correlation of Mn with As, Se, W and Zn. Other correlations are very inconsistent between lag fractions. There is a particularly strong correlation of Mn and Cu in the non-magnetic lag component and Zn is relatively poorly correlated with Mn in the magnetic component where Mn is already depleted. Manganese is concentrated in the cellular ironstone component of the fine lag (Appendix 7).

TABLE 10
CORRELATION MATRIX FOR MANGANESE

Fraction	Coarse	Fine	Magnetic	Non-Mag
n	49	48	48	48
Fe2O3	0.074	0.399	0.464	0.440
MgO	0.129	0.029	0.122	0.331
TiO_2	-0.099	0.246	0.294	0.255
As	0.065	0.392	0.234	0.432
Ba	0.014	0.302	-0.005	0.235
Co	0.250	0.208	-0.095	0.205
Cu	0.064	0.604	-0.222	0.607
Ga	-0.218	0.108	0.459	0.009
Pb	-0.017	0.372	-0.187	0.378
Se	-0.091	0.280	0.206	0.440
V	-0.245	0.233	0.723	0.204
W	0.014	0.258	0.631	0.217
Y	0.056	0.168	-0.273	0.307
Zn	0.023	0.685	0.163	0.650

Correlations of > $\pm$ 0.3 are significant (95% confidence)
See Appendix 6 for complete matrix.

8.3.16 Mo

The Mo background data all lie very close to the detection limit of 5 ppm. The coarse lag does not show any detectable Mo anomaly, though the noise level in the vicinity of the ore is slightly increased. The regional background of the fine lag shows a much higher variance than the coarse lag, largely due to one sample (8 ppm) but the local background has less variance. The fine lag is weakly to moderately anomalous over the ore and over the duricrust in all fractions. One sample in the phyllitic saprolite of the ore host shows a single point anomaly of 23 ppm in a background of 0 - 5 ppm (Robertson and Gall, 1988). Molybdenum shows little correlation with other elements.

8.3.17 Nb

Almost all the Nb data are below the detection limit and constitute noise. There is no recognisable Nb anomaly associated with the ore and Nb levels in the saprolite are similar to those in the lag. The khaki lag is significantly richer in Nb than the corresponding ferruginous lag (x 2 - 3) and the red-brown clay component of the fine lag is enriched in Nb (Appendix 7).

8.3.18 Ni

Both the ICP and XRF data are strongly correlated. The ICP data are systematically higher but the XRF data are smoother and are preferred. There is no anomalous behavior in Ni associated with the ore except for a slight dip, reflecting an absence of mafic-ultramafic rocks at that point. Nickel concentrations in the coarse lag are sporadically slightly higher over ultramafics at the east end of each line, compared to the mafic lithologies to the west but this is not reflected in the fine lag. Nickel values are typically 20 - 100 ppm in the underlying mafic saprolite. The red-brown clay in the fine lag contains the most Ni relative to the other components (Appendix 7)

8.3.19 Pb

Regional and local background concentrations of Pb are similar and show relatively little variance. The coarse lag shows a two point Pb anomaly 50 - 150 m to the east of the ore on line 38820N and a 3 point anomaly over the ore on line 38940N. Lead values in the coarse lag, on the flats to the east of the hill, are slightly elevated. The fine lag does not show any anomalous Pb. The khaki lag shows generally lower Pb values than the corresponding black lag.

Though there is a weak Pb anomaly in the saprolitic ore host, caution should be exercised where there are weak surficial lead anomalies at a site relatively close to town, where rabbit burrows are common. Support must be sought from corresponding soil samples and, if this is not found, then the possibility of ballistic contamination must be considered.

8.3.20 Rb

The Rb data lie close to the detection limit (5 ppm) and show only noise. Rubidium in the saprolite is likely to be linked to the presence of significant quantities of mica.

8.3.21 Sb

Antimony shows no anomalous behaviour in the coarse lag. Antimony in the fine lag shows moderate anomalous behaviour (7 ppm in a background of 3 ppm) and in the non-magnetic component (5 ppm in a background of 3 ppm). Antimony in the magnetic component shows a distinct step over the ore. There is a significant Sb anomaly in the saprolitic ore host and the levels are similar (8 ppm in a background of 3 ppm). The cellular ironstone seems to carry much of the Sb signal (Appendix 7).

8.3.22 Se

There appears to be a weak Se anomaly (11 ppm in a background of 6 ppm) on line 38940N. This is shown by the coarse lag, the fine lag and the non-magnetic component of the fine lag. The Se signal appears to come from the cellular ironstone component (Appendix 7). The khaki lag is marginally richer in Se than the corresponding black coarse lag. There was no recognisable Se anomaly in the saprolite at Beasley Creek but the long count XRF technique was not employed here. All the data reported by Robertson and Gall (1988) fell below their detection limit of 5 ppm.

8.3.23 Sn

Most of the data lie close to the detection limit. There appears to be a weak Sn anomaly (6 ppm in a background of 2 ppm) in the fine lag on line 38820N but not on 38940N. This appears to be reproduced in the coarse lag but does not show up in either of the fine lag components, which raises doubts as to its significance. Data from the saprolite suggest a weak, single point Sn anomaly (6 ppm) and Sn background levels are similar.

8.3.24 Sr

The regional and local backgrounds of 5 - 10 ppm are consistent. All lag fractions show a strong anomaly in Sr, some 200 - 300 m wide, centred on the ore, reaching 20 - 40 and in places 80 - 90 ppm. The fine lag (all components) shows the best anomaly contrast and the strongest Sr anomalies lie over ore on line 38940. This reflects the presence of calcrete, which is abundant at the ore position on line 38940 (Robertson and Churchward, 1989). The calrete component has been shown to be Sr-rich (Appendix 7). The correlation with similar anomalies in Ba, Ca and Mg is remarkably good. Strontium levels in the lag are an order of magnitude lower than in the underlying saprolite, where there is no Sr anomaly associated with ore (Robertson and Gall, 1988).

8.3.25 V

The ICP data are systematically lower than those obtained by XRF, though the two are highly correlated. There is no anomalous V related to ore. The coarse lag shows a much higher background over the flats to the east of the hill than over basaltic rocks. The khaki lag shows high values compared to the corresponding ferruginous lag and the red-brown clays are V-rich (Appendix 7).

8.3.26 W

Tungsten in the coarse lag shows a weak anomaly over the ore but the W anomaly in the file lag lies in the hangingwall. The anomalies are probably significant (twice detection limit). The ore host contains a distinct W anomaly of 30 - 55 ppm over a background of 3 - 10 ppm typical of the footwall rocks. Though the background levels are similar, the W anomaly in the lag is smaller (10 - 15 ppm). The use of INAA analysis for this element is considered to be well justified.

Tungsten is correlated with Fe, Ti, V and Ga and to some extent with Au, Mn and Pb. The apparent loss of W on passing from the saprolite to the lag suggests dissolution and adsorption on Fe and possibly to a lesser extent on Mn oxides. Both the red-brown clays and the cellular ironstone are enriched in W (10-12 ppm; Appendix 7).

8.3.27 Y

Yttrium shows a greater variance in the coarse than in the fine lag. There is no anomalous behaviour related to ore. The khaki lag is Y poor in relation to corresponding ferruginous lags.

8.3.28 Zn

The coarse lag has higher concentrations and a greater variance in Zn than the fine lag. There is a weak but distinct Zn anomaly in the hangingwall of the ore on line 38820N and in the footwall of the ore on line 38940N in the non-magnetic component of the fine lag. This is reflected in the total fine lag but the magnetic component shows no appreciable Zn anomaly. Zinc correlates well with Fe, Mn and Ba and to a lesser extent with Mg, As, Co, Cu, Sr and Y in the fine lag and its non-magnetic component

but it correlates with little in the magnetic component. The Zn anomaly is present in the cellular ironstone component of the fine lag (Appendix 7). The khaki lag is Zn-poor relative to the corresponding ferruginous lags.

8.2.29 Zr

There is no anomalous behaviour related to the ore. The fine lags show a general gradient of decreasing Zr from west to east. The coarse lag shows the opposite trend. The Zr levels in the coarse lags are several times lower than in the fine lag and the magnetic component of the fine lag is relatively enriched in Zr compared to the non-magnetic component and to the underlying saprolite. The Ti/Zr ratio has been briefly investigated (see Section 8.2.6). The Zr content of the red-brown clays is high, relative to the cellular ironstone and the calcrete (Appendix 7). Zirconium no longer seems to occur as zircon but is probably bound to clays and iron oxides in the lag and resides preferentially in the red-brown clay component.

9.0 CONCLUSIONS

9.1 Field Study

Detailed observation of the fine lag in the field can assist the explorationist in concentrating on the best material. The cellular ironstone component of the fine lag at Beasley Creek carries a large proportion of the useful geochemical signal. Study of a wet fine lag sample with a hand lens would be adequate.

9.2 Improvement of Geochemical Signal

Separation of the magnetic component of the fine lag gives a material which is generally more consistent but the useful geochemical signal is in most instances inferior. As the best geochemical signal appears to come from the cellular ironstone, a minor component, either a density or an electrostatic technique could be tried to separate this material and thus significantly improve the strength of the geochemical signal. This would be particularly important when dealing with an orebody which is less geochemically distinct than that at Beasley Creek.

9.3 Lag Dispersion Mechanisms

Once lag fragments have reached the top of the saprolite or the lateritic duricrust, by downward weathering of the landscape, they are either directly weathered out on the surface or incorporated in soil, hardpan and calcrete. Vertical dispersion takes place by several mechanisms, including deflation of the surface by wind and water, the burrowing action of ants, termites, rabbits, rodents and goannas, the plucking action of tree roots and clay expansion and contraction (see discussion by Carver *et al.*, 1987). Once on the surface the lag is subject to lateral dispersion.

Lateral dispersion takes place by the action of wind and water. Wind would move mainly the fine lag fractions and would be largely independent of surface gradient. The fine lag would readily be moved by water on the surface, even down a very slight gradient, but the coarse lag requires either a significant surface gradient or introduction into a drainage to move any great distance.

Several, apparently exotic, fragments were noted in the petrographic investigation (Section 6.0, Appendix 5, Figure 6D). The action of emus is one means by which small quantities of exotic material could be introduced from a considerable distance. These birds ingest quantities of sand and gravel with their food to aid the digestion of vegetable matter. Gastroliths up to 25 - 30 mm and generally of a high sphericity have been recorded. These are retained for many months when their food is dry but are readily excreted when their food is wet and plentiful. While, at first glance, gastric dispersion may appear quantitatively insignificant, over a large time span it could provide a small but signifiant means of transport for exotic material over many tens or even hundreds of kilometres. While it may not significantly alter the geochemical information, provided a sufficiently large coarse lag sample is taken, it could add some minor confusion to a petrographic investigation.

In general the finest fractions of the fine lag may show significant dispersion but the coarser fractions of the fine lag and the coarse lag itself would show progressively lesser dispersion. Apart from some rare but clearly exotic material in the coarse lag, this is shown in practice. Though target elements have a wider dispersion in the finer lag fractions, making them a good regional tool, employment of the more tedious coarse lag sampling has advantages for follow-up investigation.

9.4 Lithological Control and Dispersion

The coarse lag, the ironstone lag and the khaki lag show relatively little dispersion from their sources. The distribution of the khaki lag closely follows the lateritic duricrust and the hangingwall of the black shale orebody, but its distribution is not sufficiently universal for it to be used effectively as a geochemical sampling medium. The ironstone lag is dispersed around its small outcrops and closely follows the subcrop of the orebody and some dolerites. It appears to be spread in useful quantities no more than 200 m from source and likewise it has an inadequate distribution to be useful, except for possible follow-up work. Its potential will be assessed in a later report. The coarse lag is more widely dispersed but it is most strongly concentrated within 200 m of source.

The fine lag is widely distributed. The increase in abundance of the fine fraction of the fine lag to the north-east of the hill is probably related to colluvial sedimentation and fractionation of the lag as it passes down slope and away from source. The quartz lag appears to have been mechanically dispersed around small quartz veins, which are particularly abundant to the north-west, and have no apparent correlation with ore.

9.5 Petrography

Petrographic investigation, particularly of the coarse lag, shows relict fabrics almost certainly originated in the saprolite. The phyllitic orebody host rock is indicated by relics of mica and kaolinite. The mafic and ultramafic rocks are shown by layer silicate pseudomorphs which form confused fingerprint fabrics. Some polymictic fabrics suggest polymictic glacial sediments. The fabrics are not yet regarded as definitive, due to lateral dispersion, the complexities of saprolitic processes and iron replacement. The information is nonetheless valuable and may be combined with other techniques such as geochemistry, radiometry, remote sensing and magnetometry to determine underlying lithologies without the need for drilling. Preliminary examination of the gross fabric, using a binocular microscope, of wet or varnished, freshly-sawn surfaces of samples of coarse lag may help the field geologist. It is hoped that further study of saprolitic fabrics in the Weathering Processes Research Project (AMIRA P241) will refine this.

The petrography suggests the following sequence of probably overlapping processes:-

1) The metamorphic mineral assemblage was weathered to a saprolitic assemblage. Feldspars and amphiboles were replaced by clays and hydrated iron oxides. This was followed by limited solution and redeposition of clays as authigenic minerals within the saprolite (e.g., as kaolinite accordion structures).

2) Replacement of parts of the saprolitic mineral assemblage by hydrated iron oxides occurred in the lower mottled zone. Saprolitic minerals were pseudomorphed in extreme detail. Micas appear to have largely resisted this process, though they have suffered some degradation in crystallinity and small-scale penetration by Fe, accompanied by loss of some K and minor hydration (illite). Later solution and redeposition of iron has partly replaced the pseudomorphed saprolitic fabrics with spongy goethite. There were several cycles of this process.

3) Solution of the saprolitic clays, surrounding the iron-rich nodules, occurred at the boundary between saprolite and pedolith. This was accompanied by solution and redeposition (re-texturing) of the clays and some collapse of the saprolite. The iron-rich nodules protected or partly protected their contained saprolitic fabrics from further dissolution, compaction of the saprolite and resultant distortion. This may have overlapped in part with 2.

4) Below the lateritic duricrust, some limited, but continued, solution and re-precipitation of goethite, to form cutans, occurred on some ferruginous nodules and there was partial destruction of preserved saprolitic fabrics with probable co-precipitation of gold (see Appendix 5).

5) Within and below the lateritic duricrust, there were cycles of continued solution of saprolitic clays and some of the goethite of the nodules, accompanied by precipitation of several cycles of red and yellow clays between the nodules and in cavities. Clay cutans were formed on some pisoliths, which were subsequently partly dissolved and/or fragmented and then recemented by clay (see Appendix 5).

6) At or near the top of the duricrust, solution of clays and goethite occurred along fractures to form vesicles, accompanied by further precipitation of goethite in the fractures and vesicles and goethite permeation of the clays near fractures. Clay-rich hardened mottles were turned into pisoliths by solution and re-precipitation of clays and iron oxides.

7) The laterite profile was partly stripped and the ferruginous nodules lay near the surface, in the soil. Some vesicles became filled with hardpan, clay and opaline silica. There was some gold dissolution and re-precipitation.

8) The nodules reached the surface by deflation of the soil where they now contribute to the lag. Clay coatings were largely removed and some lag particles developed a desert varnish.

9.6 Mineralogy

The black ferruginous lag consists mainly of goethite and hematite with small amounts of kaolinite, illite and quartz. There is also some, as yet indeterminate, complex interstratified clay. Much of the hematite appears to have formed by dehydration of goethite and the two are complementary. Background rocks tend to be richer in kaolinite, quartz and hematite and poorer in goethite than those nearer ore. The khaki lag is hematite-rich and its goethite is extensively substituted with Al.

Equivalent materials to the khaki lag in the lateritic duricrust consists of gibbsite, hematite and minor goethite but the khaki lag contains kaolinite instead of gibbsite.

Electron microprobe analyses of the mica relics indicate a slight K deficiency, suggesting that they are hydrated (illite); this is an intermediate step in mica breakdown. Goethite surrounding these mica relics contains appreciable quantities of Al, Si and K, suggesting sub-micron relics of mica. The matted goethite pseudomorphs, after layer silicates, contain appreciable quantities of Al and Si, suggesting remnant sub-micron clays. The structural formulae of the goethites indicate a wide range of dehydration to hematite but those that were analysed with the electron microprobe showed comparatively little Al substitution.

9.7 Geochemistry

Geochemical background has been established using four samples which straddle the deposit to the north and south and were collected about 600 - 700 m from the centre of the pit. This has been reinforced by extending the two lag sample lines to the east to about 800 m from the pit centre. Though these background sample sites overlie a variety of lithologies, they have proved valuable as a background reference.

Apart from gold, the orebody and its host are depicted by positive anomalies in the alkaline earth elements Mg, Ca, Sr and Ba and by the chalcophile elements As, Co, Cu, Zn, Mo (weak), Pb (possible) and Sb, and by the lithophile elements W, Mn and Fe. In addition Si, Cr and Zr show broad negative anomalies. Gold is the most distinctive, giving a very broad anomaly of 1000 ppb and the coarse lags show very strong and localised anomalies of 12 000 ppb which pinpoint the ore. Arsenic is also effective in defining the target. It is thought that the anomalies in Ca, Mg and Sr reflect the calcrete developed high in the landscape, which, at Beasley Creek, so happens to coincide with the ore host. The very distinctive Mn and Ba anomalies are thought to be related to the ore host rock rather than to the ore itself. The less distinctive anomalies in Cu, Mo, W, Se, Sb and Zn are probably ore-related. These anomalies, and the lag fractions in which they are reflected, are summarised in Table 11. The cellular ironstone is thought to carry much of the anomalous As, Cu, Mn and Zn, as well as some of the Au, Co, Sb, and Se. It appears to represent a gossanous component.

Both the coarse and the fine lags are effective sampling media. The broad Au anomalies in the coarse lag have higher spikes, reaching over 5 ppm, which define the location of the orebody more closely than the more mechanically-dispersed fine lag. The fine lag is better for defining the general area of mineralisation, so it is an excellent means for a first pass survey, and the coarse lag could be used for follow up. It would be advisable to use as large a coarse lag sample as possible (2 kg) for Au representivity but this is generally severely limited by availability of the material.

The fine lag gave better results for Sb, W and Zn. The non-magnetic component of the fine lag was generally superior to the magnetic component, which failed to give satisfactory results for Co, Cu, Se and Zn. These same elements showed a slightly improved signal to noise ratio in the non-magnetic component, compared to the total fine lag sample. As the non-magnetic component made up about 75% of the total sample, only a slightly improved performance would be expected by analysing it separately. It is concluded that no useful advantage would be gained at Beasley Creek by analysis of the magnetic component of the fine lag.

The width of the broad Au anomaly (600 - 900 m) exceeds that which would be expected from mechanical dispersion alone. Petrographic study suggests mechanical dispersions of 50 - 150 m from source for the coarse lag (Appendix 5) and a slightly greater, though indeterminate, dispersion distance for the fine lag. Elements other than Au show anomalies of 100 - 300 m width (Table 11). It seems

TABLE 11
SUMMARY OF ANOMALY TYPES, WIDTHS
AND POSSIBLE SOURCES

	COARSE LAG		FINE LAG						Possible Source
					Magnetic		Non-Magnetic		
	Anom type	Width (m)	Anom type	Width (m)	Anom type	Width (m)	Anom type	Width (m)	
SiO2	-		U	700	-		U	700	
Al2O3	-		U	200	-		U	200	
Fe2O3	-		M	700	-		M	700	
MgO	√	300	√	300	?	200	√	300	Calcrete
CaO	√	200	√	200	√	200	√	200	Calcrete
TiO2	-		-		-		-		
Ag	-		-		-		-		
As	√	100	√	100	?		√	100	Ore
Au	√	900/100	√	900	√	600	√	700	Supergene
Ba	√	300	√	300	√	300	√	300	Ore Host
Bi	-		-		-		-		
Cd	-		-		-		-		
Ce	-		-		-		-		
Co	√	100	√	100	-		√	100	Ore
Cr	-		U		U		U		
Cu	√	100	√	200	-		√	200	Ore
Ga	-		-		-		-		
Ge	-		-		-		-		
In	-		-		-		-		
La	-		-		-		-		
Mn	√	200	√	200	?		√	200	Ore Host
Mo	-		?		-		-		
Nb	-		-		-		-		
Ni	-		-		-		-		
Pb	√	100	-		-		-		?Ore?
Rb	-		-		-		-		
Sb	-		√	300	?		?	100	Ore
Se	√	100	√	100	-		√	100	Ore
Sn	?		?		-		-		
Sr	√	300	√	200	√	200	√	200	Calcrete
V	-		-		-		-		
W	?		√	100	?		?		Ore
Y	-		-		-		-		
Zn	?		√	100	-		√	100	Ore
Zr	-		-		-		-		

Anomaly Types	
√	Positive Anomaly
U	Wide Depletion
M	Wide enhancement
?	Uncertain

that gold was already dispersed in the ferruginous, nodular precursors to the lag during their saprolitic history and this wide gold anomaly reflects a previous chemical rather than a mechanical dispersion. This notion is supported by the generally late-stage positions occupied by gold grains (Figures 7G and H) and will be further tested by profile investigations along line 38820 N at a later date.

The gold at Beasley Creek is related to zones of intense ferruginisation in the host phyllite. The ferruginous lag is a viable geochemical sampling medium as key indicator elements are readily adsorbed by goethite which is its major component. Elements which show useful anomalies as well as a significant correlation with iron are As, Au, Ba, Cu, Mn, Pb, Se, W and Zn.

10.0 ACKNOWLEDGEMENTS

Sample preparation was by R.A. Janes, J.F. Crabb and G.D. Longman. The XRF geochemical analyses were performed by M.K.W. Hart, and the ICP analyses by J.E. Wildman and M. Richardson. INAA analysis was by Becquerel Laboratories. M.J. Lintern, M.J. Willing, D.C. Wright and K.A. Howe assisted with gold check analyses. XRD data were collected by M.R. Annett-Stuart. Polished sections were prepared by A.G. Bowyer. Assistance on the SEM and Cameca microprobe was ably given by B.W. Robinson and G. Burkhalter. R.C. Morris advised on identification of opaque minerals and photomicrography and E.H. Nickel and J. Grice with mineral calculations. R.A. Anand and R.A. Eggleton (ANU) advised on XRD determination of Al substitution. C.P.S. de Rebeira (CSIRO Division of Wild Life and Ecology) advised on emu eating habits. Drafting and artwork was by A.D. Vartesi. J.L. Perdrix and J. Porter assisted with checking and formatting the final document. C.R.M. Butt and R.E. Smith both supplied critical commentary on the manuscript. Western Mining Corporation Ltd., assisted with accommodation and logistics while in Laverton. All this is acknowledged with appreciation. Especial thanks goes to H.M. Churchward and L.M. Lawrance, who assisted with collection of lag samples and to C. Reddell, M. Fox and J. Hronsky for their assistance while at Beasley Creek and later.

11.0 REFERENCES

Anand, R. R., Smith, R.E., Innes, J., Churchward, H.M., Perdrix, J.L. and Grunsky, E.C. 1989. Laterite types and associated ferruginous materials, Yilgarn Block, W.A. Terminology, classification and atlas. CSIRO Division of Exploration Geoscience. Restricted Report 60R.

Banfield, J.F. and Eggleton, R.A. 1988. Transmission electron microscope study of biotite weathering. *Clays and Clay Minerals.* **36**, 47-60.

Carver, R.N., Chenoweth, L.M., Mazzucchelli, R.H, Oates, C.J. and Robbins, T.W. 1987. "Lag" - A geochemical sampling medium for arid regions. *Journal of Geochemical Exploration.* **28**, 183-199.

Deer, W.A., Howie, R.A. and Zussman, J. 1967. *An introduction to the rock-forming minerals.* Longmans, London. 528 pp.

Hallberg, J.A. 1984. A geochemical aid to igneous rock type identification in deeply weathered terrain. *Journal of Geochemical Exploration* **20**, 1-8.

Hart, M.K.W. 1989. Analysis for total iron, chromium, vanadium and titanium in varying matrix geological samples by XRF, using pressed power samples. Standards in x-ray analysis. Australian X-ray Analytical Association (W.A. Branch) Fifth State Conference. 117-129.

Holmes, A. 1944. *Principles of physical geology.* Thomas Nelson and Sons Ltd. London. 532 pp.

Morris, R.C. 1985. Genesis of iron ore in banded iron-formation by supergene and supergene-metamorphic processes - a conceptual model. In K.H. Wolf (Ed). *Handbook of strata-bound and stratiform ore deposits. Regional studies and specific deposits. Vol 13.* Elsevier. 73-235.

Norrish, K. and Chappell, B.W. 1977. X-ray fluorescence spectrometry. in J. Zussman (Ed). *Physical methods in determinative mineralogy.* Academic Press, London. 201-272.

Robertson, I.D.M. and Crabb, J. 1988. A case-hardened carbon steel swingmill. CSIRO Division of Exploration Geoscience technical files. 6 pp.

Robertson, I.D.M. and Eggleton, R.A. (in prep). The weathering of granitic muscovite to kaolinite and halloysite and plagioclase-derived kaolinite to halloysite. *Clays and Clay Minerals.*

Robertson, I.D.M. and Gall, S.F. 1988. A mineralogical, geochemical and petrographic study of rocks of drillhole BCD1 from the Beasley Creek Gold Mine - Laverton, W.A. CSIRO Division of Exploration Geoscience, Restricted Report MG 67R, 44pp.

Robertson, I.D.M. and Churchward, H.M. The pre-mining geomorphology and surface geology of the Beasley Creek Gold Mine, Laverton, W.A. CSIRO Division of Exploration Geoscience, Restricted Report 26R, 39 pp.

Schulze, D.G. 1984. The influence of aluminium on iron oxides. VIII. Unit-cell dimensions of Al substituted goethites and estimation of Al from them. *Clays and Clay Minerals.* **32**, 36-44.

Wang, Q. 1988. Mineralogical aspects of monzonite alteration: An investigation by electron microscopy and chemistry. Ph.D. Thesis. Australian National University, 192 pp.

Williams, H., Turner, F.J. and Gilbert, C.M. 1955. *Petrography - an introduction to the study of rocks in thin section.* W.H. Freeman and Co San Francisco. 406 pp.